UNIVERSITY OF SOUTHAMPTON

FACULTY OF PHYSICAL SCIENCES AND ENGINEERING

Optoelectronics Research Centre

Manufacturing Novel Fibre

by

Paul Bastock

Thesis for the degree of Doctor of Philosophy

2015

UNIVERSITY OF SOUTHAMPTON

ABSTRACT

FACULTY OF PHYSICAL SCIENCES AND ENGINEERING

Optoelectronics Research Centre

Thesis for the degree of Doctor of Philosophy

MANUFACTURING NOVEL FIBRE

Paul Bastock

The work described in this thesis has been funded by the "Engineering and Physical Sciences Research Council's Centre for Innovative Manufacturing in Photonics" and has been part of the work undertaken by the "Non-Silica Glasses and Related Fibre Technology" work package, within the "Novel Glass and Fibre" group at the Optoelectronics Research Centre.

Original contributions to the field include the development of a novel fibre drawing tower, which has allowed over three hundred fibre draws to be accomplished, resulting in composite metal-glass fibre and infrared transmitting fibre manufacturing processes being established. Most significantly, a refined fibre drawing procedure to produce up to 50 km of continuous glass-encapsulated microwire has been created. Fibre has been fabricated with an outer diameter of around 23 μm and inner diameter of around 4 μm, featuring standard deviations of just 2.2 and 0.8 μm for outer and inner diameters respectively, over kilometres of length. A large portion of the work reported in this thesis has been in collaboration with industrial and academic partners, including Rolls Royce, Shell, National Physical Laboratory, Nanyang Technological University, Laboratory of Ultrafast Spectrometry and others.

Characterisation of optical materials has founded relationships with many partners including the University of Oxford and SPI Lasers Ltd. Analysis has been carried out for many groups within the Optoelectronics Research Centre, including the Photovoltaic, Compound Glass, Silica Fibre Fabrication and Integrated Photonics groups. Other academic units at the University of Southampton including the 'Electronics and Computer Science', Chemistry and 'Engineering and the Environment' departments have also had valuable material characterisation performed with the use of the facilities described in this work. Impurity analysis of optical glasses and raw materials has established a relationship with Northern Analytical Laboratory Inc., who has provided continued analysis for the advancing glass melting facility mentioned in this thesis.

Table of Contents

List of Tables

List of Figures

DECLARATION OF AUTHORSHIP

I, Paul Bastock

declare that this thesis and the work presented in it are my own and has been generated by me as the result of my own original research.

Manufacturing Novel Fibre

I confirm that:

1. This work was done wholly or mainly while in candidature for a research degree at this University;
2. Where any part of this thesis has previously been submitted for a degree or any other qualification at this University or any other institution, this has been clearly stated;
3. Where I have consulted the published work of others, this is always clearly attributed;
4. Where I have quoted from the work of others, the source is always given. With the exception of such quotations, this thesis is entirely my own work;
5. I have acknowledged all main sources of help;
6. Where the thesis is based on work done by myself jointly with others, I have made clear exactly what was done by others and what I have contributed myself;
7. Parts of this work have been published as: (See List of Publications)

Signed: .....

Date:.....

Acknowledgements

I would like to thank my supervisor, Professor Dan Hewak for giving me the opportunity to work in the Novel Glass and Fibre Group and his encouragement throughout my PhD.

Our group technician Chris Craig deserves great thanks for his continued support throughout my PhD and in particular, all his help with the glass-encapsulated microfibre project. Moral support has continually been provided and I recognise his work being beyond what is expected from him. Spirits are always kept high when working with Chris! Chris is also to thank for the glass melting of all GLS glass used in the work reported here.

Facility manager Ed Weatherby has provided technical help, and has gotten jobs done quickly for me on multiple occasions, and has always been keen to give a helping hand when needed.

Dr. Kevin Huang, Jin Yao, Khouler Khan and especially Behrad Gholipour have all given advice and hands-on aid for experiments throughout my PhD and deserve great thanks for their help. Behrad is also acknowledged for his depositions in the glass-encapsulated nanowire work reported here.

Thanks to the ORC support staff, Paul Allwood, Mark Lessey, Ollie Matthews and Trevor Austin for their help and advice over the years.

The scientific glass blowers from Chemistry, Paul Frampton and Lee Mulholland have gotten jobs done for me quickly when needed and have always happily made glassware for me, no matter how complex.

Support staff from ECS, Ken Frampton and Mark Long have offered much advice and have done somewhat tricky jobs for me in the past, which has helped a lot during particular projects.

Thanks to all my family, friends and loved ones for their support over the course of my PhD.

The support of the UK's Engineering and Physical Science Research Centre is gratefully acknowledged for the funding of my studentship.

Funding provided from the EPSRC Centre for Innovative Manufacturing in Photonics.

Seed-corn funding provided by the EPSRC funded Metamaterials Programme.

List of Abbreviations

EPSRC – Engineering and Physical Sciences Research Council

GLS – Gallium-lanthanum-sulfide

EDX – Energy-dispersive X-ray spectroscopy

XPS - X-ray photoelectron spectroscopy

ICP-MS - Inductively coupled plasma mass spectrometry

SIMS - Secondary ion mass spectrometry

GDMS - Glow discharge mass spectrometry

xN - Purity, where x is the number of 9's e.g. 4N = 99.99% purity

T_x – Temperature of the onset of crystallisation

T_δ – Fibre drawing temperature

T_g – Onset of glass transformation temperature

T_m – Onset of melting temperature

T_p – Temperature of the peak crystallisation

T_w – Onset of weight loss temperature

DSC - Differential scanning calorimeter

TMA - Thermo-mechanical analyser

DTA - Differential thermal analyser

TGA - Thermogravimetric analyser

K_{gl} - Hrubý parameter

SBW – Spectral bandwidth

C.T.E. – Coefficient of thermal expansion

NTU - Nanyang Technological University

PGB – Lead-gallium-bismuth

FLITES - Fibre-Laser Imaging of Gas Turbine Exhaust Species

EFE - Environmentally friendly engine

UHC - Unburned hydrocarbons

TFLAS - Tuneable fibre-laser absorption spectroscopy

HMFG – Heavy metal fluoride glasses

CVD – Chemical vapour deposition

OSA – Optical spectrum analyser

Chapter 1: **Introduction**

1.1 Novel Fibres

The term ‘fibre’ can often bring many perceptions to mind, and only some immediately think of an optical fibre. Fibres exist in many forms, both synthetic and from the natural world. A common type of naturally made fibre, which is essentially made from pure protein and can be found in most households, is silk. Use of fibres has been dated to prehistoric ages, functioning as rope, and the modern day manufacture of textiles still utilises both natural and synthetic fibres. Manufactured glass fibre is used in so many consumer products that the production of glass fibre makes up a significant portion of the world economy. However, considering the many uses of fibre, the field of glass fibre is relatively small, and that of optical fibre extremely specialised, albeit essential in many modern day telecommunication, medical and scientific apparatuses.

The most commonplace type of optical fibre is comprised of silica glass, which has become a well-established transmission medium for many telecommunication systems with good reason. Silica fibre offers environmental stability over long durations of service and its refined fabrication methods have evolved to produce extremely low optical loss over extensive distances. Because of these exceptional properties, good reason must be made to produce optical fibre of different material.

This thesis details the work carried out towards creating multiple types of novel glass-based fibres for optical and electrical applications. There are two key types of novel fibre produced in this work: mid-infrared transmitting fibre and metal-core glass fibre.

Infrared transmitting fibres have gathered significant interest since first being fabricated in the 1960’s from a family of glasses called chalcogenides [1]. Chalcogenide glasses are most commonly used to transmit in the near to mid-infrared wavelength region (3 – 30 μm), and by definition contain one or more of the chalcogen elements: sulphur, selenium or tellurium. An underlying problem associated with infrared transmitting fibres is the difficulty in purifying the raw materials, resulting in high optical loss in comparison to silica fibres. Just one part-per-million of iron contained in a chalcogenide glass can create 3 $dB.m^{-1}$ of optical loss over a large area of the mid-infrared [2]. While solid-core silica fibres offer an ultralow loss of $1.48x10^{-4}$ $dB.m^{-1}$ at 1.57 μm [3], the lowest loss chalcogenide fibres currently comprise of As_2S_3 glass; which feature losses of around 0.05 $dB.m^{-1}$ at 3.6 μm [4]. There are still years of progress to be made before chalcogenide fibres can feature losses that rival silica fibre. However, there are many short-range optical processes that operate in the mid-infrared, which require optical fibre

to transmit the relevant light power. Solid-core silica fibre does not fit the requirements for this type of application due to its inherent absorption at these wavelengths, whereas chalcogenide fibres offer promise.

Aside from pure glass fibre, composite fibre, namely metal-core glass fibre (first developed by Taylor in 1924 [5]), has found uses in an exceptional amount of applications ranging from microelectronics to reinforced textiles [6]. There has been much progress in the subject area of composite fibres and recent developments have achieved extremely complex fibre structures that allow for “all-in-fibre chemical sensing” [7] or “functional fabrics” [8] for example.

In order to manufacture the aforementioned novel fibres, a specialised fibre drawing facility is required. In this work, an unconventional fibre drawing tower has been developed, which includes a modular furnace that can accommodate the vast range of fibre materials, temperatures and drawing conditions necessary to achieve the breadth of fibres drawn and reported in this thesis.

1.2 Motivation and Goals

Progression in the field of infrared optics is essential to pave a way for the efficient advancement in many scientific areas such as chemical sensing [9], radiometry [10], laser power delivery [11], thermal imaging [12] and laser development [13]. Due to infrared optics being a vital component in these applications, a large industrial demand has been created for infrared transmitting lenses and fibres with low optical loss. One of the most efficient ways of guiding infrared light from one source to another is via an optical fibre, and the current standard of infrared transmitting fibre on the market is not suitable for most of the mentioned applications in terms of cost, durability and optical loss. Therefore, the development and manufacture of an infrared transmitting fibre with high durability and low optical loss, to rival the current fibres on the market, is an exciting prospect to be involved in that can benefit so many fields. To achieve this, one of the goals of this work is to improve the purity of infrared transmitting glass made in-house, and in this way reduce the fibre loss.

A fibre design that has many applications in optical [14, 15], electrical [16, 17] and mechanical [6] sectors, is that of a simple metal core and glass cladding. Due to the immediate access to so many industries, creating a facility to manufacture this fibre structure has founded an extremely valuable resource to the Optoelectronics Research Centre’s repertoire of capabilities. Already, numerous research groups have expressed considerable interest in this type of fibre, and by developing the capability to mass-produce the fibre; abundant samples can be readily supplied to interested researchers, which has opened a door to effective collaborative projects.

Unfortunately, research is recognised to be plighted by high costs and secrets, which often slows progress in both research and the industries that it benefits. By working in collaboration with several academic and industrial-based partners throughout the work reported in this thesis, a sincere effort has been made to share knowledge and results. The extremely high price of many infrared components that can help save lives in the medical sector, by delivering CO_2 laser power during surgery [18] or aid chemical sensing for environmental studies [19], often creates a bottleneck for progress to be made in these areas. By developing an improved infrared transmitting fibre with an ambition of manufacturing such a product, costs will be driven down for consumers. A consequent end-goal of offering an affordable mid-infrared transmitting fibre and lenses to the market will allow many applications in the mentioned sectors to progress, which may have previously been held back for economic reasons.

In summary, the goals of the work reported in this thesis are to:

1. Design and implement a modular fibre drawing facility for various types of fibre.
2. Characterise and develop bulk infrared transmitting glass for fibre production.
3. Develop fibre drawing procedures for improved quality infrared transmitting glass.
4. Manufacture refined metal-core fibre for various device applications.

Chapter 2: **High Purity Materials**

2.1 Introduction

Raw materials are situated at the very beginning of the many steps toward fibre manufacture, and their purity is considered critical to achieving low loss fibre. Many of the impurities found in raw materials can be removed within the first few steps of in-house high purity glass manufacture; however, beginning with the highest purity raw materials provides valuable headway towards generating high purity bulk glass. An important factor not to be overlooked is that impurities can also be introduced during the glass synthesis procedure. Whether from the crucible, the furnace chamber or from a purge gas supply, precautions must be taken to avoid such occurrences when manufacturing high purity materials for optical applications.

A material is considered not to be of high purity if it contains any foreign substances that are detrimental to the performance of device fabricated from the material. Methods for identifying, tracing back, and reducing impurities are discussed in this chapter as well as what effects impurities have on bulk glass and optical fibre. Focus will be centred on the manufacture of the mid-infrared transmitting chalcogenide glass, gallium-lanthanum-sulfide (GLS), which is created for preform fabrication and then drawn into optical fibre.

2.2 The Importance of High Purity Materials

Identifying impurities contained within the bulk GLS glass produced in-house is essential for endeavouring to make low loss GLS fibre. Impurities contained within the bulk GLS will continue to inhabit the glass, even in the fibre end product, in which case they can act as undesirable absorbing and scattering centres to form optical losses within the fibre. Not only this, some impurities will act as nucleation points for crystallisation during fibre drawing, which in turn also results in a high loss fibre.

So far, impurities have been discussed in a very general sense and a much more in-depth analysis and understanding is needed in order to make improvements on both GLS bulk glass and fibre. This chapter will outline the detrimental effects impurities can have on bulk glass and the polished preform ready to be drawn into fibre.

There are two primary loss mechanisms recognised to occur within optical glass, the first of which is intrinsic, whose losses are attributable to three inherent mechanisms: ultraviolet absorption (caused by electronic absorption bands), Rayleigh, Brillouin and Raman scattering, and infrared absorption (caused by interaction between the vibrating bonds and incident light of

the same frequency). This subchapter will focus on the second loss mechanism, extrinsic losses, which are accredited to be dominant in terms of optical signal deterioration within the infrared wavelength regime. These losses arise because of impurities and imperfections within the glass matrix acting as absorbing and scattering centres as opposed to inherent, intrinsic loss mechanisms above-mentioned.

If an optical fibre were pure, containing no impurities or imperfections, then all absorption would be intrinsic. A theoretically projected minimum loss of an optical fibre is a result of purely intrinsic losses, and interestingly, infrared transmitting fibres are predicted to be able to possess as much as three orders of magnitude less loss than predicted for silica fibre [1]. Unfortunately, no infrared transmitting fibre has been fabricated with a loss as low as silica fibre, and the key reason behind this is due to the abundance of impurities contained within the relevant raw materials, and the difficulty in removing them. Although, if as much time and resources were spent on infrared fibre research as there has been on silica, one could ask themselves what level of standard infrared fibres could have reached. Impurities of particular concern contained within the raw materials that constitute GLS (Ga_2S_3 and La_2S_3) are the first row transition metals, hydroxide ions [20] and dissolved gases [21], due to their abundance, difficulty of removal and their very broad and strong absorption features in the mid-infrared. In comparison to other optical fibre materials, chalcogenide glasses have a large refractive index, this enhances the absorption cross-section of the ions contained in the glass matrix [22], resulting in strong absorption from an ion that may be negligible if it were contained in a lower index glass. Due to lanthanum's inherent chemical similarity to cerium, these elements coexist and are extremely difficult to separate [23], consequently cerium becomes a problematic impurity within La_2S_3.

It has been established that impurities contained within raw materials can impair the final fibre product by acting as an absorbing impurity or a scattering centre. In general, chemical impurities cause extrinsic absorption and, along with physical defects, also cause extrinsic scattering of incident light within the glass fibre [20]. In terms of infrared absorbing impurities, these hinder both the final fibre product and the fibre drawing process. During use as a passive mid-infrared transmitting fibre, the impurities can absorb the signal, creating a fibre with a high loss factor. Not only this, but during fibre drawing, an absorbing impurity can heat up faster than the GLS preform and locally initiate crystallisation if the absorbing particle reaches a temperature higher than the crystallisation temperature of GLS. This also contributes to the loss in a fibre. Extrinsic scattering is a large loss mechanism featured within the current GLS fibre being fabricated, which is mostly accountable to crystallisation. Crystal grain boundaries of significant size interfere with the incident light and cause it to diverge in course, or scatter.

The amount of extrinsic loss mechanisms that exist and can detriment passive fibre performance has been highlighted. It is recognised that physical defects that cause scattering in an optical fibre are often initially caused by impurities contained within the bulk glass raw materials. Furthermore, these impurities can act as extrinsic absorbing features within an optical fibre, even if they have not caused physical defects that have initiated crystallisation, bubbles or cracks. Due to the severe performance impairment that impurities cause within optical fibres, means of reducing the impurity content within bulk GLS glass created in-house, for fibre preforms, is essential to fabricate low loss fibre.

2.3 Impurity Analysis Review and Implementation

In order to identify and quantify impurities contained within raw materials and bulk glass, a review of impurity analysis techniques has been carried out. All of the techniques reviewed have been performed on raw materials or bulk GLS glass; however, one technique in particular, glow discharge mass spectrometry, has been recognised to generate results more efficiently and accurately than others.

The ideal impurity analysis procedure would involve minimal preparation of a sample, and result in a full elemental breakdown of what the sample contains in parts-per-billion accuracy across the entire periodic table. Mass spectrometry comes closest to offering such results, however mass spectrometry itself is an extremely broad subject area, containing numerous analysing techniques and sample atomising mechanisms. Mass spectrometry depends on the formation of gas-phase ions that can be isolated based on their mass-to-charge ratio and a detector that can identify and count each of the ions. The following material characterisation techniques are investigated and their procedures are discussed along with suitability towards impurity analysis of GLS glass and raw materials: energy-dispersive X-ray spectroscopy (EDX), X-ray photoelectron spectroscopy (XPS), inductively coupled plasma mass spectrometry (ICP-MS), secondary ion mass spectrometry (SIMS) and glow discharge mass spectrometry (GDMS).

As a first step towards finding the ideal impurity analysis technique for GLS glass and raw materials, EDX was explored. EDX is a useful tool for the quick inspection of a material of unknown composition, to approximately identify what elements are contained within it, or to verify that a particular element is present. EDX works on the fundamental principle that every element has a unique atomic structure, which allows for elemental identification from an X-ray emission spectrum of the sample being analysed. To induce an X-ray emission from a sample, a high-energy X-ray, electron or proton beam is focused onto the sample. This process can excite an electron in the inner shell of an atom; ejecting it from the shell. An electron hole is then created where the ejected electron used to be, and subsequently, an electron from an outer,

higher energy shell will fill the hole. The difference in energy between the higher and lower energy shell is then released in the form of an X-ray, which is measured by an energy dispersive spectrometer that also records the intensity of the X-rays emitted from the sample. The energy of the X-rays measured by the spectrometer are assigned to particular elements and the intensity of X-rays are used to quantify the particular element abundance. EDX is often categorised as a modest analysis tool due to the relatively low accuracy of identification and quantification of elements within the sample. In terms of identification, although each element emits an X-ray of particular energy, many have overlapping peaks from different X-ray families. Furthermore, any atom within the analyte can emit an X-ray when excited by the incident beam, but does not radiate in any particular direction, so the X-ray may not be directed at the spectrometer or could be re-absorbed by the analyte. Samples of a high density absorb more of the emitted X-rays than a less dense sample and accuracy is particularly hindered within inhomogeneous or rough samples, which can cause an elevated X-ray absorbing effect. Nonetheless, EDX is a useful tool when determining approximate stoichiometric information of a small sample area, but is not suited for the impurity analysis of bulk GLS glass or raw materials.

XPS is known to be a more accurate method of determining sample composition, particularly in thin films, therefore was assessed to determine its suitability for impurity analysis. XPS is a non-destructive surface analysis technique widely used due to its relatively simple operation and data analysis. The process involves irradiating a sample, to a depth that generally extends to around 5 - 10 nm, with a mono-energetic X-ray (1486 eV), which excites the electrons of the sample atoms. If the binding energy of the electrons is lower than the incident X-ray energy, they are emitted from the atom as a photoelectron. The mono-energetic X-ray is produced through the manner described by EDX, where an electron beam is fired at an aluminium target; the emitted X-rays from the aluminium target are 1486 eV, which are then focused onto the analyte to create the XPS excitation process. The majority of the photoelectrons emitted from the top 10 nm of the sample surface will escape from the analyte without being reabsorbed and are transported to an electron energy analyser via charged hemispherical plates. This transportation process (Figure 2.1) determines the binding energy of the photoelectrons, which are characteristic of particular elements. The potential between the negative and positively charged hemispherical plates is swept, allowing only photoelectrons of particular eV to pass through at a time; matching the signal produced from the electron energy analyser to the hemisphere’s potential allows for both determination and quantification of individual elements. Each element contains multiple binding energies, which are representative of its electron orbitals. The kinetic energy of the emitted photoelectrons is the difference between the incident energy (1486 eV from the X-ray) and the aforementioned binding energy. Therefore, if the kinetic energy can be measured, the binding energy of the photoelectron can be calculated

through simple subtraction and therefore the element that the photoelectron belonged to can be determined.

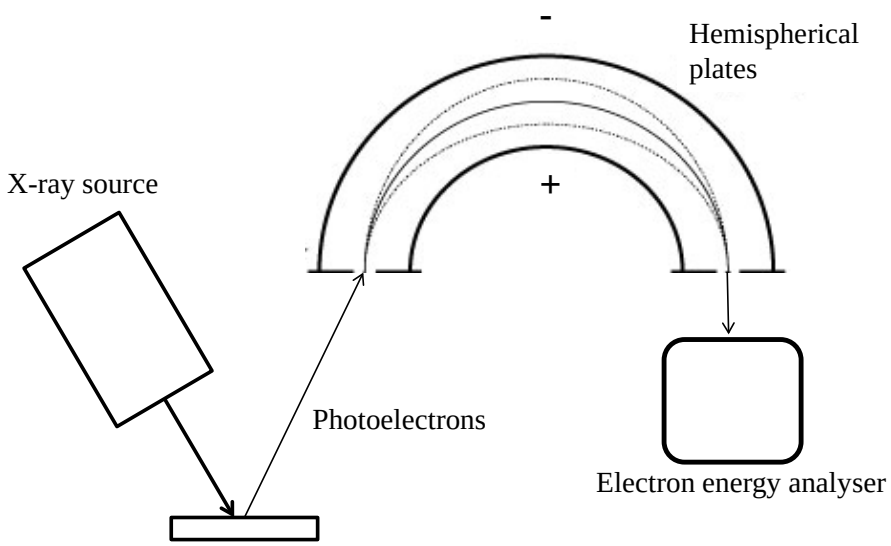

Figure 2.1 Schematic of XPS process

XPS is an extremely effective material analysis technique for small samples, however, due to the limitation of only analysing samples to a very small depth, XPS has also been considered unsuitable for the impurity analysis of bulk GLS glass and raw material powders.

Mass spectrometry is recognised to be a suitable method of producing quantitative impurity analysis data [24], and has therefore been evaluated for the suitability of analysing GLS glass and raw material powders. ICP-MS, SIMS and GDMS have all been endeavoured in attempt to realise the benefits of each, to determine the most suitable technique for this particular purpose. Mass spectrometry effectively measures a samples mass-to-charge ratio and abundance. A typical apparatus consists of three distinctive components: an ion source, which converts the sample into gas phase ions, a mass analyser that separates the ions based on their mass-to-charge ratio, and a detector, which measures the intensity of the signal generated by those ions. The subject of mass spectrometry is extremely vast as there are several types of ion sources, mass analysers and detectors. Overviews of the specific operation of the three types of mass spectrometry used in this work are presented and results gained are discussed.

ICP-MS is an analytical technique mainly used in geochemical laboratories, where it has been adopted as the analytical method of choice due to its superior detection capabilities, particularly for rare earth elements. The ionisation process consists of either a sample in solution (usually in diluted nitric acid) being introduced into the core of an inductively coupled argon plasma, in the form of aerosol droplets, or a solid sample being laser ablated and similarly being introduced

into the plasma. The droplets or particles are instantly atomised within the plasma and successively lose electrons and become (singly) charged positive ions. The most common mass analyser used in ICP-MS is a "quadrupole mass filter" (illustrated in Figure 2.2), which separates ions based on their mass-to-charge ratio. The quadrupole is comprised of four rods arranged in a square whereby alternating AC and DC voltages are applied to the opposite pairs. The voltages are rapidly switched, and a radio frequency field is also applied around the quadrupole, which creates an electrostatic filter that only allows ions of a single mass-to-charge ratio pass through the rods to the detector at a time. This is an extremely fast process, and a full range of mass-to-charge ratio data-sets can be plotted almost simultaneously after the intensity of each mass-to-charge value is recorded by the detector. The resulting information is regarded as isotopic since different isotopes of the same element have different masses, therefore the gathered data can distinguish between both elements and isotopes, however some isotopes of dissimilar elements do overlap, which is a disadvantage associated with conventional ICP-MS.

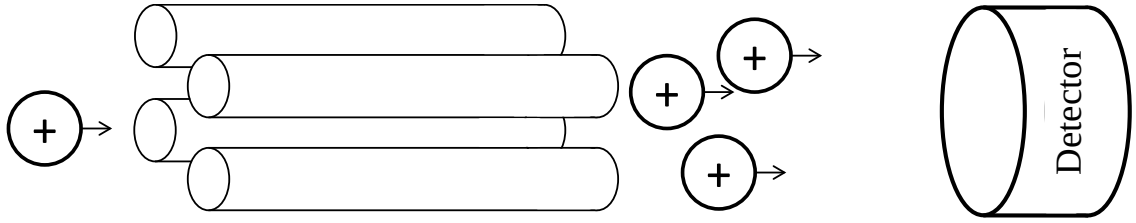

Figure 2.2 ICP-MS quadrupole mass filter and detector

ICP-MS has been carried out at Glass Technology Services Ltd., Ilika plc. and the National Oceanography Centre to give a count per unit-time of each isotope detected; however, quantifying the results involves purchasing an individual standard for each element of interest, to calibrate the equipment. Each standard is relatively high in cost, and with a requirement of a full elemental analysis, this method is not cost effective. Although ICP-MS has given useful data as to what contaminants are present in the GLS raw materials, without the ability to quantify the results, alternative impurity analysis techniques have been explored.

SIMS is a technique most commonly used on thin films to determine compositional data that can be imaged to create a depth profile of a film. The process can also be rastered in order to determine elemental concentrations across a sample surface. The ionisation process consists of a pulsed primary ion beam (usually caesium due to its inherently large mass) being used to dislocate and ionise species from the sample surface. The caesium primary ion beam is generated by heating a solid sample of caesium, whereby the vapour produced strikes a heated tungsten plate, causing the vapour to become thermally ionised. Once the ions are created, they then escape through a small aperture; creating a caesium ion beam. Upon the beam hitting the sample surface, secondary ions are created, which are accelerated into a mass analyser. A "time-

of-flight" mass analyser has been used in the case of the analyses carried out at Loughborough Surface Analysis, Surface Science Western and Imperial College London. The emitted secondary ions make their way into the time-of-flight analyser by applying a high voltage potential between the sample surface and the mass analyser. The secondary ions travel through the time-of-flight mass analyser with different velocities, depending on their mass-to-charge ratio. A full mass spectrum is obtained by measuring the exact arrival times of the secondary ions at the detector and performing a simple time-to-mass conversion to determine what ions are present. For each primary ion beam pulse, a new mass spectrum is generated. An issue that became apparent with the SIMS technique is that quantifying the detected elements, again, requires standards to create relative sensitivity factors for each element of interest. Although SIMS provides extremely useful information on thin film thicknesses and concentration factors, this method is not suited to bulk analysis. The main drawback associated with SIMS is that quantitative results are very difficult to produce except for the specific case of trace concentrations with calibration standards in hand. There is also a severe matrix effect coupled with SIMS [25], which is accountable to variations in sputtering yield over time.

GDMS is a technique most commonly used in semiconductor and high purity metal industries, for the analysis of trace elements. Its primary function is that of impurity analysis, and can offer the greatest detection limits of any bulk mass spectrometry technique. The method of GDMS has the immediate advantage of the atomisation and ionisation processes being separated in both space and time. This results in only minor variations in sensitivities and the matrix effect is almost entirely diminished, so quantification is possible without the need of matrix-matched standards [26]. Quantitative GDMS results of GLS glasses and raw materials has been performed by Northern Analytical Laboratory, Inc. in parts-per-million (by molecular weight) resolution. The equipment used for this analysis has been the VG9000, which is recognised as the most popular GDMS instrument of the one hundred or-so appliances that are used world-wide [26].

GDMS relies on the phenomenon that if an electrical potential is applied between two electrodes (negatively biased cathode and positively biased anode) in a low-pressure, inert gas atmosphere, an electrical discharge will occur [27]. The glass or powder analyte is processed into a small pin, typically 1 – 3 mm in diameter and 10 - 15 mm in length, which acts as the negatively biased cathode. A sample sputtering process is then induced by providing an electric field to a glow discharge (which is a specific type of plasma) created within the atomisation chamber. For a gas discharge to occur from the glow discharge, a fraction of the gas particles must be ionised by application of an electric field. The positively charged gas discharge ions accelerate towards the negatively biased cathode (sample), which upon impact begins sputtering, effectively atomising the sample pin. The strong negative electric bias on the cathode stops secondary ions

from leaving the sample surface like that in SIMS. Only neutral species from the cathode can diffuse into the plasma of the glow discharge whereby the atoms are ionised by collision and are then extracted through a small slit and accelerated into a high-resolution mass analyser. The mass analyser used in the VG9000 is a "magnetic sector" whereby fields generated by the flowing ions interact with a magnetic field imposed on their flight [28]. The ions flow through a curved path with a radius proportional to their mass-to-charge ratio (as shown in Figure 2.3), which separates ions of different mass in space. The ion beam then passes through an electrostatic analyser in order to reduce the energy spread of the ions. The electrostatic analyser deflects the beam by 90 ° to select and transmit nominal ion energy and the walls absorb the unwanted ions; the remaining ions are delivered to a detector that quantifies the count of each element, alongside a computer.

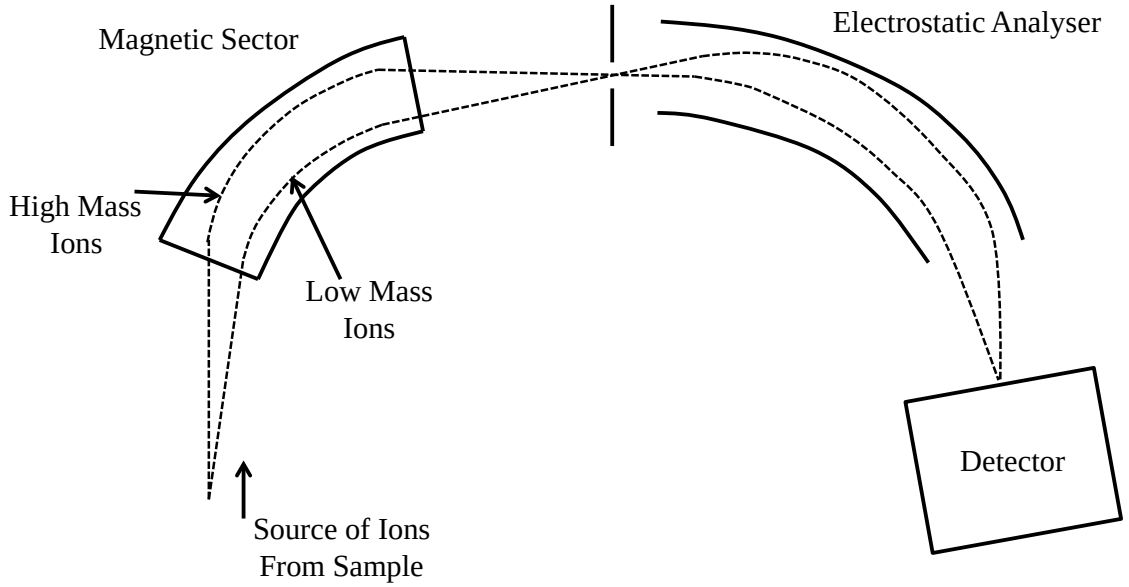

Figure 2.3 GDMS mass analyser and detector schematic

In this section, a review of potential impurity analysis techniques has been discussed along with the concept behind each instrument. GDMS has been established as the most suitable method of attaining impurity analysis of GLS bulk glass and raw material powders due to the ease of generating quantitative results in parts-per-million resolution, minimal sample preparation and relative low cost. Examples of the reader-friendly GDMS results are shown in Appendix A.

2.4 Bulk GLS Glass Manufacturing Process

It has been described why high purity materials are important and what analysis technique has been employed to identify impurities within raw materials used for in-house glass melting. Not only do the raw materials have to be of high purity, it is also important to realise that foreign

particles can be introduced to the glass during melting. For example, carbon or silica from the crucible or furnace wall can create nucleation sites within the glass; these act as a direct cause for the onset of crystallisation during fibre drawing, which leads to extremely high optical losses within the resultant fibre. The removal and prevention of such impurities is extremely important and such methods of doing so should be carried out methodically. Many steps can be taken to ensure glass synthesis and melting is carried out under the best possible conditions, some of which will be discussed in this subchapter.

Firstly, it should be made clear how the GLS synthesis and melting system operates, an illustration of which is shown below in Figure 2.4.

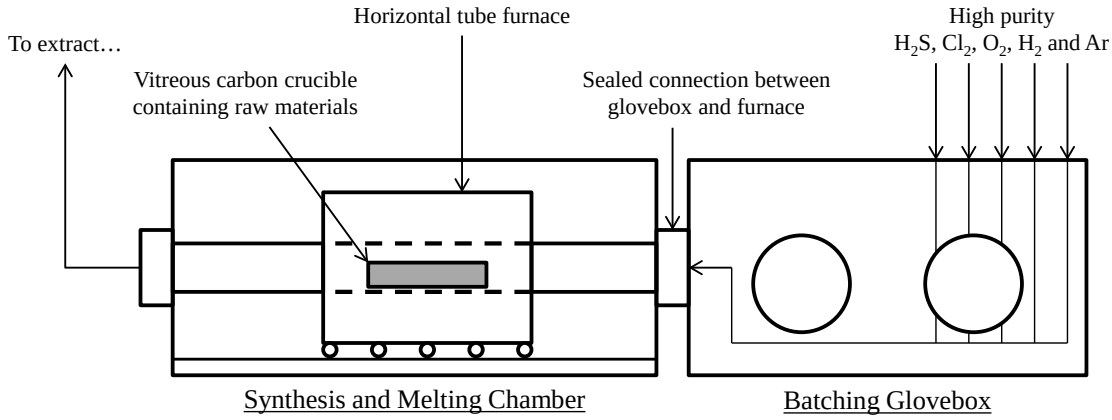

Figure 2.4 Current GLS synthesis and melting system

Raw materials purchased from specialist suppliers are stored in the batching glovebox, which is continuously purged with high purity argon. Commercially bought Ga_2S_3 and La_2S_3 raw materials are batched and mixed within the batching glovebox using high accuracy scales before being placed inside a vitreous carbon crucible. The loaded crucible is then carefully transferred into the tube furnace, which is also being purged from the batching glovebox. The crucible is positioned in the middle of the tube furnace, and a recipe is programmed into the furnace to start the melting process. Various gasses can be introduced into the furnace whilst in operation, to create an inert or reactive atmosphere. Depending on what gases are added to the furnace, many compounds can be reduced. For example, Shuichi et al. have demonstrated the reduction of H_2O, OH^- and SH^- content in Ge-S glass through the introduction of a S_2Cl_2 vapour flow over raw materials at elevated temperatures [29]. After the melt has finished, the furnace, which is secured onto runners, is pushed to one side to allow the glass melt to quench before being annealed.

The purity of the bulk GLS glass being made in-house is currently plighted by a lack of high purity raw material suppliers. The Ga_2S_3 currently being used is of 99.99 % purity (4N) and the

La_2S_3 only 3N. These raw materials are currently of the highest purity that are available, and within monetary budget. The synthesis and melting system has also been designed to make the raw materials for GLS in-house, to create higher purity materials than can currently be bought. 7N gallium metal is available for purchase, as is 5N LaF_3, and by converting these materials into Ga_2S_3 and La_2S_3 in-house, GLS raw materials can be produced with higher purity than can be directly purchased. Conversions would take place in the following three steps:

$$LaF_3 + O_2 \rightarrow La_2O_3 + F_2 \uparrow$$

$$La_2O_3 + H_2S \rightarrow La_2S_3 + H_2O \uparrow$$

$$Ga + H_2S \rightarrow Ga_2S_3 + H_2 \uparrow$$

This process can offer much tighter quality control than is currently in place; the unknown manufacturing process associated with buying Ga_2S_3 and La_2S_3 from a supplier can be removed from the current GLS production process. Through continuous monitoring of dewpoint meters, which are installed on the gas delivery lines, quality control of in-house conversions (in terms of moisture content) is significantly enhanced compared to buying from suppliers. Another advantage becomes apparent through converting raw materials in-house, of continuity between batches being much more stringent; currently, variations in colour between batches of raw materials from the same supplier can be seen, which suggests discrepancies in material composition.

Creating raw materials in-house has many advantages; however, precautions must be taken into account to complete a conversion or glass melt in an atmosphere, which is of suitably high quality. One of the main attributes towards creating a high-quality conversion, synthesis and melting environment is to purge the system with ultrahigh purity gas. By installing ultrafine point-of-use gas filters into the gas delivery lines, dramatic improvement to glass quality has been realised, although this alone is not sufficient to create the best glass possible. By pre-heating the tube furnace for 24 hours at high temperature, the silica tube that has been cleaned with hydrofluoric acid and deionised water between melts is suitably dried, prior to being used for conversion or glass melting. Efforts like these mentioned make a big difference in glass quality and should provide motivation to making even small changes in procedure or hardware to further improve glass quality.

Lack of availability of high purity raw materials is also accompanied by difficulties in sourcing high quality vitreous carbon crucibles in which the GLS glass melts are contained. Conventional glass melting crucibles are made from platinum, silica or alumina; however, none of these materials are appropriate due to reactivity with GLS during melting. Properly manufactured vitreous carbon crucibles will not react with GLS; however, if the carbon crucible has not been

properly vitrified, particles of carbon can infuse into the GLS during melting. Likewise, high purity silica tubing is used for the interior of the furnace wall to provide a clean environment, which remains stable at high temperatures, and does not devitrify and drop particles of silica into the GLS melt.

An absorption plot illustrating the difference between two separate 65:35 (65 mol% Ga_2S_3 and 35 mol% La_2S_3) GLS bulk samples is shown in

Figure 2.5. There are two main differences in these melts: the raw material supplier and the glass melt and synthesis conditions.

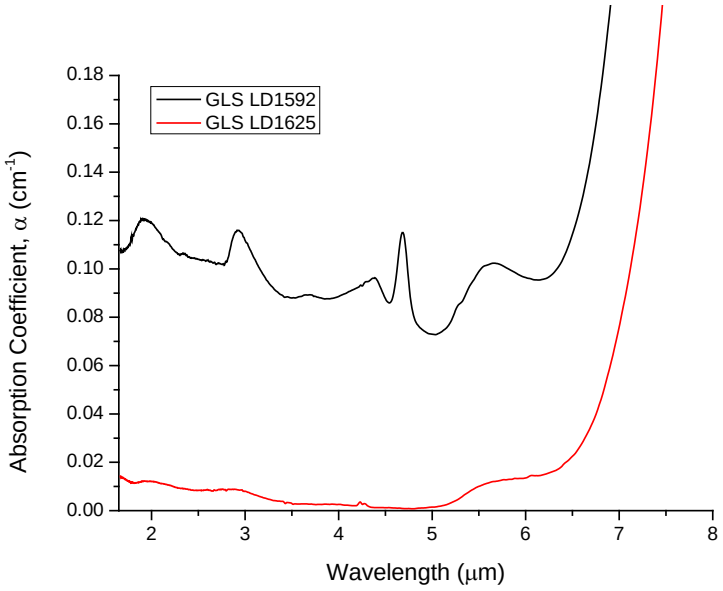

Figure 2.5 Absorption plot illustrating bulk GLS development

LD1592 is made from 65 mol% Ga_2S_3 (4N) from Great Western Inorganics Inc. and 35 mol% La_2S_3 (3N) from Testbourne Ltd. The glass melt was carried out in a basic vertical furnace, which is not equipped with ultrafine gas filters like the newly developed horizontal furnace. A simple melt recipe was used, where the homogenously mixed raw materials were heated to 1150 °C at 10 °C.min^{-1}, held for 24 hours and consequentially quenched and annealed. LD1625 is made from 65 mol% Ga_2S_3 (4N) from Great Western Inorganics Inc. and 35 mol% La_2S_3 (3N) from Lorad Chemical Corporation. The raw materials were dried at 800 °C for 24 hours prior to melting and were sequentially melted under the same recipe as LD1592, but within the upgraded synthesis and melting system. Although the melt and synthesis conditions are different between LD1592 and LD1625, a major factor in reducing the absorption so dramatically is undoubtedly due to the raw materials used. Glow discharge mass spectrometry results (Appendix A) clearly show a big difference for impurities contained in Testbourne Ltd. and Lorad Chemical Corporation La_2S_3 powder. Nevertheless, it should be noted that the addition of

gas line filters also contributed a good deal towards the reduction in absorption between the two samples. It can be noted that no oxygen, nitrogen or carbon data is found in Appendix A and this is due to a lack of standards for these elements. The relative sensitivity standards for these elements have a much larger spread over different material matrices than most other elements.

The current stage of development of the bulk GLS glass synthesis and melting system has been outlined and the reasoning behind certain aspects of the equipment is explained. The precautions mentioned are crucial in order to produce low loss GLS fibre and an ongoing development of the system should be performed in parallel to GLS fibre improvement.

2.5 Conclusion

This chapter has summarised the GLS bulk glass making process along with what actions need to be taken into account during the synthesis and melting procedure. In order to produce glass suitable for optical components and fibres, it has been established that high purity raw materials are of upmost importance, as is the way they are treated during glass melting. Impurities can make their way into a glass melt from many sources, which have been discussed, and techniques on how to quantify impurities contained within glass and raw materials has been reviewed. In order to track progress made during the continuous development of the GLS synthesis and melting system, GDMS has been employed to perform impurity analysis due to its advantages over alternative techniques including cost and ease of procedure.

Chapter 3: **Glass Characterisation**

3.1 Introduction

Following each glass melting trial (as described in Chapter 2), thermal and optical analysis has been routinely performed. One of the main features attributable to GLS is its large glass-forming region. This allows glass compositions to be tailored and optimised for particular device applications. Improvements in the glass melting facility (as discussed in Chapter 2) led to improvements in bulk glass quality. Each modification to the melt system was followed by a glass melt and assessment of the glass purity; allowing evaluation, on an ongoing basis, of the effectiveness of these improvements. Slight variation in GLS stoichiometry results in changes to the glass optical and physical properties. Creating a clear picture of how the glass characteristics vary with stoichiometry is therefore quite essential. The following chapter provides details of the thermal and optical analysis equipment used. Further detail is provided in standard operating procedures found in Appendices B - D.

3.2 Thermal Analysis

One of the main setbacks during the fabrication of GLS optical fibre is the glass' tendency to crystallise during the fibre drawing process. This is because the crystallisation temperature (T_x ~ 680 °C) lies very close to the fibre drawing temperature (T_δ) of GLS, which are just two of many glass features that can be identified using thermal analysis. From the many glass properties that can be determined, the suitability of a glass for fibre drawing can be accurately concluded by thermal analysis. An ideal instrument to establish glass suitability for fibre drawing is a viscometer, which can generate a plot of viscosity as a function of temperature and confirm exactly what temperature is needed to soften the glass to its T_δ. Fibre drawing is carried out at a viscosity of around 10^4 poise (Pa.s) and the respective temperature can be compared to the T_x of the glass, which will ideally be significantly higher than the temperature at 10^4 poise to allow for fibre drawing to take place comfortably. Although this particular piece of equipment is not used throughout the work reported in this thesis, alternative methods have been used to establish glass thermal properties, which indirectly provide viscosity data similar to that of a viscometer.

In this work, there are three separate thermal analysis devices that have been regularly used to characterise bulk glass, films and raw materials: the Perkin Elmer Diamond series of differential scanning calorimeter (DSC), thermo-mechanical analyser (TMA) and combined differential thermal analyser (DTA) and a thermogravimetric analyser (TGA).

The DSC measures the heat change in a material together with the temperature at which these changes occur, as the sample is subject to a predefined heat cycle. Upon heating, cooling or isothermal hold, any transformation taking place in a material is accompanied by an exchange of heat; the DSC enables the temperature at which this transformation occurs to be determined and the energy exchange from it to be quantified. The property measured by the DSC is expressed as heat flow; the flow of energy radiating out of, or absorbing into the sample, expressed in mW. The Watt is the unit of power, which is defined as a Joule per second, in other words, the flow of energy per unit-time, hence, heat flow. The heat flow measured by the DSC is not absolute, but rather, relative to a reference, which sits in a separate furnace to the sample. The sample (around 10 mg in weight) is contained within a sealed aluminium pan, as seen in Appendix B (DSC standard operating procedure), and an identical empty pan is used as a reference throughout the analysis. The heat flow displayed to the user is the difference in heat flow between the sample and reference, detected by separate thermocouples on which each sample pan sits. An increase in heat flow is recognised as an exothermic reaction, for example, crystallisation of the sample, and inversely, a decrease in heat flow is recognised as an endothermic reaction, for example, melting of the sample. The amplitude of the heat flow peak determines how big a reaction has occurred, with the integral of that peak reflecting the amount of heat released in Joules. The DSC is calibrated to work with a ramp rate of 300 °C.min^{-1} and has a current maximum operating temperature of 300 °C. A helium purge is connected to provide a highly conductive gas atmosphere for rapid heating and cooling.

The TMA determines the dimensional changes of a material as a function of temperature and/or time under a defined mechanical force. Any dimensional change is quantified and correlated to glass transitions or physical properties. A small sample of precise dimensions, often a cube or cylinder, is mounted in the selected TMA module, which is surrounded by a furnace. There are multiple modules that can be used with the TMA, which include expansion and compression parallel plate probes, a three-point bending probe, penetration probes, and an elongation probe kit. The use of these modules is described in Appendix C (TMA standard operating procedure), where a description of each module can be found. A thermocouple is positioned close to the probe tip within the furnace, where the sample is located, and provides a live feedback of the approximate sample temperature; the exact position of the probe is also recorded in-situ, which has a credible accuracy of ± 10 nm. As a material expands, the probe is forced upwards and the slope created of length as a function of temperature is used to calculate the coefficient of thermal expansion of the material. When a sample reaches its glass transition temperature (T_g), the probe will experience an increase in height if under tension and conversely, a decrease in height if under compression. A constant force can be applied (compression or tension) with a varying temperature, or constant temperature with varying force, depending on the analysis

chosen to be carried out. Sample preparation is important so that an accurate analysis can be performed; if a sample does not have sharp edges or parallel cuts, the imprecise volume will introduce error into thermal expansion measurements. A simpler alternative to preparing cubic specimens is to cane the sample. A cane is a large diameter fibre fabricated at a much slower speed than that for fibre drawing and using a higher viscosity. Cutting this cane with two parallel cuts creates a cylindrical specimen as opposed to the six cuts required for a cube. The TMA is calibrated to work with a ramp rate of 10 °C.min^{-1} and has a maximum operating temperature, limited by the silica modules, of 1200 °C, although ceramic modules are available for use up to 1500 °C. Purge gasses available to the TMA are argon, nitrogen, oxygen and air.

The DTA and TGA are contained within the same apparatus and both sets of data are calculated simultaneously. The DTA measures the difference in temperature between a sample and a reference as they undergo temperature scanning in a controlled atmosphere. Both sample and reference are confined within the same uniform-temperature furnace and thermodynamic events that undergo an endothermic or exothermic reaction are recorded as a function of temperature in parallel to the TGA calculating the mass change under the same conditions. Extremely sensitive 'thermobalances' quantify weight change between sample and reference, which is recorded as a function of temperature. The thermobalances on which the sample crucibles sit, record the DTA signal via a thermocouple at the same time as the thermogravimetric measurement via a microbalance, hence the name thermobalance. A sample of around 10 mg is prepared and can be of any liquid or solid form. Sample preparation is very simple as the sample usually consists of a small sacrificial shard of glass or a small superfluous sample of powder or liquid that is matched to a suitable crucible material (usually platinum or alumina). It is important to make sure that the analyte will not react with the crucible under the temperature conditions set in the recipe. A reference is used much like the DSC measurement, so the signal produced is from the sample itself, which is displayed as heat flow and weight as a function of temperature. In addition to detecting the sample weight loss/gain events, the synchronised DTA signal shows thermal effects that are not accompanied by a change in mass, for example T_g, T_x or melting temperature (T_m). The TG/DTA is calibrated to work with a ramp rate of 10 °C.min^{-1} with a maximum operating temperature of 1500 °C and purge gasses of argon, nitrogen, oxygen and air are available. A standard operating procedure for the TG/DTA is included as Appendix D.

A typical GLS heat flow plot as a function of temperature is illustrated in Figure 3.1. This particular plot was generated with the use of the DTA and clearly shows T_g, T_x, peak crystallisation temperature (T_p) and T_m. In terms of fibre drawing stability, heat flow plots like this provide extremely useful information. Bulk glass can be assessed in terms of its approximate fibre drawing suitability, given the onset temperatures shown in Figure 3.1. The T_g is the onset temperature from glass solid to liquid phases, hence fibre drawing is carried out at a

temperature above T_g. However, depending on the glass viscosity curve, the temperature between T_g and T_m can vary substantially. A large T_x - T_g is desirable for stability during drawing, as a large temperature difference between T_g and T_x implies that T_δ will not be as close to T_x as if T_x - T_g were small. A broad, weak, crystallisation peak (half-width of the peak given by T_p - T_x) is advantageous as this means that the crystallisation event is not rapid, where only a small structural re-arrangement is required to induce crystallisation. A large T_p - T_x results in much slower growth of nuclei due to a smaller driving force; this allows for the GLS to be taken to a slightly higher temperature, perhaps enough for improved fibre drawing conditions. Lastly, a small T_m - T_p infers that crystallisation will occur closer to T_m, and therefore far from T_δ.

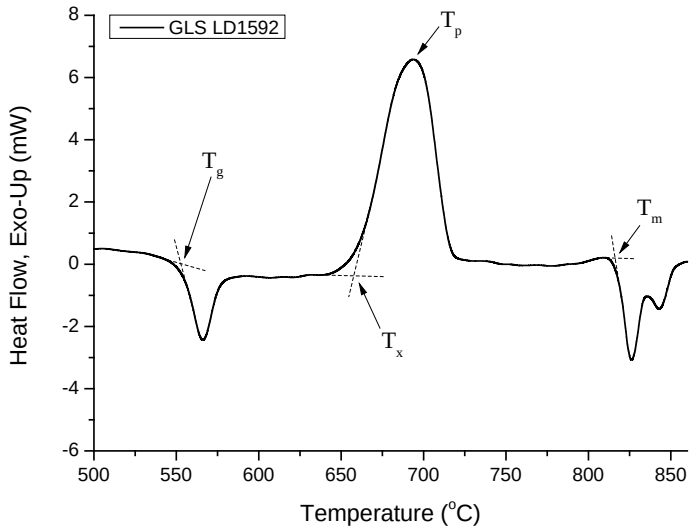

Figure 3.1 Typical DTA curve for GLS (LD1592, 65:35)

All three transition temperature differences (T_x - T_g, T_p - T_x and T_m - T_p) are of importance and one doesn't necessarily outweigh another in terms of fibre drawing suitability. This somewhat rudimentary method of determining glass suitability for fibre drawing is a useful measure of glass stability. A stability parameter, termed the Hrubý parameter [30], can be employed for glasses whose viscosity required for fibre drawing is accessible within the T_x - T_g region. Equation 3.1 defines the Hrubý parameter (K_{gl}) for such glasses, whereby a high value suggests improved fibre drawing stability.

$$K_{gl} = \frac{T_x - T_g}{T_m - T_x} \qquad (3.1)$$

Without the use of a viscometer to determine the optimal fibre drawing temperature of a particular glass, alternative approaches have been utilised. A glass viscosity of around 10^4 poise

is suitable for fibre drawing, and this viscosity is usually depicted in terms of temperature: the fibre drawing temperature. Figure 3.2 portrays a general glass viscosity curve, which is used as reference when referring to viscosity-temperatures and represents a full glass viscosity passage, from flowing to plastic state. Above 10^9 poise the viscosity becomes increasingly time dependant, therefore the delay required to achieve structural equilibrium with any increase in viscosity becomes so great that by 10^{13} poise, the glass can be considered solid, or frozen, under normal cooling conditions. Stresses can be relieved at this viscosity after a 15 minute wait [31], referred to as annealing, but the viscosity is still large enough to hold structural integrity.

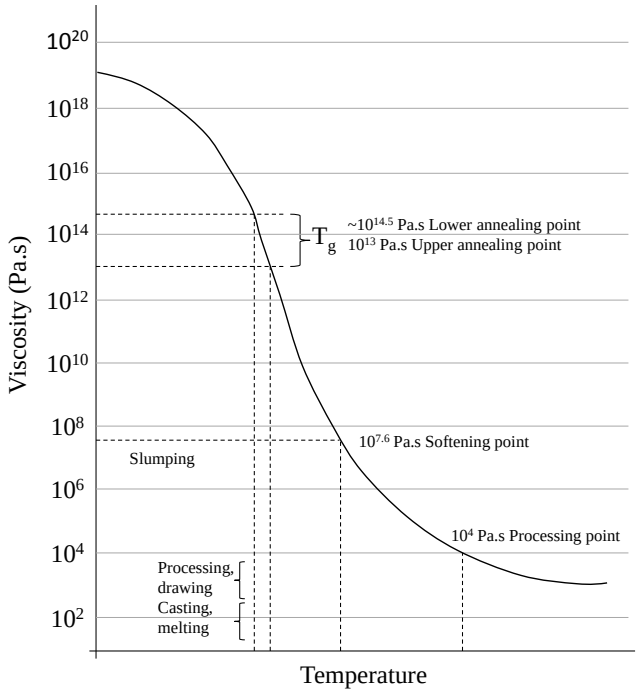

Figure 3.2 General glass viscosity course as a function of temperature, redrawn from Schott Optical Glass Catalogue

With the equipment available, and the knowledge that bulk GLS's fibre drawing temperature lies between the T_g and T_x, a reasonable estimate of the fibre drawing temperature of GLS has been realised. As shown in Figure 3.3, a DTA plot of GLS is overlaid with a TMA plot generated from the same glass. The DTA shows a T_g of 544 °C and T_x of 669 °C. The overlaid TMA confirms that T_δ is located between T_g and T_x, but also gives an onset temperature for the deformation of the GLS under a 50 mN static tension. The TMA results in Figure 3.3 were obtained from a sample of 13.85 mm length and 1 x 2.95 mm cross-section, which was clamped into the elongation module and heated to 800 °C at a ramp rate of 10 °C.min^{-1} under a 50 mN static tension. DTA was performed on a 16.4 mg shard of GLS with a ramp rate of 10 °C.min^{-1} and a pre-dwell of 1 hour at 40 °C to allow the DTA to purge with argon, so as not to induce

any oxidation on the GLS sample during heating. This precaution has been employed on all DTA experiments with oxygen reactive materials.

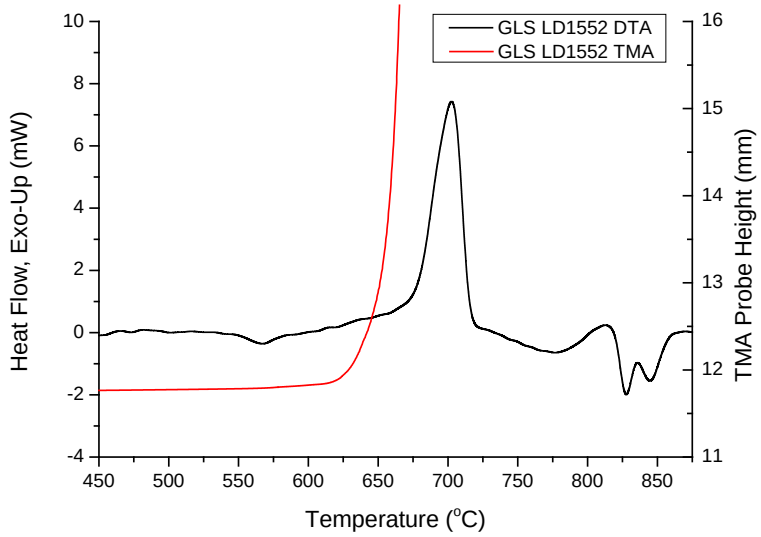

Figure 3.3 DTA of GLS LD1522 (65:35) with TMA tension probe overlay

Although a method to gain an estimated fibre drawing temperature for GLS has been realised, other precautions must be made during the drawing process. Subjecting the GLS fibre preform to temperatures close to T_x may induce the formation of homogeneous nuclei [32], increasing the likelihood of crystallisation during subsequent or prolonged heat treatment. Therefore, when a GLS preform is being drawn into a fibre, one must ensure that minimum time is spent at temperatures near T_x. A table summarising the capabilities of the thermal analysis equipment discussed is displayed below in Table 3.1, which can be used as reference when deciding what material features are to be determined.

Table 3.1 In-house thermal analysis capabilities

TMA	DSC	TGA	DTA
Glass transitions	Crystallisation	Thermal degradation	Crystallisation
Coeff. of expansion	Glass transitions	Absorption	Glass transitions
Young's modulus	Boiling point	Adsorption	Atmospheric stability
Creep	Thermal stability	Desorption	Thermal stability
Stress relaxation			
Tensile properties			
Softening point			

3.3 Visible and Infrared Spectroscopy

Chalcogenide glasses are amongst the few materials that possess the ability to transmit well in the infrared and are able to be formed into high quality optical components. Usually, an optical component is chosen based on the composition of which it is made. One of the main attributes being the optical loss at wavelengths of interest, therefore a material that can transmit with minimal losses over a wide range of wavelengths is especially sought-after. This is because it can be utilised for many applications operating at various wavelengths, as opposed to a component designed for use within just a narrow bandwidth. In order to produce a visual graph showing absorption as a function of wavelength of a particular glass sample, a spectrometer is used. Two separate devices are necessary to cover the entire transparency window of GLS: an FTIR and a UV-Vis-NIR spectrometer. Detailed procedures of how to produce absorption plots are described in the following subchapter for future reference.

A Varian 670-IR FTIR spectrometer is used in conjunction with Resolutions Pro software to generate absorption plots with a range capable of spanning from 1.6 – 25 μm by means of a heated ceramic infrared source. A 'deuterated L-alanine doped triglycene sulphate' detector is installed in the FTIR, which has a spectral range of 0.8 – 28 μm, covering the entire infrared signal output. Within the 'method editor' of Resolutions Pro, 99 scans are set for both sample and background, so that sufficient amounts of scans are averaged for an accurate result. The resolution, which is defined as the smallest wavelength separation for which two distinct spectral lines of equal intensity can be distinguished, is set to 8 cm^{-1}. Spectral resolution helps distinguish closely spaced absorption peaks and is commonly set to 8 cm^{-1} or 4 cm^{-1} for solid samples. The scan speed is typically set based on the detector type, which has been 0.32 $cm.s^{-1}$ in all measurements reported in this thesis. The scan-type is set to 'absorbance', the values for which are simply converted from transmission data, using Equation 3.2.

$$Absorbance\ (cm^{-1}) = \log\frac{100}{\%Transmittance} = -\log Transmittance \qquad (3.2)$$

The transmittance is a percentage of the light received by the detector, where 100% would indicate the same intensity as was recorded in the background scan. Absorbance data is not corrected for sample thickness; however, there is a relatively simple solution when attaining the absorption of bulk GLS samples. This can be achieved by creating multiple samples of the same glass composition, but of various thicknesses and polishing them identically. If three samples of various thicknesses are made, the following procedure will generate results that have proved to produce reliable data. A background scan is taken with the thin sample held in the sample holder, and then subsequent sample scans are taken with the medium, then thick thickness

sample held in the sample holder. A background scan is then taken with the medium thickness sample in the sample holder and lastly, a sample scan with the thick sample held in the sample holder. This produces three plots, which when corrected for thickness, should be near identical. The experiment should be repeated multiple times to ensure results are consistent. To correct the absorption for thickness, the data-sets are simply divided through by the effective sample thickness in cm (difference in thickness between the two samples under evaluation). This method includes the benefit of correcting for sample surface reflections, assuming that samples are polished and are positioned in the sample holder identically.

Before absorption measurements are commenced, a few precautions must be taken into account. Before any FTIR analysis, a signal monitor scan is started and a response signal higher than 7 V should be seen with an empty sample holder in place. If the signal is significantly lower than this, one should consider either using a sample holder with a larger aperture, or increasing the beam attenuator throughput. If the analyte cannot be positioned in a larger aperture sample holder or there is still a low signal after increasing the beam attenuator throughput, a 'power boost' can be applied. An essential feature to include in any FTIR measurement is an inert gas purge. Dry nitrogen has been used to purge the entire FTIR system and sample compartment throughout this work, and Figure 3.4 demonstrates how much noise from atmospheric absorption is reduced by doing so. There are four distinct absorbing regions evident on the non-purged plot; gas-phase moisture is causing absorption at 2.8 and 5.5 – 7.5 µm and CO_2 gas is causing absorption at both 4.2 and 15 µm.

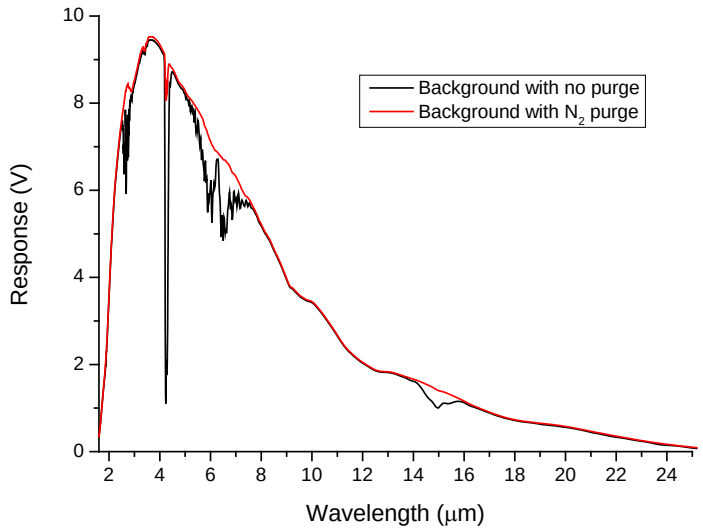

Figure 3.4 FTIR scans with and without a dry nitrogen purge

To extend an absorption plot down to lower wavelengths and reach bulk GLS's electronic absorption edge, a Varian Cary 500 Scan UV-Vis-NIR spectrometer has been used running Varian Win Scan Application software. A wavelength span capability of 175 nm – 3.3 μm is made available on this spectrometer with three light sources (tungsten, deuterium and optical mercury) and a combination of a photomultiplier tube detector and lead sulfide detector for short and long wavelengths respectively. The wavelengths at which the detectors and light sources switch can be slightly modified within the software so that a change is not made at a wavelength where an analyte absorption feature is expected to be. When the detector or light source do switch, a small error is produced in the absorption plot, which is often not fully corrected by the background scan. Within the setup of the Varian Win Scan Application software, absorptivity mode is selected, which plots data in the form of absorption, using Equation 3.2 alongside collected transmission data. The scan kinetics that have proven to create accurate results are a 0.1 s average time, 1 nm data interval and a 600 $nm.min^{-1}$ scan rate. The average time represents the number of chopper cycles the spectrophotometer averages the collected signal over; one chopper cycle is 0.033 s, so an averaging time of 0.1 s results in the scan data point being the average of three readings from the detector. The data interval sets the increment of the wavelength step between each data point and the scan rate sets the rate at which the spectrometer scans the wavelength range. A spectral bandwidth (SBW) of 2 nm is used in conjunction with the double beam mode, which allows for a sample and reference to be analysed simultaneously. The SBW affects both the signal-to-noise ratio and the spectral resolution of the instrument. A large SBW will irradiate the sample with several wavelengths of light, therefore reducing the ability of the instrument to distinguish peaks, but providing a high light throughput and good signal-to-noise performance. Conversely, a small SBW will allow the instrument to resolve peaks that are close together, but will reduce the amount of light reaching the detector, creating a weaker signal to the detector. The 'zero/baseline correction' is used so that both a 100 % transmission baseline correction and a zero line correction are applied to the sample scan.

A similar approach to the FTIR method is used once the set-up has been finished, with the main difference being that reference and sample scans are taken concurrently. The aforementioned thin and medium thickness samples are held in the reference and sample holders respectively and an absorption plot is created. This is repeated with the thick sample in the sample holder, and lastly with the medium sample in the reference position and thick sample in the sample holder. A zero/baseline correction is performed before each scan, to produce a reliable result. The resultant data-sets are corrected for thickness by dividing through by the effective sample thickness, duplicating the method used to correct the FTIR data-sets for thickness. The three

resulting absorption plots should be near identical and the experiment should be repeated if this is not the case.

Before beginning analysis on the UV-Vis-NIR, alignment must be performed and time should be spent making sure the sample holders are well aligned with the light source, for maximum signal efficiency. Furthermore, once the background steps have been completed, it is important to 'zero' the instrument, within the Varian software, so data collected is not offset at all. It is also recommended by the manufacturer that the apparatus be allowed to warm up for 2 hours prior to use for optimum performance.

The absorption plots obtained through use of both instruments are created with an assumption that the incident light upon the samples is exactly perpendicular. This assumption ensures that no complex angular reflectance corrections have to be employed. It is therefore very important to ensure that samples are held in the sample holders securely and that the face of the sample is in good contact with the face of the sample holder.

An experiment to assess measurement repeatability has been conducted on both instruments. The absorption of 1 mm thick polished samples of GLS (LD1625) were measured five times over on both instruments, whereby a separate background was taken before each individual scan to ensure individuality between measurements. A single GLS sample was measured with the FTIR for both background and sample measurements, whilst two identical samples were used in the UV-Vis-NIR; one positioned in each of the sample and reference holders. Each absorption plot should ideally show a zero reading across the entire wavelength range, but it was revealed that there is a small uncertainty error over repeated experiments. A standard deviation of the five measurements taken from both instruments is plotted in Figure 3.5 and Figure 3.6. This demonstration of accuracy for both devices has revealed that each can generate repeatable results down to around 0.5 $dB.m^{-1}$ and 0.005 $dB.m^{-1}$ on the FTIR and UV-Vis-NIR respectively. The higher deviation peaks visible in the UV-Vis-NIR plot are likely due to gas absorbing species and the increase in deviation towards the higher wavelengths can be attributable to heat noise from the instrument itself. The U-shape created by the FTIR standard deviation plot is due to lower detector sensitivity towards the limits of the detector wavelength range.

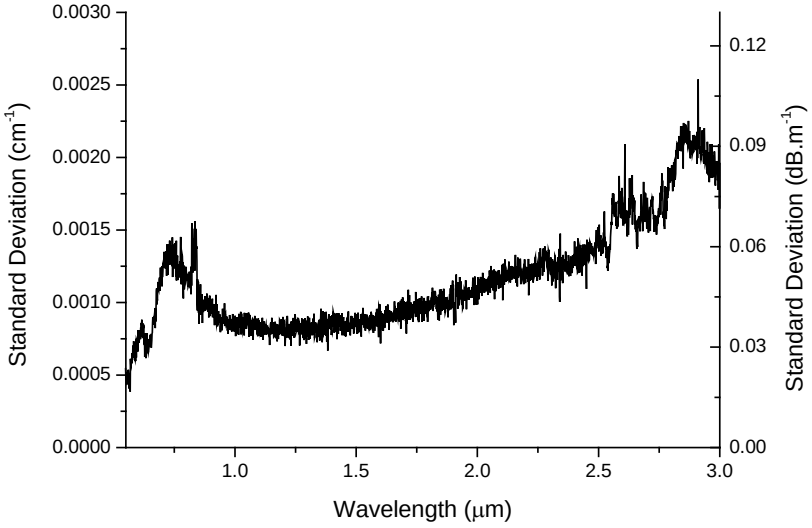

Figure 3.5 Standard deviation of absorption through 1 mm thick GLS samples (LD1625), measured with the UV-Vis-NIR spectrometer

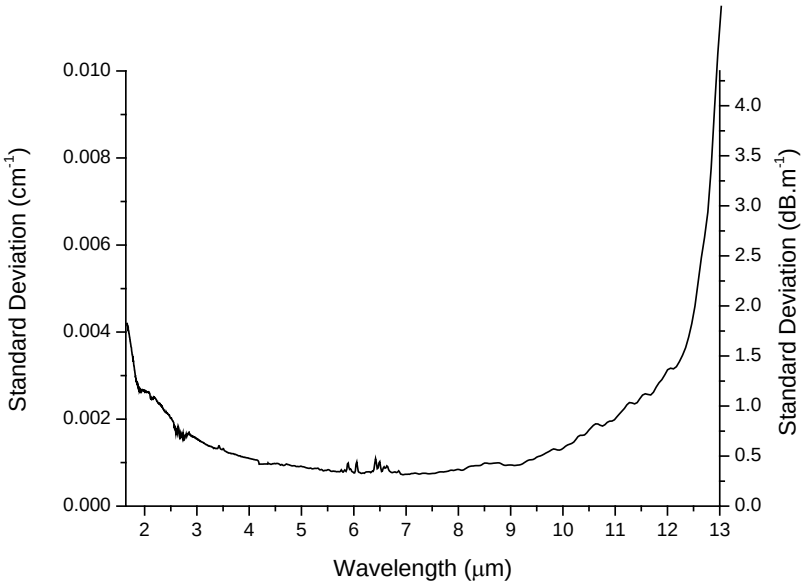

Figure 3.6 Standard deviation of absorption through 1mm thick GLS sample (LD1625), measured with the FTIR spectrometer

3.4 A Thermal and Optical Study of GLS

GLS is a chalcogenide glass recognised for its valuable optical and thermal properties. It is an ideal candidate to supersede arsenic-based fibre technology due to its lower toxicity (no arsenic content), greater hardness, higher thermal stability (T_g over 500 °C), lower thermal expansion ($10x10^{-6}$ K^{-1}), lower solubility and higher laser damage threshold. That said, arsenic-based

chalcogenide fibre technology is very mature and state of the art mid-infrared transmitting fibres available to the market are predominantly of this composition. Recent advances in these types of fibres and glass composition have already found applications in commercially available thermal imaging equipment [33, 34]. Upon further refinement, arsenic-based chalcogenides are predicted to find applications within more compact and sensitive infrared optical sensors for medical, biological and industrial applications. However, like many glasses, current GLS fibre technology is limited by its relatively high optical loss, and this is predominantly due to impurities introduced by the bulk glass fabrication process or inherent in the raw materials. Arsenic-based glasses are manufactured using a sealed ampoule technique [35] with extremely high purity raw materials and melted under a vacuum, after which they can be distilled without any compositional change occurring. On the other hand, La_2S_3, which is used to manufacture bulk GLS, contains some impurities (namely co-lanthanides and transition metals) that are extremely difficult to separate from the raw material. Although arsenic-based optical fibres have been fabricated that show very low losses [36-40], GLS-based optical fibre has been predicted to be able to host comparable losses [41]. However, the study reported in this subchapter does not focus on ultrahigh purity glass for passive applications, but rather concentrates on a wider picture. In order to apply GLS in practical applications, a study of the entire glass-forming region has been carried out to understand how this glass changes in terms of performance through variation of its stoichiometry.

Raw materials stored in a dry nitrogen purged glovebox; 4N Ga_2S_3, purchased from Great Western Inorganics and 3N La_2S_3, purchased from Testbourne Ltd., were batched using scales with an accuracy of 0.5 mg and mixed on a roller for 1 hour. The homogenously mixed powders of 18 g batches were then transferred into small vitreous carbon crucibles and melted for 24 hours at 1150 °C whilst under an argon purge. The glasses were annealed at 490 °C for 24 hours, before slowly being cooled to room temperature. Each glass sample was then cut into 15 mm diameter discs of various thicknesses and optically polished by Crystran Ltd. with ethanediol-suspended diamond particles, ready for characterisation, as shown in Figure 3.7. Small cubes were also cut in-house (Figure 3.8) using a precision dicing saw for TMA measurements (due to not having GLS canes readily available) and the remaining GLS was used for TG/DTA.

Figure 3.7 15 mm diameter polished GLS discs

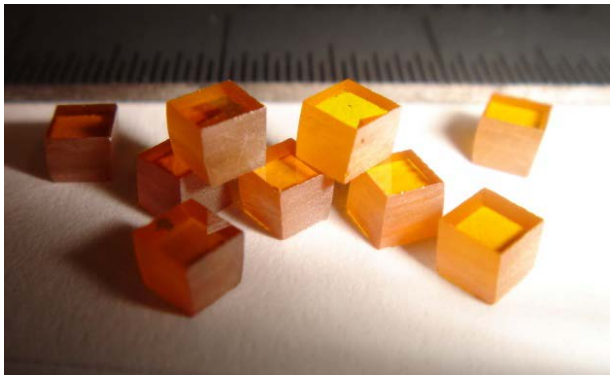

Figure 3.8 Small GLS cubes cut in-house for use on TMA

To determine the various GLS sample transparency regions and absorption as a function of wavelength, two optical spectrometers were used (UV-Vis-NIR and FTIR) to gain a wavelength range from 175 nm - beyond 15 µm, comfortably covering the entire GLS transparency range. Procedures on both pieces of equipment were carried out under an absorption mode in the relevant software and corrected for thickness as described in the previous subchapter. Reflection was taken into account by using identically polished thinner samples as reference in the dual beam UV-Vis-NIR, and as background in FTIR measurements. A purge of dry nitrogen gas was used during FTIR measurements to reduce noise from atmospheric absorption in the sample chamber.

From the plots shown in Figure 3.9, Figure 3.10 and Figure 3.11, it can be seen that 60:40 GLS has the widest transparency window, although all glasses are somewhat comparable. 45:55 GLS shows larger absorption due to the evident phase separation boundaries (Figure 3.12), which cause scattering of incident light. This occurrence is due to the GLS composition lying slightly outside the GLS glass-forming region, reported by Guittard et al. [42]. A phase diagram of the Ga_2S_3 – La_2S_3 system is also sown in Figure 3.13. Clear absorption peaks seen at around 2.9 and 4.7 µm correspond to O-H and Ce^{3+} absorption respectively, which are both inherently contained within the La_2S_3 used in this study.

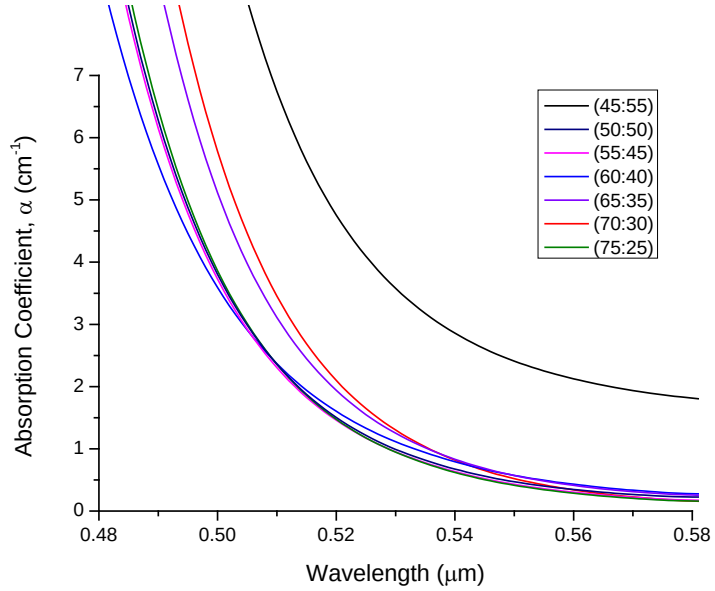

Figure 3.9 Electronic absorption edge of GLS samples, measured with the UV-Vis-NIR spectrometer

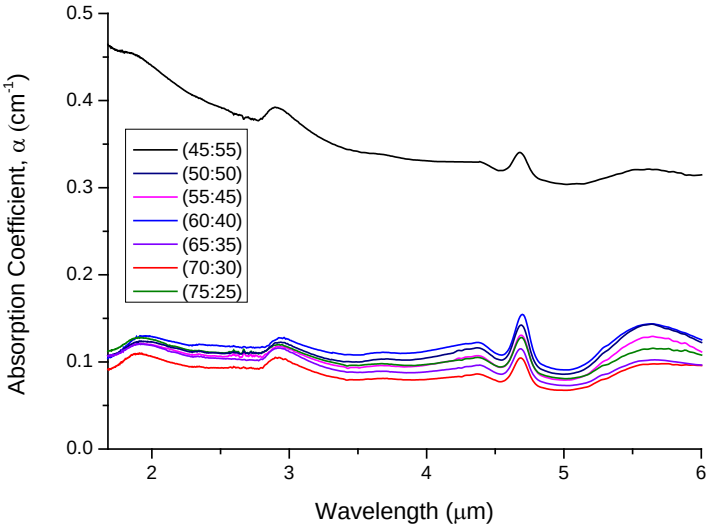

Figure 3.10 Evident absorption peaks in transmission region of GLS samples, measured with the FTIR spectrometer

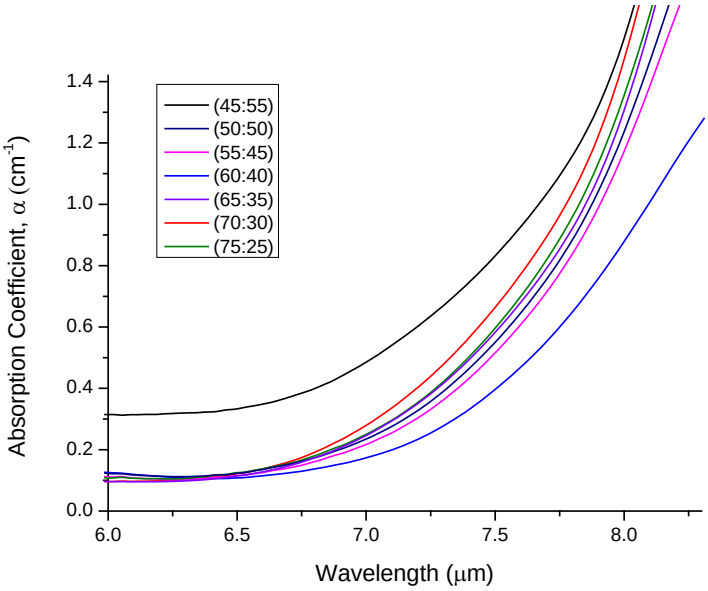

Figure 3.11 Infrared absorption edge of GLS samples, measured with the FTIR spectrometer

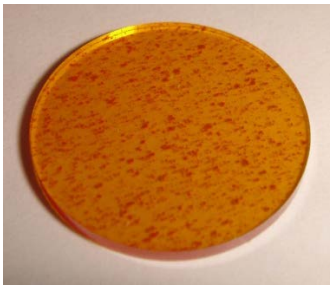

Figure 3.12 Phase-separated 45:55 GLS

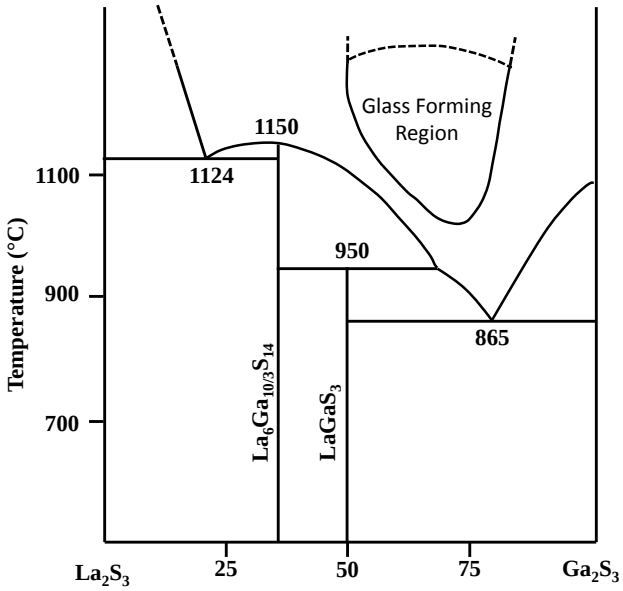

Figure 3.13 Glass-forming region in the Ga_2S_3-La_2S_3 system (Re-draw from Kumta et al. [43])

The refractive index of the GLS series was measured using a Horiba UVISEL 2 Scientific Spectroscopic Ellipsometer and results are summarised in Table 3.2. The refractive index decreases as a function of increasing wavelength, with 60:40 GLS bearing the highest refractive index of 2.51 and 45:55 GLS possessing the lowest index of 2.28, at 0.65 and 2.15 µm respectively. A Perkin Elmer Diamond TG/DTA was used to gain important glass thermal properties: T_g, T_x, T_p, T_m and the onset of weight loss (T_w). All of which are displayed in Table 3.3.

The correlation between these thermal properties provides valuable information that can be used to determine fibre drawing parameters. The coefficient of thermal expansion between 20 and 300 °C ($C.T.E_{(20\text{-}300\ °C)}$) was measured using the TMA in "Penetration – Rectangle" geometry and with the penetration module installed. A "Force Linear Program" was used with a 100 mN static force and 10 °C.min^{-1} temperature scan rate. The results of these measurements are displayed in Table 3.4 along with density of each sample, which was measured by weighing samples of known volume with high accuracy scales that have a µg resolution at room temperature. The Hrubý Parameter is also displayed, indicating the fibre drawing stability of each composition.

Table 3.2 Refractive index of GLS samples measured with spectroscopic ellipsometer

Glass Composition	$n_{(0.65\mu m)}$	$n_{(1.025\mu m)}$	$n_{(1.4\mu m)}$	$n_{(1.775\mu m)}$	$n_{(2.15\mu m)}$
45:55	2.36	2.29	2.28	2.28	2.28
50:50	2.48	2.38	2.37	2.35	2.34
55:45	2.47	2.40	2.39	2.39	2.32
60:40	2.51	2.38	2.36	2.35	2.35
65:35	2.49	2.40	2.38	2.37	2.34
70:30	2.45	2.38	2.37	2.37	2.32
75:25	2.49	2.39	2.38	2.36	2.36

Table 3.3 Thermal properties of GLS samples measured with TG/DTA

Glass Composition	T_g (°C)	T_x (°C)	T_p (°C)	T_m (°C)	T_w (°C)
45:55	527.9	659.0	667.6	816.7	873.9
50:50	584.8	694.3	731.2	839.4	915.9
55:45	583.7	702.7	735.1	839.6	917.7
60:40	607.8	681.2	717.4	885.4	912.0
65:35	563.8	679.2	728.6	829.3	939.7
70:30	553.0	660.3	694.0	815.8	904.4
75:25	571.4	693.7	735.2	839.2	961.2

Table 3.4 Physical properties of GLS samples measured with TG/DTA, TMA and high accuracy scales

Glass Composition	T_x-T_g (°C)	T_p-T_x (°C)	T_m-T_p (°C)	C.T.$E_{(20\text{-}300\ °C)}$ x10^{-6}(K^{-1})	Density (g.cm^{-3})	Hrubý Parameter
45:55	131.1	8.5	149.1	5.27	4.00	0.83
50:50	109.4	36.9	108.2	6.74	4.27	0.75
55:45	118.9	32.4	104.5	6.17	4.34	0.87
60:40	73.4	36.3	168.0	6.86	4.48	0.36
65:35	115.5	49.3	100.7	6.84	4.19	0.77
70:30	107.3	33.7	121.8	6.04	4.11	0.69
75:25	122.3	41.4	104.0	7.30	4.27	0.84

It can be noted that 45:55 GLS and 70:30 GLS possess the lowest thermal onset temperatures, similarly to having lowest refractive index and coefficient of thermal expansion. Whereas 55:45 GLS bears the overall highest thermal onset temperatures. In terms of thermal stability, 65:35 GLS boasts the smallest T_m - T_p and largest T_p - T_x, yet 75:25 GLS retains a second best position in terms of all three temperature difference values. Therefore, potentially concluding that 75:25 GLS is the most suitable composition in terms of fibre drawing stability. The density of the GLS samples closely follows the trends set by thermal analysis, where the lowest

densities are attributable to the lowest thermal onset temperatures, and follows trend to highest values.

GLS has many uses for both active and passive optical devices within the mid-infrared wavelength regime; the most basic use being a mid-infrared transmitting lens. GLS optical fibres are able to transmit light from around 1 – 6 μm and as glass quality improves and impurities diminish, losses may become comparable with the current leader in fibre optic mid-infrared transmission: hollow core fibres [44-55]. Chalcogenide optical fibres have been developed to transmit in the mid-infrared with low losses in the form of hollow core photonic crystal fibres [56]. Following from this development, fibre structures such as a negative curvature hollow core [11, 57, 58] could be the necessary progressive step for GLS optical fibre to become a market-leading product. GLS has extremely high rare earth solubility and can therefore contain high dopant levels owing to efficient emission at specific wavelengths, and this attribute need not be limited to optical fibre. GLS microspheres can be used for micro-resonators [59] and GLS films, which can be made from sputtering [60], pulsed laser deposition [61] or spin-coating [62] are used in devices such as integrated optics [63] and phase-change memory [64] devices. The use of GLS has evolved in recent years from a simple mid-infrared transmitting bulk glass, to the versatile material we know today, which makes a reliable foundation for many optical devices.

The thermal and optical properties of bulk GLS glass have been measured and individually discussed. This adaptable glass composition can be tailored to the user's desire in terms of optical and thermal performance and can be used in many device applications. Although not too many trends can be seen in terms of low to high La_2S_3 content, considerable differences between the series of glass compositions has been summarised in the form of tables and graphs that can be used as reference when determining which GLS ratio is most suitable for the user's desired application.

3.5 Conclusion

Thermal analysis equipment available in-house has been discussed and the individual capabilities have been outlined. The equipment has been used to gain useful information regarding fibre drawing and will continue to provide analysis throughout in-house glass development. Absorption plots as a function of wavelength for GLS samples of various thicknesses have been created and the method of doing so has been described in detail. This method has been established to produce reliable results, which can be applied to various other samples with little modification in procedure. A comprehensive thermal and optical study of GLS has been completed, which has offered a useful reference of GLS stoichiometry for

particular device applications, where specific glass properties are required. The composition of GLS currently used in fibre drawing trials is 65:35; however, 75:25 will be adopted as a possible composition to supersede 65:35, due to its thermal stability characteristics.

Characterisation of any new material prior to device fabrication is a necessary procedure to ensure that it is fully compatible with the processing technique and final device form. Having completed characterisation on a bulk material that has not been used for a particular application before; a safeguard has effectively been put in place, which creates boundaries on the material capabilities.

Chapter 4: **Fibre drawing**

4.1 Introduction

The art of fibre drawing has come a long way since Rene de Reaumur's achievement of making spun glass in 1713 [65] and Charles Vernon Boys' ingenious method of making quartz fibre with the use of a pine crossbow and an arrow of straw, simply attached to a small fragment of molten quartz with sealing-wax [66]. The most advanced fibre drawing towers in the world are dedicated to manufacturing extremely low loss optical fibre at the rate of 2 $km.min^{-1}$. These mass-production dedicated towers are adorned with copious amounts of sensors and data-logging equipment and can run up to 24 hours a day to meet the high demand of optical communication links throughout the globe.

These highly developed systems, which draw fibre at up to 2 $km.min^{-1}$ and stand 40 m tall are devoted to manufacturing only a few, extremely well-refined, telecommunication fibre designs. However, a much more simplistic approach has been adopted for the design of 'Novel Glass Tower II', which has been used throughout the course of the work reported in this thesis. The design and operation of Novel Glass Tower II is discussed in detail and accompanied by a standard operating procedure found in Appendix E.

Over three hundred fibre draws have been achieved throughout the work mentioned in this thesis, a list of which is presented in Appendix F. Details of each individual draw are recorded, which include details of preform, furnace set-up, draw conditions and results. Due to the difficulty of drawing GLS into fibre, a review of the headway made to date is outlined along with the understanding behind the fibre drawing process.

A feasibility trial to produce metal-core fibre has achieved a result sufficiently positive to attract an industrial funded project, which is discussed in Chapter 6. Here, metal-core fibres with complex cross-sections have been produced and a new preform fabrication process has successfully been developed.

4.2 Novel Glass Tower II Development

At the beginning of the work reported in this thesis, a blank canvas was offered in terms of a stripped-back fibre drawing tower structure. In place was the tower frame, with preform feed and fibre take-up units installed. Along with these key parts, a medium frequency generator and remote head were pre-installed with a fibre diameter gauge and cane puller. This left the tower with no furnace, and most noteworthy, without the abundance of sensors, guides and pulleys

that encumber not only industrial fibre drawing systems, but also the other three fibre drawing towers at the ORC. A picture of the fibre drawing tower in its current configuration is shown in Figure 4.1.

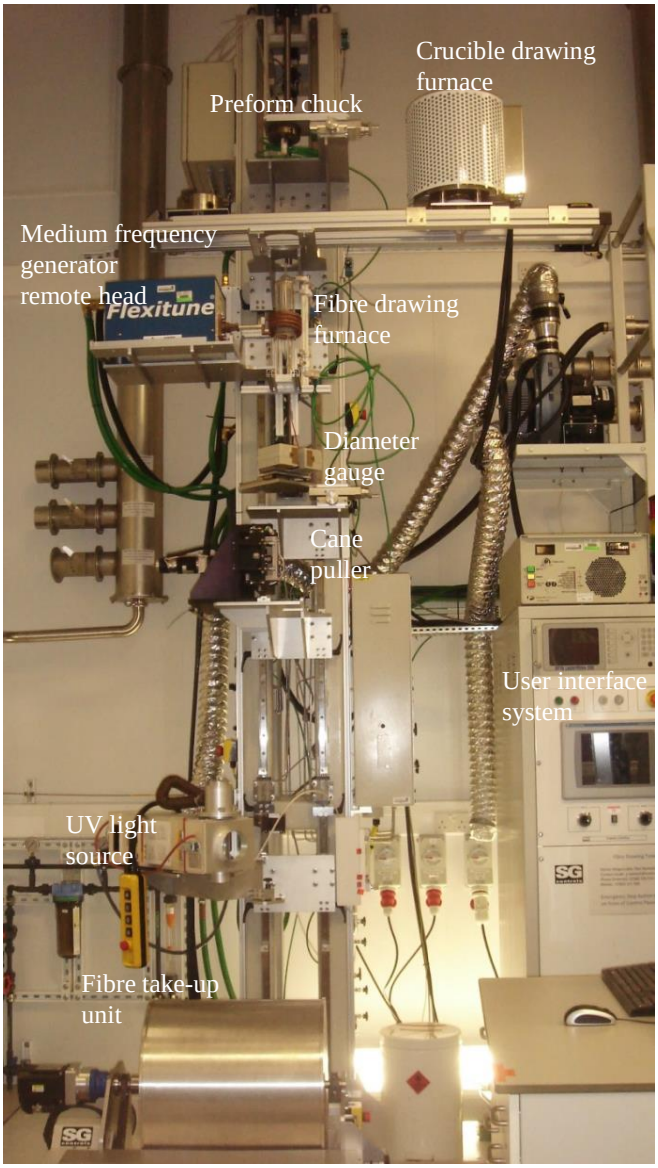

Figure 4.1 Current configuration of Novel Glass Tower II

In this work, a fibre drawing furnace was designed to be modified with ease and to accommodate preforms of a variety of shapes and sizes. Not only this, but the furnace can have a complete over-haul in terms of configuration within just a few minutes. Existing systems for drawing soft glasses are usually single-operational and are not designed to be modified a great deal. A furnace body comprised entirely of silica has been designed (an example of one configuration is depicted in Figure 4.2) and has continually been remodelled and developed throughout the course of the fibre drawing reported here. The susceptor (heating element), which is held within the fibre drawing furnace, is a ring made out of either grade 303 stainless

steel, Inconel or graphite. The medium frequency generator radiates an automatically tuned frequency of around 25 kHz through a water-cooled copper coil that encloses the fibre drawing furnace. A current of around 200 A is alternated through the coil, which produces a reversing magnetic field. Placing a conducting object (susceptor) within the alternating magnetic field causes the material to heat up due to localised electrical currents (eddy currents), which are created within the susceptor. These eddy currents flow against the susceptors electrical resistance, causing it to heat up. There are many parameters that are automatically controlled and monitored by the medium frequency generator unit, which include the inverter output power, voltage and frequency, the tuning circuit reactive current and power, the coil voltage and current, and the coil/load Q value. A desired temperature is communicated to the medium frequency generator via the user interface. Through feedback from a thermocouple positioned in the core of the susceptor, the required parameters are generated for the coil to radiate the correct degree of magnetic field for the susceptor to reach the input temperature.

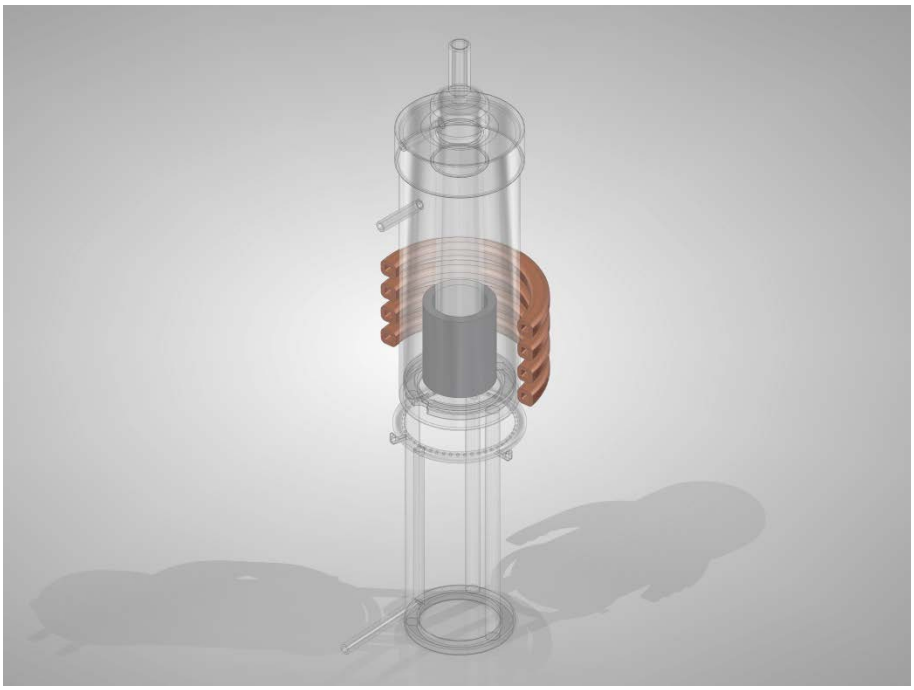

Figure 4.2 40 cm tall fibre drawing furnace with cooling ring, graphite susceptor and copper coil

A change in the coil dimensions in terms of diameter or number of turns has an impact on the coupling efficiency between the coil and susceptor, likewise, changing the susceptor dimensions or material also has an impact on the coupling efficiency. To achieve low temperatures below 500 °C, an inefficient coupling is necessary. This is achieved by using a large diameter coil so that there is a sufficient distance between the susceptor and coil, resulting in less of the magnetic field coupling into the susceptor. On the other hand, to achieve high temperatures and precise temperature control, a high coupling efficiency is required; therefore, a small gap

between the coil and susceptor is necessary. However, the medium frequency generator has an inverter output power limit of 10 kW, which is more than enough power to reach temperatures beyond 2000 °C. The material choice of the susceptor depends mostly on the desired temperature range to be used. The susceptor material 303 stainless steel softens around 1100 °C for example, which makes it unsuitable for drawing the likes of borosilicate that requires a susceptor temperature of around 1200 °C. In this case, a graphite susceptor is more appropriate as long as a sufficient inert gas purge is supplied to engulf the graphite, preventing it from oxidising and consequently degrading. The susceptor shape influences the hot zone (a vertical length within the furnace that possesses the maximum temperature) that the preform is subjected to; a tall susceptor creates a longer hot zone within the furnace and conversely, a short susceptor creates a shorter hot zone. Figure 4.3 and Figure 4.4 illustrates a temperature profile of two graphite susceptors of the same thickness and height but of different diameters. The recorded temperature was achieved by positioning a thermocouple in the centre of the furnace to mimic the conditions of what a preform would be subject to and sweeping from the bottom to the top of the susceptor, with time allowed for temperature readings to settle. The temperature profile is very similar between the two susceptors; however, the larger diameter susceptor has a greater offset between the set temperature and the ‘preform temperature’. This greater offset is simply due to the larger gap between the centre of the furnace and susceptor, allowing more heat to dissipate before radiating into the preform. It can also be noted that the hot zone in the smaller diameter susceptor in Figure 4.3 lies at around 20 mm from the bottom, whereas the larger diameter susceptor in Figure 4.4 is at around 25 mm from the bottom of the susceptor. This difference is contributable to the change in coil between experiments; this was done to gain better temperature control of each respective susceptor. A temperature variation as a function of gas purge rate has also been recorded and concurrently, a significant difference between the core and surface temperature of a preform was discovered. This experiment was carried out by securing a thermocouple in the core of a silica preform that has been partially bored through, and repeating the experiment with the thermocouple tip touching the surface of the preform at the exact same vertical position. The temperatures recorded from this experiment are shown in Figure 4.5 and was repeated three times with duplicate results. The gas purge used in the experiment was argon flowing solely from the preform holder. A 6-turn coil was used with a 25 mm tall 303 stainless steel susceptor with 10 mm thickness and 50 mm outer diameter. When any changes are made to the configuration of the fibre drawing furnace, whether that is a change to the glassware, coil or susceptor, a temperature profile should be created like those in the following figures, as a way of calibrating the furnace.

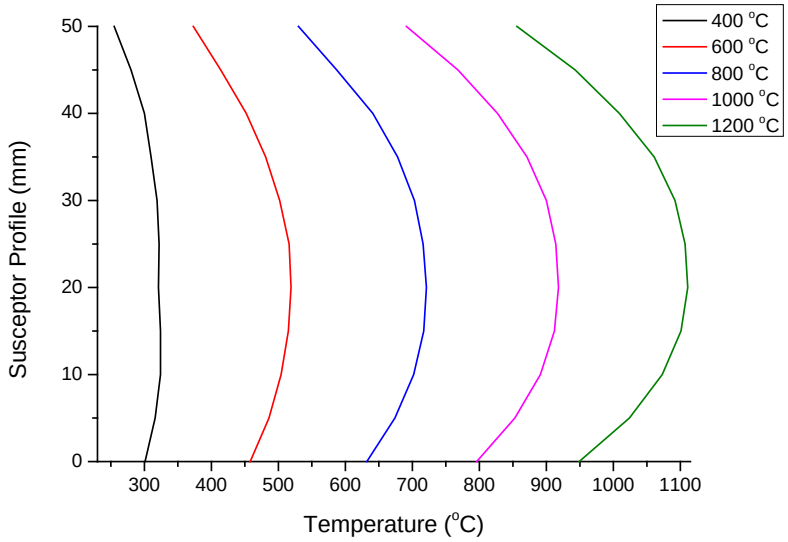

Figure 4.3 Temperature profile of 50 mm tall, 5 mm thick, 40 mm outer diameter graphite susceptor at various set temperatures with 4-turn coil and 4 l.min^{-1} argon purge

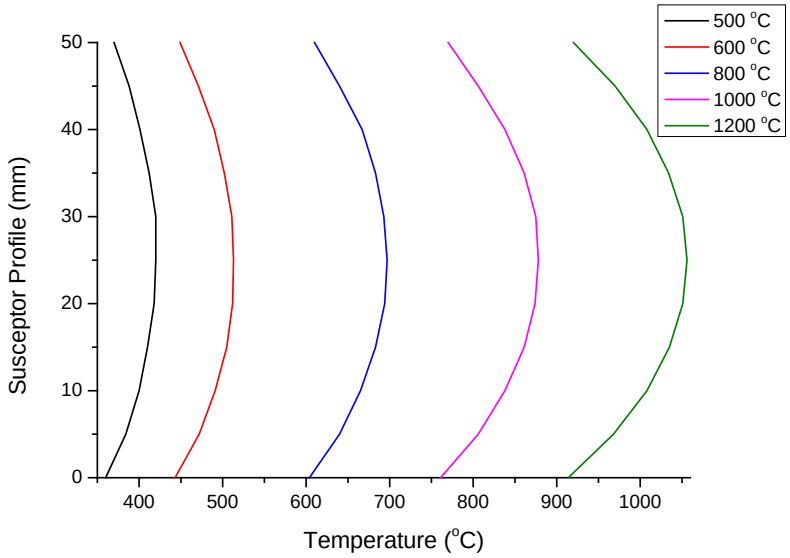

Figure 4.4 Temperature profile of 50 mm tall, 5 mm thick, 60 mm outer diameter graphite susceptor at various set temperatures with 6-turn coil and 4 l.min^{-1} argon purge

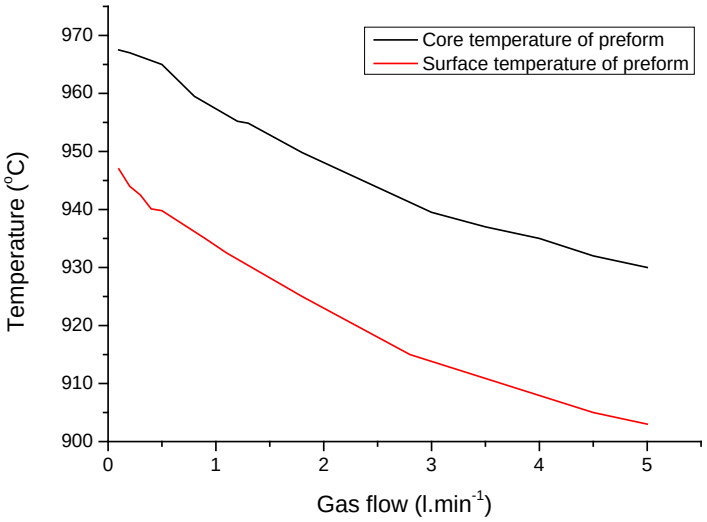

Figure 4.5 Core and surface temperature of 15 mm outer diameter and 2 mm bore diameter silica preform at various argon gas purge flow rates

The current silica furnace design, in the form of engineering diagrams, has been included in Appendix G so that repeatability of furnace building will not become an issue. Figure 4.2 represents the fibre drawing furnace in its most commonly used configuration and a few features can be discussed. It can be seen that there are three 6 mm gas inlets on the furnace extending to the left. These are for three separate gas purge purposes. The top inlet purges the centre of the furnace where the preform is situated, to create an atmosphere suitable for the preform material whilst being subject to its fibre drawing temperature. The middle inlet reaches into the outer concentric chamber where the susceptor is located, to prevent the susceptor material from oxidising at elevated temperatures; typically a 4 $l.min^{-1}$ argon purge. The bottom inlet supplies the gas-cooling ring, which cools the fibre as soon as it exits the furnace for a rapid quench. The gas used for this purpose is usually nitrogen due to its high thermal conductivity compared to the other available gasses (oxygen or argon).

There are five main glass components to the furnace: the stand, cooling ring, furnace body, susceptor holder and furnace cap. The susceptor holder is a somewhat unconventional addition as it creates a separate chamber for the susceptor to the furnace core. Temperature profiles have been performed to confirm that the silica tubing separating the two sections makes no difference to the temperature within the furnace. The separate chambers create a barrier, protecting the preform from any contamination that may occur from drifting particles of graphite, stainless steel or Inconel. Such particles can create crystallisation nuclei, or scattering and absorbing centres in the resultant fibre. The susceptor holder and furnace cap have been made in various sizes to accommodate a number of different susceptor and preform dimensions.

The preform can be held in place using two different techniques, predominantly depending on the size of the preform; either by the use of a silica preform holder (Figure 4.6) or by the chuck that is attached directly to the preform feed platform on the tower. For long preforms of relatively inexpensive material like borosilicate, the preform chuck is used due to its rigidity. An appropriate furnace cap is used so that the preform diameter is only slightly less than the inner diameter of the furnace cap inlet and a similar consideration is used when determining which susceptor and susceptor holder to put in place. Common preform dimensions that have been used for GLS and other novel glasses are around 10 mm in diameter and 100 mm in length. These relatively small glass rods require a preform holder to efficiently hold the rod in the centre of the furnace and create minimal waste; this efficiency aspect is especially important for GLS preforms, which are relatively expensive to manufacture. The preform holder used in this work is made entirely of silica and requires a small amount of nickel-chromium wire, to secure the preform in place. The nickel-chromium wire is fastened around notches cut into the top of the preform (as shown in Figure 4.6) and are threaded through the holes in the bottom of the preform holder to create a secure hold, with minimal contact between glass and metal. Many preform holders consist of a metal chuck, which lock onto the glass preform, and this can be extremely detrimental towards glass that is susceptible to crystallisation. The metal chuck can also act as a susceptor within the furnace and can heat the preform from the top. Due to the large area of contact from the chuck, crystallisation can occur because of this added heat; this was the inspiration behind the current preform holder design. The preform holder is held in place with a Chemcon fitting that allows a gas purge to flow through the inside of the preform holder directly onto the preform.

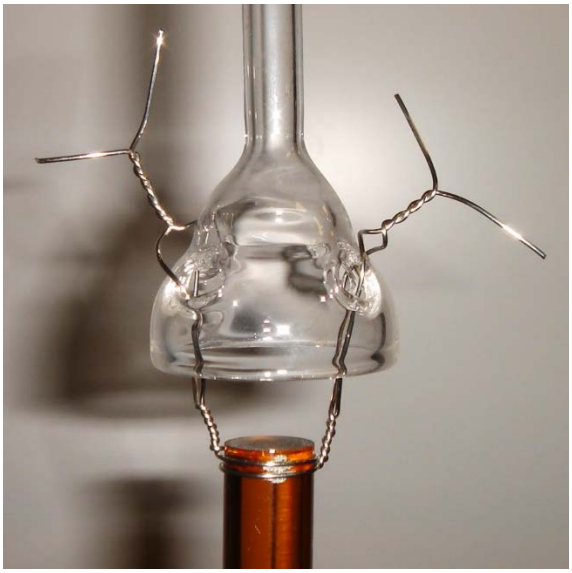

Figure 4.6 GLS preform held in preform holder with nickel-chromium wire

Aside from the furnace, the two principal components of a fibre drawing tower are the feed mechanism and the fibre take-up unit. The diameter of the resultant fibre is controlled through both of these components, which must be in accord to produce fibre of a desired diameter. An increase in take-up speed results in a decrease in fibre diameter and conversely, an increase in feed rate results in a larger diameter fibre being produced. A fibre drawing 'parameter calculator' is attached as Appendix H, where preform dimensions are required as an input and suitable fibre drawing parameters are displayed. The feed mechanism that preforms are attached to can move between 0 and 10 $mm.min^{-1}$, which has been sufficient for all fibre draws to date, however, the take-up drum has been modified to be able to operate up to around 500 $m.min^{-1}$. This modification has been achieved by changing the gearhead from a 28:1 to 16:1 ratio. The motor maximum speed is 5000 rpm, so with a 16:1 gearhead installed, a maximum operating rate of 490 $m.min^{-1}$ can be achieved on the 500 mm diameter take-up drum. This modification can be also be reverted when high speeds are not necessary.

An additional tube furnace, with a longer hot zone, was introduced onto the tower, which is labelled in Figure 4.1, for crucible drawing. This furnace is able to melt a large volume of glass much more efficiently than the fibre drawing furnace, which has a much shorter hot zone length and is limited by the longest induction coil available that only has 6 turns. The tube furnace can be pushed out of position as it sits on runners, which allows for simple transformation between preform and crucible drawing set-ups.

The modular state of Novel Glass Tower II has been discussed and reasoning behind particular configurations has been explained. The tower is currently set up to be able to produce a variety of fibres, but is by no means permanently configured. The modular nature of the tower enables the user to change most features, depending on the preform material or size to be drawn.

4.3 GLS Preform and Fibre Fabrication

GLS has been pursued as the material of choice to produce infrared transmitting fibre due to its availability in high purity form, as detailed in Chapter 2 and properties described in Chapter 3. Brady was also able to draw a significant amount of GLS fibre with varying success, as described in [2], which provided useful knowledge transfer on fibre drawing procedures. Small-core GLS fibre was fabricated by Brady containing losses of around 20 – 30 $dB.m^{-1}$ at 1.5 µm, therefore encouragement for success has been offered in terms of past results. However, before the glass can be drawn into fibre, it must be made into a preform. Preform manufacture of GLS is somewhat unconventional in that it does not follow the trend set by ultralow loss silica fibre preform production. Exceptionally low loss silica preforms are produced by a modified chemical vapour deposition [67] and this technique would be the logical method to create GLS

preforms on first thought. However, there are a few drawbacks associated with creating GLS preforms in this manner, which deems the process currently unfeasible. Firstly, the CVD growth rate of GLS is very low, and secondly, the precursors needed to produce GLS by chemical vapour deposition are extremely expensive to purchase and are currently not available in ultrahigh purity. Furthermore, the coefficient of thermal expansion of GLS is much higher than that of silica, so material cracking may become evident during CVD in a conventional traversing burner set-up due to the frequent heat-cycles.

The principle measurement of quality of an optical fibre is its optical loss per unit-length, typically measured in $dB.m^{-1}$. This parameter is directly influenced by the quality of the fibre preform, although a high quality preform does not necessarily guarantee a low loss fibre. The fibre drawing process of GLS is considered challenging in comparison to many other optical fibre materials. The method used to fabricate GLS fibre reported in this thesis will be discussed along with preform preparation.

The method used to create GLS preforms (shown in Figure 4.7) in this work has been to cut rods from a glass ingot created in-house. Ideally, the GLS preforms would be entirely produced in-house, however, due to lack rod-polishing equipment in hand, a third party, Crystran Ltd., are employed to do so. The method used by Crystran Ltd. is to cut the glass melt into a rectangle cuboid and subsequently roll to an oversize diameter rod. The rod shape is made using 303 silicon carbide grit at first, and a finer grit size is employed to create the final diameter. A three-step diamond polishing process is then used, beginning with an 8 µm grit size and refining to 1 µm and finally a 0.7 µm finish by hand. Around 10 minutes is spent on each grit size as the surface is largely judged by eye, although the finishing stage can take a lot longer. While Crystran Ltd. exercises a procedure that generates relatively repeatable results, there are some drawbacks to having the preforms made by a third party. Firstly, the glass ingot leaves cleanroom conditions and is subject to a harsh environment throughout the rod making process, and secondly, the polishing technician can differ between batches, resulting in slight variations in preform quality. The consistency of preform condition is essential for successful fibre drawing to take place over time. A recipe is currently being refined to produce GLS fibre under optimal conditions and this optimisation process becomes extremely difficult if preform quality varies between fibre draws, as an additional variable is introduced into the fibre draw. Initial GLS fibre draws have proved troublesome due to poor quality preform polishing. Fibre has been drawn, as detailed in fibre drawing run sheets around ‘Run 250 – 260’ (all run-sheets are kept electronically on the Novel Glass and Fibre Group shared drive); however, surface crystallisation was apparent in all of the resultant fibre. It can be seen in Figure 4.8 that there are many inclusions in the surface of the GLS preform and through EDX analysis, the majority of the inclusions were confirmed to be carbon, whilst a small amount of the apparent inclusions

were simply chips made from polishing. The carbon source was established as being diamond polishing residue left behind, due to its particle size. An example of which is shown in Figure 4.9, however these particles proved extremely difficult to fully remove.

Figure 4.7 Polished GLS preforms (LD1552 and LD1554)

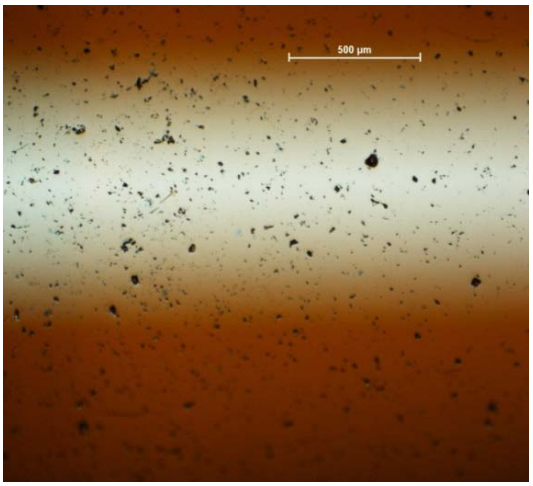

Figure 4.8 Optical microscope image of GLS (LD1554) preform

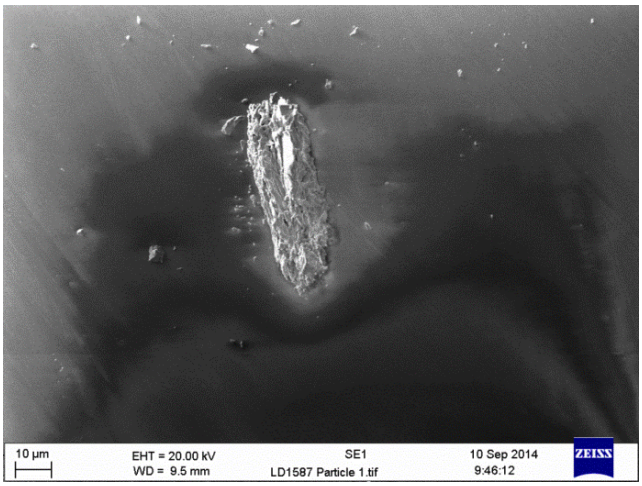

Figure 4.9 SEM image of carbon particle on GLS (LD1554) preform

Sonicating the preforms in various solvents proved ineffective, therefore reactive ion etching was endeavoured in order to target the carbon deposits left on the preforms. The selective etching from this process seemed appropriate so as not to disturb the polished surface of the preforms. A range of recipes were used, however, improved surface quality was not evident on the GLS preforms after reactive ion etching. A thorough literature search revealed only one publication detailing GLS etching; a patent by Itoh et al. [68], which contains a recipe for wet etching GLS of composition 70 mol% Ga_2S_3 : 30 mol% La_2S_3. The potassium hydroxide-based recipe was tried under various conditions, however, only worsened the condition of the preforms. A report [69], was consulted that summarises various GLSO etching trials and details a recipe comprising of fluoroboric, nitric and boric acid, which concluded to have produced improved preform surface quality. Unfortunately, this result was not reproducible; however, this could have been influenced by the lack of La_2O_3 content in present GLS preforms. The surface quality of the GLS preforms used in this work worsens towards the ends of each preform length. However, many of the preforms received from Crystran Ltd. exhibited high quality polishing towards the centre of the preform length. Most recently fabricated preforms have been subjected to an additional polishing step and sonication in a detergent solution, Alconox, in attempt to produce preforms of continuous high quality.

The concentrated effort to create preforms of exceptional surface quality is fully rationalised from evidence of fibre drawing results. Small inclusions or flaws on the preform surface can act as a nucleation centre and initiate crystallisation. This phenomenon became apparent during a substantial amount of GLS fibre draws, the consequence of which resulted in surface crystallisation, pictured in Figure 4.10. These surface crystals act as both scattering centres and a weak point in the fibre length, preventing the fibre from being handled without snapping easily. Most of the GLS fibre drawn to date has been able to wind onto a 0.3 m diameter polystyrene bobbin, however, bending the fibre to a diameter less than this, often results in a snap.

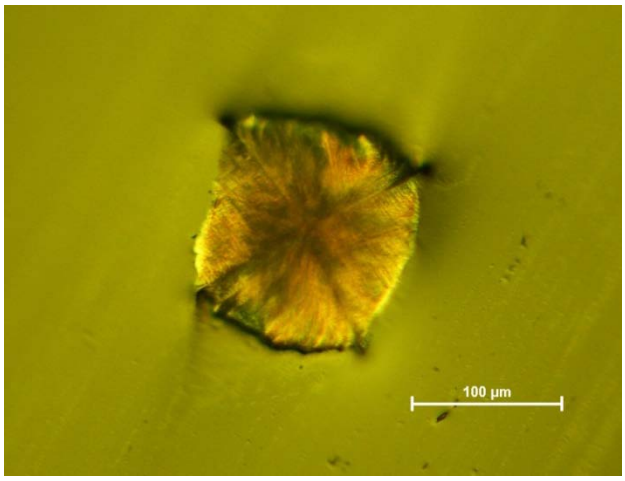

Figure 4.10 Surface crystallisation on GLS fibre, taken with optical microscope

Surface crystallisation is different from bulk crystallisation in that a single crystallite forms without transforming a significant volume of the fibre or preform into a crystalline state. The bulk preform material remains amorphous whilst separate crystallites can spread out along the length of the fibre. It is hypothesised that due to the crystallites large size and relatively small quantity, this suggests a "low rate of nucleation and high growth rate" [70]. The nature of fibre drawing provides an inherently rapid quench rate of the softened glass to room temperature upon exit of the furnace. Therefore subduing further crystallisation and hence preventing bulk crystallisation from occurring, since the glass has been cooled before significant crystal growth. GLS is made from materials with large atoms and weak bond strengths. This is what allows transmission into the infrared, due to the fundamental molecular vibrations lying in the infrared; however, susceptibility to crystallisation is a direct implication of the lack of strong covalent bonds. Network stabilisers can be added into the glass matrix, for example oxides, which are generally resistant to crystallisation [60, 71]. This addition allowed Brady [2] to fabricate GLSO fibre successfully, due to the higher stabilisation properties of the glass. Nevertheless, GLS shows extremely promising initial fibre drawing results, with short lengths of credible fibre already fabricated and with the benefit of having a wider transparency window than that of GLSO. Run 285 produced some good quality 65:35 GLS (LD1642C), which was measured to contain an optical loss of 34.7 $dB.m^{-1}$ at 6.65 µm. This result crudely projects a loss of around 22 $dB.m^{-1}$ between 3 – 5 µm. The fibre loss measurement at 6.65 µm was accomplished using the conventional cutback method and a quantum-cascade laser point source. The projected losses have been estimated by using the LD1625 absorption plot in

Figure 2.5 and fitting the absorption at 6.65 µm to replicate 34.7 $dB.m^{-1}$ and correcting the rest of the plot's data-points.

Most successful GLS fibre draws have been with 8 mm diameter 65:35 GLS preforms and an extended furnace interior, which provides an improved barrier against atmospheric gas entering the furnace. This is because the purge gas is supplied from the top, and effectively pushes atmospheric gas out through the bottom of the furnace. With this configuration, a susceptor temperature of around 800 °C, argon purge of 0.5 $l.min^{-1}$, feed rate of 4 $mm.min^{-1}$ and pull rate of 25 $m.min^{-1}$ is used. However, as previously mentioned, an optimal fibre drawing condition is still to be established.

4.4 Non-Circular Metal-Core Fibre

As part of the work under the EPSRC, a brief feasibility study on the manufacture of various glass-encapsulated metal patterns by means of fibre drawing has been carried out. The motivation behind this project was to manufacture extremely long lengths of a single cross-sectional metal pattern in order to stack-and-draw this pattern into an array, which could sequentially be sliced into metamaterial pattern arrays, much like previously reported work [72-78].

In short, metamaterial patterns are a man-made structure, which responds to light in ways not observed in naturally occurring materials [79]. Arranging particular sub-wavelength metallic shapes into an array on a substrate will cause light to interact with this material in intriguing ways, such as creating a perfectly absorbing surface [80] or a negative refractive index [81]. Metamaterial patterns are commonly fabricated using relatively slow-yielding techniques, for example, focused-ion beam milling, electron-beam lithography or direct laser writing. Of course, with any proven technology worthy of mass production, time becomes a factor of great interest. Faster production techniques have been investigated such as inkjet and laser printing [82, 83], which have gained reputable results. However, fibre drawing is a recognised fabrication method for producing extremely long lengths of multi-material, unidirectional patterns in relatively short timeframes, so was employed as a method for creating such features.

Metal-core glass fibre fabrication was first developed by Taylor in 1924 [5] and has since progressed into a means of fabricating glass-encapsulated microwire, which is used in many applications from connection wires on printed circuit boards to ballistic protection textiles [6]. With inspiration from the “Taylor wire process”, an innovative concept of complex-cross-section glass preform fabrication was developed, which involves the fusing of multiple glass ‘building blocks’. Glass preforms can be formed into a secure structure by simply aligning the building blocks into the desired shape and thermally fusing them into place. A similar process of forming polymer (polysulfone) preforms has been used by Gumennik et al. [7] and Jansen et al.

[84] have reported work on drawing glass fibre with complex cross-section that has also been taken as inspiration for the work described here.

The method firstly involves using a conventional glass-cutting saw to cut glass blocks into various key shapes. Figure 4.11 shows three examples of fused Schott glass preforms, one of which has a metal insert, ready for fibre drawing. Preforms of various assemblies were thermally fused into shape by carefully aligning the individually cut pieces of glass, which can be separately identified in Figure 4.11. The entire assembly is then heated to the glass softening point in an enclosed furnace. This consolidation is a key step to maintaining shape geometry during the fibre draw. The softening point of each glass used was determined from the glass data sheet supplied by Schott Glass Ltd. A generic recipe for fusing the glass preforms was used where the softening point was reached at a ramp rate of 5 °C.min^{-1} and a dwell of 30 minutes was applied before ramping back to room temperature at 20 °C.min^{-1}. A mixed gas purge of high purity nitrogen and oxygen were used throughout fusing, both at 1 l.min^{-1}. In order to stop the glass preforms from sticking to the flat silica substrates on which they were fused, a layer of carbon paper was kept between the silica and Schott glass.

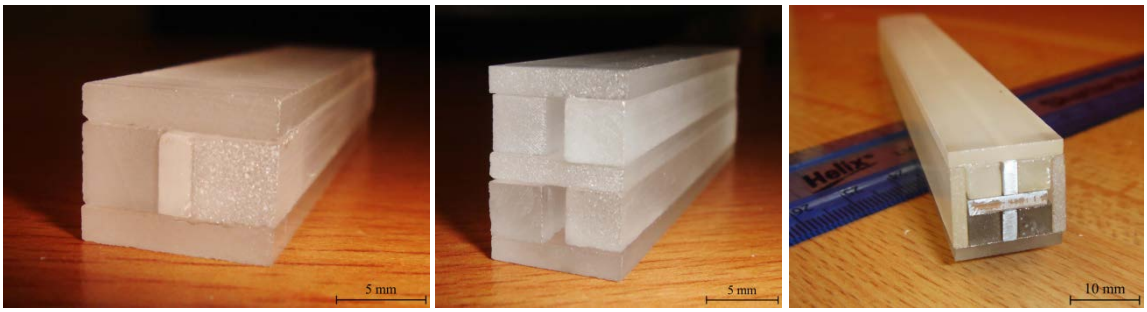

Figure 4.11 Fused Schott glass preforms. Left: single-core LLF2 glass with sealed end. Middle: double-core LLF2 glass. Right: cross-shaped core F2 glass with aluminium sheet insert

Traditional methods of fabricating complex preform structures involves ultrasonic milling and drilling of bulk glass, or extrusion of glass using complex dies. These approaches are expensive, time consuming, shape limited and for some materials can be temperature limited. The building block method described is extremely versatile and quick in comparison. By starting with a few basic glass shapes, many designs can be built up and simply fused together in a matter of hours.

The metals and glasses used in this study were chosen on a basis of their thermal properties, ensuring the glass working temperature was sufficiently higher than the metals melting temperature. The high thermal expansion of the metal (22.2, 23.4 and 29.7 x10^{-6} K^{-1} for aluminium, tin and zinc respectively) proved beneficial in reducing the air gaps between the metal and glass interface of the fibre. At high temperature, the metal has expanded, creating a

smooth surface between it and the softened glass. Upon cooling, the soft glass contracts with the metal, with surface tension ensuring the two materials hold together. The glass is still soft after the metal has frozen, therefore it can form around the metal before solidifying itself. However, a fast quench-rate is important to maintain a continuous metallic core. If the metal does not solidify as soon as the preform has been drawn into a fibre, the metal has a tendency to bead due to surface tension, however, if the fibre is cooled fast enough on exit of the furnace, the metal will freeze and maintain continuity. To produce a high quality interface between metal and glass fibre, pre-drawing precautions must be followed, for example, appropriate cleaning of the metal before inserting into the glass preform is necessary. Vigorously wiping the metal with an acetone soaked cloth removes any residual contaminants found on its surface. Glass is wiped clean with citrus degreaser and subsequently cleaned in a sonicated bath of acetone for 30 minutes and rinsed with deionised water, prior to drying in a vacuum oven for 24 hours. These cleaning steps ensure that all cutting wax and fluids are removed. Contaminated glass or metal can cause the evolution of gasses at the glass-metal interface and create weak points along the fibre length, resulting in a fibre snap during drawing or a flawed product. It was also realised that the un-polished, matt surface of the glass pieces are essential for sound fusing to be achieved. Polished samples that have been subject to the same consolidation recipe would not bond together properly. The reason behind the un-polished surfaces bonding more effectively is due to the added surface area, which allows better heat circulation. In an email conversation on the 14th of April 2015, M. Souza explained that the matt surface is full of peaks at the micron level, and these tips of the peaks melt more efficiently. At the softening point, these peaks slump and consolidate, bending and curling as they deform, and the interaction results in a rapid bonding of the glass peaks once surface tension is overcome. A force greater than gravity alone is required to fuse polished samples together of this weight, as the air gap, which remains between the polished surfaces, creates a barrier to the fuse [85].

High purity metal wire is inserted into the glass preform and is molten to fill the entirety of the core; a heat gun is sufficient to melt tin wire into the preform, and a general-purpose chamber furnace is used to melt zinc and aluminium under an inert gas purge. During fibre drawing, a mixed purge gas of oxygen and argon is used and a feed rate of around 1 mm.min^{-1}. The drop temperature of the preform is slowly reached to allow for the molten metal to equilibrate and for thermal expansion to settle.

Schott glasses F2, F5 and LLF2 have been used to successfully fabricate various non-circular metal-glass fibres, each with both tin and zinc cores. Continuity of the metallic core has been confirmed over distances of in excess of 50 m by simply gaining resistance readings through contact of exposed core at the fibre ends. Inspection by optical microscope (Figure 4.12) also confirmed metallic core continuity, high quality glass-metal interface and uniformity. Shape

geometry has been maintained down to tens of microns in diameter, with Figure 4.13 showing some slightly larger examples of this, as cleaving the metal-core fibre for imaging proved troublesome.

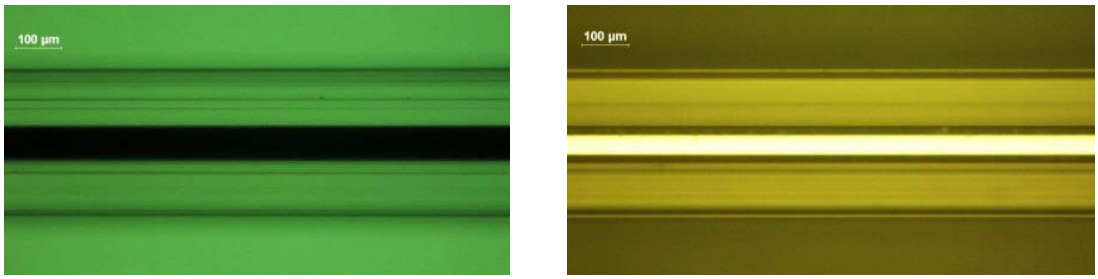

Figure 4.12 Side profile of Schott F2 fibre with zinc core, taken with optical microscope in transmission on left and reflection on right

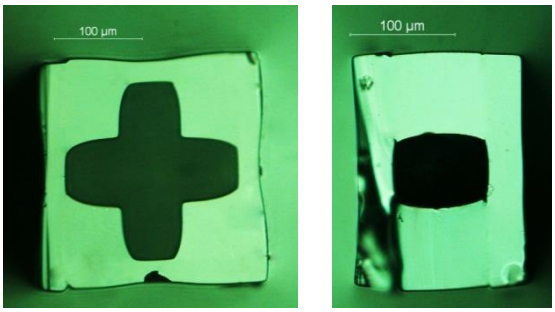

Figure 4.13 Left: Schott LLF2 hollow fibre cross-section. Right: Schott F2 fibre with tin-core cross-section, taken with optical microscope

Extrusion has also been used to produce preforms of the same structure created by the building block fusing method. Extrusion did not yield improved results, but conversely resulted in preforms with moderately rounded corners, bowed longitudinal length and a substantial increase in preform production time. Canes have been fabricated with the intention of stacking and drawing to produce a fibre possessing a cross-sectional array of the metallic shape, similar to that process shown in Figure 4.14. This fibre would then be cleaved into small samples containing the planar metallic feature array. Canes were successfully fused together to create a stacked preform, with capillary force being sufficient to keep the metal confined within the core of the canes. Effective fusing was found to be achieved when the touching surfaces of the canes were slightly ground with emery paper to create a matt finish prior to stacking, however, care must be taken to wipe the ground surface clean with an acetone soaked wipe to ensure all glass debris is removed. Unfortunately, no high calibre fibre was drawn of this design before resources had been exhausted and new projects undertaken.

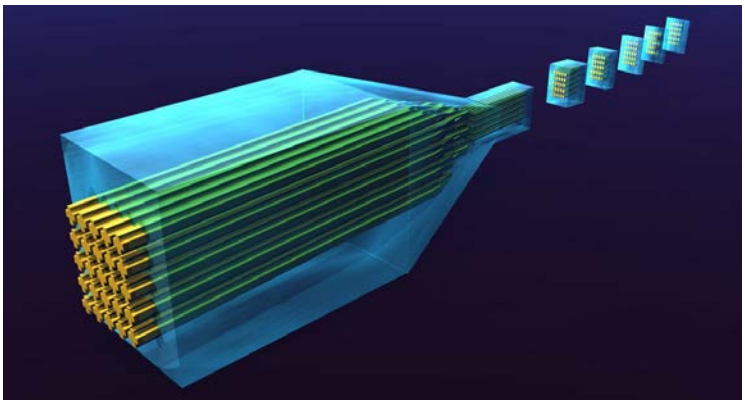

Figure 4.14 Stack and draw of cross shape canes, then cut into metamaterial samples

In addition to the main project aim of fabricating metamaterial patterns through fibre drawing, other potential applications have been realised for the fibres produced. The bending radius of the resultant fibre varies with orientation and shape. For example, rectangular shaped fibres have a dramatic change in bending radius over a 90 ° rotation. Therefore, depending on the orientation of the fibre with respect to the working direction, a variable flexibility can be employed. Textile-based applications can utilise this feature to introduce orientation dependant flexibility. Another application for such glass-metal composite fibres could be the fabrication of extremely high surface area fibre-capacitors. Similar work has been patented by Tuncer et al. [86-88] using a matrix of fibres with an electrically conductive core and insulating cladding. Other work has also been developed to incorporate fibre capacitors into “smart apparel” by weaving directly into fabric during manufacture [89]. Furthermore, ambitious products such as aircraft and building wrappings and embedded wireless communication devices have been reported as a use for fibre-based electrical energy storage devices [90].

A fibre-based capacitor requires multiple fibres with an electrically conductive core and dielectric cladding. The fibres are arranged into a matrix bundle pattern, resulting in two distinguishable sets. The first set of fibres is arranged so that at least one fibre core of the second set is positioned adjacent, to create a capacitance between the first and second set of fibre cores. Separate electrodes contact the two independent sets of fibre cores, so an electric capacitance is generated between the two sets of fibre cores, and between the two separate electrodes. The metal-core fibres produced in the work reported here, can potentially be suited for this application, but have an interesting advantage over published work in this area. The irregular shapes that have been fabricated, particularly the cross-shaped core fibre, enlarges the effective surface area of the metal core, promoting a larger potential capacitance per unit-length of fibre used.

Metal-core fibres have been fabricated from various materials and numerous shapes. Long lengths of fibre have been confirmed to bear a continuous metallic core with excellent glass-

metal interface and uniformity. Conservation of shape geometry has been demonstrated down to tens of microns in cross-sectional diameter, and the stacking of canes to create pattern array preforms has been established. Extrusion of the same glass structures has been demonstrated, however, has been concluded not to benefit the fibre fabrication process.

4.5 Collaborative Fibre Fabrication Projects

Due to the diverse capabilities that have been made available to Novel Glass Tower II, many different types of fibre can be drawn, which has led to the establishment of multiple collaborative fibre fabrication projects. Many small projects have been undertaken throughout the work reported in this thesis, alongside the main goals outlined in Chapter 1. An overview of some of these projects is outlined in the following subchapter, and the progress made for each is discussed.

In collaboration with the 'Advanced Solid State Sources' group at the ORC, the fabrication of neodymium doped silicate (Nd:silicate) fibre for use within a fibre amplifier has made good progress towards the target geometry. An active fibre to be pumped at 808 nm, to produce an amplified signal at 1064 nm is in development, and initial fibre drawing trials have begun. A circular core-clad preform structure has been produced with Nd:silicate glass, and refinement of the core-clad interface within the fibre is still underway. To determine the glass working temperature range of the Nd:silicate, DTA has been used. With the obtained thermal information, successful caning has been achieved, which has allowed for the next fabrication step of rod-in-tube drawing taking place. Clad preforms have been made by ultrasonic drilling silicate rods to create tubes. A series of hydrofluoric acid etching trials have been used to enhance the surface quality of the interior bore, which has improved the core-clad interface of the fibre. Various cane and fibre draws have been accomplished under a variety of vacuum strengths, to refine the drawing conditions, however, small air gaps between the core and clad materials are still evident in the resultant fibre. In parallel to this work, for the same application, Schott borosilicate BK7 is being fabricated into a planar waveguide, with final dimensions similar to that of a cane; around 100 – 200 μm width. A three layer planar structure of around 10 x 10 x 50 mm is fused together to create a preform, similar to the work described in the previous subchapter. The preform consists of three layers: Schott BK7 – Nd:BK7 – BK7, and once fused, the preform is caned to produce a waveguide with a 100 – 200 μm width. Fusing trials are still ongoing but promising initial results provide confidence for success.

Training on Novel Glass Tower II and relevant glass characterisation equipment has been provided for two visiting researchers from Nanyang Technological University (NTU), Singapore. As well as providing training, fibre drawing projects were also started with the

visitors, and initial results have made headway for continuation at NTU, with similar fibre drawing facilities. Two separate projects were undertaken in collaboration with the visiting researchers: the fabrication of active lead-gallium-bismuth (PGB) glass fibre for nonlinear applications, and speciality nanofibre fabrication.

PGB is an infrared transmitting material similar to GLS, which offers high nonlinearity and high thermal stability. With nonlinearities two orders of magnitude higher than that of fluoride-based fibres [91], PGB offers great prospect as an active fibre within the mid-infrared wavelength regime. Although the fabrication process of PGB is relatively immature, the design and demonstration of PGB optical fibre fabrication has been achieved. Fabrication steps from glass melting, through preform fabrication to fibre drawing is detailed in a conference paper written by Tse et al., 2014 [91], which includes results of both passive and active PGB fibre.

A novel technique of creating preforms for the manufacture of glass-embedded nanowires has been developed and results have been published [14, 92, 93]. By simply cutting a Schott oxide glass preform longitudinally in half and consequentially polishing the exposed facets, a planar surface is exposed on which patterns can be deposited. Deposition begins with photolithography, to create a mask, and sputtering is then used to deposit the material pattern. Once the material has been sputtered and mask removed, the two halves of the Scott glass preform are fused back together, similar to the technique described in the previous subchapter, and illustrated in Figure 4.15.

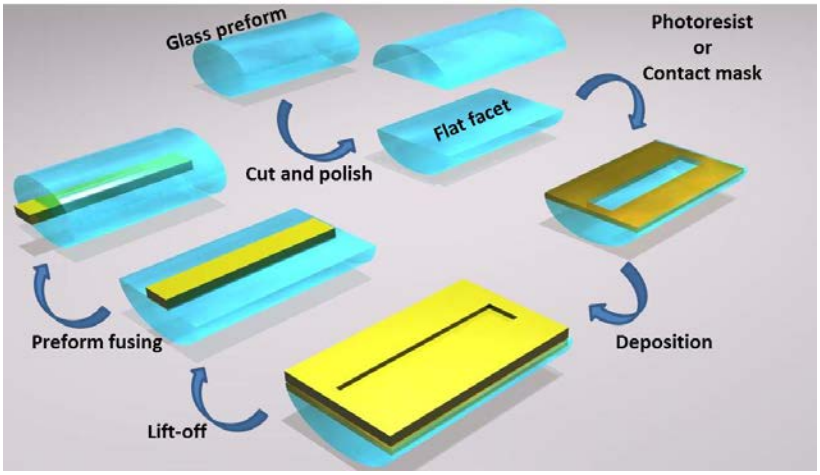

Figure 4.15 Nanofibre preform fabrication method

Materials such as gold have been used as the patterning material, and by exploiting the fact that thin films tend to have a melting point depression, fibre can be drawn at a temperature significantly lower than the bulk, deposited material, melting point. The resultant fibre from this type of preform contains nanowires of the deposited film, as shown in Figure 4.16. The

interaction between these nanowires and an input laser pulse, which is launched into the fibre tip, creates a plasmonic response, as discussed in [14, 92, 93].

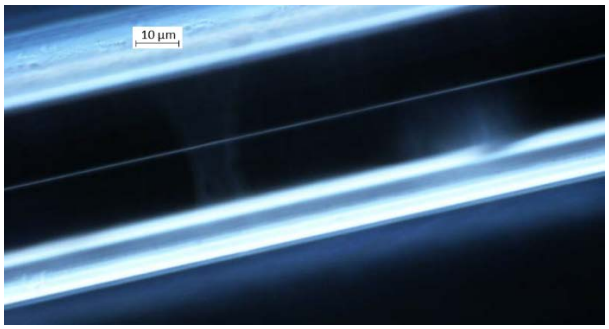

Figure 4.16 Optical microscope image of single gold nanowire concealed in the core of Schott N-SF8 glass fibre

Nanowires are used in various applications other than that already mentioned, including biosensing [94-96], super-capacitor electrodes [97] and nanoscale interconnects [98]. These applications require nanowires that are not glass-encapsulated, but free to be able to manipulate. Upon etching the glass away from the fibres fabricated in-house, nanowires are released, which have an extremely large aspect ratio. Examples of the unconfined gold nanowires are shown in Figure 4.17, which are just a couple-hundred nanometres in diameter. The method used to etch the Schott glass away from the confined nanowires was wet etching. Firstly, a glass slide was completely coated in gold via four separate electron beam physical vapour depositions; this glass slide would then carry the glass-encapsulated nanowires without being attacked by the etchant. Multiple fibres were secured onto the gold-coated slide and then dipped into 10 % hydrofluoric acid for 15 minutes. This etch time was sufficient to remove most of the Schott glass surrounding the gold nanowires; revealing extremely long lengths compared to existing published work, which reports gold nanowire just a few microns in length [99, 100].

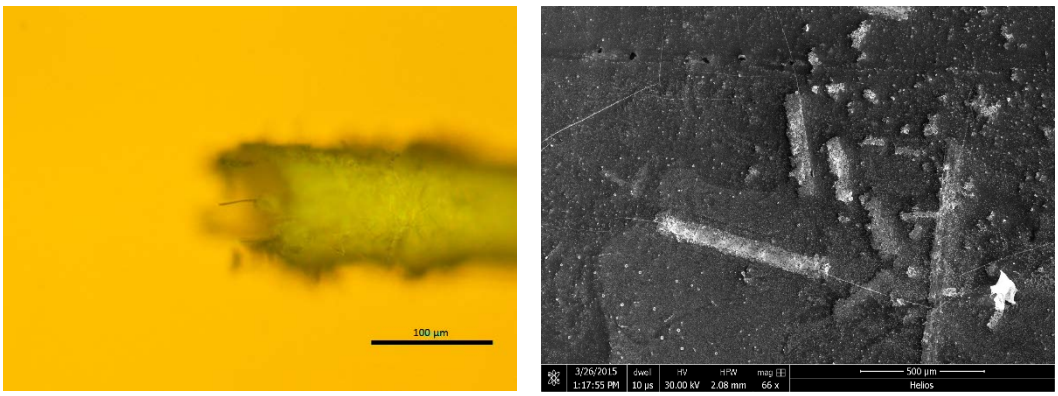

Figure 4.17 SEM images of gold nanowires revealed by wet etching

As well as accomplishing good results with the mentioned planar fabrication technique, the fabrication of chalcogenide nanowire arrays has been instigated, and research using these structures is being undertaken at NTU. The method behind this project was inspired by the work of Yaman et al., 2011 [101] whereby a rod, or cane, of chalcogenide material is inserted into an outer jacket and drawn into fibre. The resultant fibre is then stacked together, inserted into a subsequent outer jacket, and drawn to create microfibres. Upon repeating this process once more, many nanowires are produced, which have extremely interesting applications in flexible sensor platforms, phase-change memory and nonlinear photonics amongst many other things. Work towards creating similar results by using an As_2S_3 core and thermally matched polymer jacket has commenced and the fibre drawing tower furnace has been suitably modified to accommodate such fibre draws. This included the redesign of the induction coil, glassware and susceptor in order to achieve steady low temperatures, which are required for the soft As_2S_3 and polymer cladding material.

In addition to the collaborative projects mentioned, many other short timeframe projects have been carried out with the use of Novel Glass Tower II, which have generated useful results in terms of data and founded relationships between research groups. As a prime example of the benefits associated with collaborative projects, the use of extremely advanced characterisation equipment, not available at the ORC is now accessible through contacts at NTU. This scenario works both ways, for when equipment or facilities at the ORC may be of use to collaborative partners.

4.6 Conclusion

The development of Novel Glass Tower II and reasoning behind individual modifications has been detailed, accompanied by a standard operating procedure found in Appendix E. Although the tower is currently configured to manufacture numerous types of fibre, continued development is ongoing and encouraged. A fibre coating system is currently being installed, with an aspiration to include a spray coating option. This technique would benefit fragile fibre materials that can easily break during conventional fibre coating methods.

Collaborative fibre drawing projects carried out on Novel Glass Tower II have been discussed and the progress made on the particular projects has been described. GLS optical fibre manufacture is underway and will continue to be developed as the principal infrared transmitting optical fibre made on Novel Glass Tower II. Initial results have been promising and further work will be carried out.

Chapter 5: **Industrial Projects**

5.1 Introduction

The research described in this thesis, on the manufacture of novel fibre, has not been applied to the solitary research-driven path towards a publication count. Several industry-led projects have been embarked on, resulting in new collaborations and leading to the discovery of novel fibre fabrication techniques. One example is the fabrication of glass-encapsulated microwire, which has been successfully developed from conceptualisation to market-ready product during a six month project. Furthermore, passive GLS fibre for mid-infrared laser applications is being developed for the use of gas sensing in a collaborative project, FLITES (Fibre-Laser Imaging of Gas Turbine Exhaust Species), involving the University of Manchester, University of Strathclyde, Rolls-Royce and Shell. Shorter termed industrial-based projects are also outlined in the following chapter, where the project goals, results attained and the motivation behind each is described.

5.2 Manufacturing Glass-Encapsulated Microwire

A six month industrial project was taken on with an ultimate objective of manufacturing highly conductive glass-insulated microwire for electrical applications. An ambitious target for the outer diameter of just 23 µm was set with a metallic core diameter of around 4 µm. A pre-insulated, high quality microwire, ready to be used within many applications including micro-circuitry and composite textiles has been consequentially produced.

Funding for this short-term project was secured following successful proof of principle fabrication of non-circular metal-core fibre as discussed in Chapter 4. However, a different approach was necessary for the project at hand. Metals that suit the condition of high conductivity possess much higher working temperatures, compared to the materials used within the non-circular metal-core fibre project. Modifications of the fibre drawing tower itself were also needed because the furnace temperature and fibre take-up speed did not meet requirements for producing such small diameter fibre from the necessary materials.

To meet the objective of making a highly conductive microwire, a suitable metal had to be chosen that can be melted below the softening point of the glass cladding, and ideally below the softening point of silica; the material that the fibre drawing furnace is made of. The most conductive metal is well known to be silver, which has an electrical resistivity of 15.87 nΩ.m, closely followed by copper, gold and aluminium that have an electrical resistivity of 16.78,

22.14 and 26.50 nΩ.m respectively. The melting point of these metals range from a modest 660 °C for aluminium, to the more demanding 1085 °C for copper. Previous fibre draws containing low melting point metals had been achieved, therefore aluminium was chosen due to its low melting point, low cost and large availability. Borosilicate was chosen due to it being the material of choice in many previously published metal-core fibre results [5, 6, 17, 102]; Schott Duran borosilicate tubing (81 wt% SiO_2, 13 wt% B_2O_2, 4 wt% Na_2O+K_2O, 2 wt% Al_2O_3) can be bought in bulk with a quick delivery time and a choice of many dimensions, so was devoted to the entirety of the project.

Firstly, Schott Duran borosilicate tubing with an outer diameter of 8.5 mm was used to establish whether fibre could be continuously drawn at such small dimensions without a metal core. With a feed rate of 1 $mm.min^{-1}$, a fibre take-up speed of 160 $m.min^{-1}$ is needed to generate fibre with an outer diameter of 20 µm. This was achieved without difficulty; therefore introducing a metal core to the preform was then investigated. A susceptor temperature of 1200 °C was being used for the borosilicate tubing fibre draws, which was the upper temperature limit of the fibre drawing furnace. This limitation was instated by the software running the fibre drawing tower control system and prevented core materials such as copper from being drawn. Nevertheless, high purity tin was used as a core material and fibre was drawn with an outer diameter of less than 40 µm. The second limitation of the fibre drawing tower was then apparent – a diameter gauge with a lower detection limit of 40 µm. In its place, a Zimmer OHG A/2 High-Temperature Optical Diameter Monitor was installed, used in conjunction with a high accuracy Fluke 45 Dual Display Multimeter to record the output voltage from the Zimmer, which measures a fibre diameter of 0 – 2 mm. Although aluminium is reported to react with the SiO_2 contained within borosilicate glass at high temperatures [102], previous fibre draws containing an aluminium core and Schott F2 glass cladding resulted in short lengths of reasonable quality fibre, which created optimism towards recreating this type of fibre. The best aluminium core fibre results were obtained by bringing the entire preform up to 1000 °C and dwelling for 10 minutes before ramping up to the fibre drawing temperature. As soon as the preform starts to neck, the preform feed is started and the fibre is attached to the take-up drum, which is then taken up to a fast drawing speed. This would yield a reasonable amount of aluminium core fibre (example shown in Figure 5.1), but following multiple trials and not generating improved results, a reconsideration was required. The software controlling the fibre drawing tower was stripped of all its limits, which allowed higher temperatures to be achieved, and a new metal core material was chosen. Copper transpired to be a less costly material to buy in bulk wire form, and hence immediately took position of aluminium as the core material for future fibre draws.

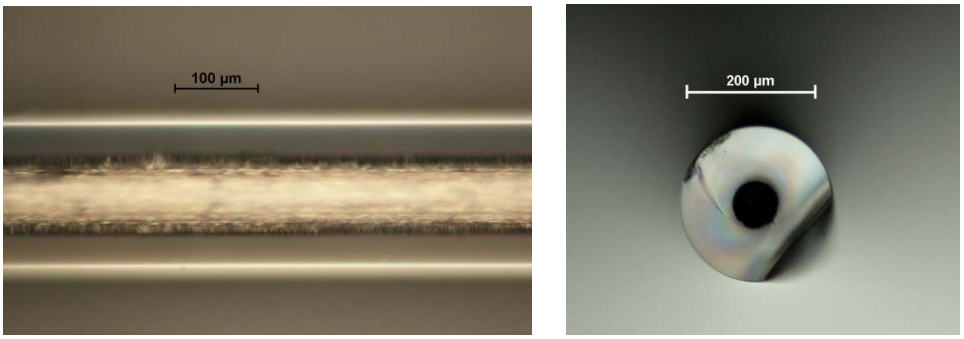

Figure 5.1 Left: side profile of aluminium-core, borosilicate fibre. Right: cross-section of aluminium-core, borosilicate fibre, taken with optical microscope

Many fibre snaps occurred during initial copper-core fibre draws, however, reasoning behind each fibre snap was realised. Most fibre snaps were due to the copper not melting fully, or too much copper flowing into the preform neck at once. These issues emerged to be mainly temperature related, but the feed rate, pull rate and volume of copper used, all became apparent as contributing factors towards fibre snaps. Substantial variations in fibre drawing results were being realised between identical draw conditions and this issue transpired to be due to a faulty line filter within the medium frequency generator. This issue consumed a large amount of the allotted project time, however once rectified, fibre draws became perfected, with trial and error being the main method of headway.

The following fibre drawing conditions allow the continuous drawing of copper-core fibre up to 50 km in length, with an outer diameter of around 23 µm and core diameter of around 4 µm, as pictured in Figure 5.2. Diameter fluctuations have been measured over tens of kilometres with an outer diameter standard deviation of 2.2 µm and inner diameter standard deviation of 0.8 µm A Schott Duran borosilicate preform of 6 mm outer diameter and 2.5 mm inner diameter is fused at one end to create a seal, and four lengths of 0.5 mm diameter copper wire are inserted into the preform. No gas purge is supplied to the centre of the furnace, where the preform is situated, but a 5 $l.min^{-1}$ nitrogen gas flow is delivered through the cooling ring. A 50 mm tall, 30 mm inner diameter and 40 mm outer diameter graphite susceptor under a 4 $l.min^{-1}$ argon purge is heated to 1320 °C at 100 $°C.min^{-1}$. The take-up drum is pre-started, at a take-up rate of 20 $m.min^{-1}$. As soon as the preform starts to neck, a feed rate of 6 $mm.min^{-1}$ is started and the set speed of the take-up drum is increased to 70 $m.min^{-1}$. The fibre is attached to the take-up drum at 20 $m.min^{-1}$ as opposed to 70 $m.min^{-1}$ due to the difficulty of attaching the fibre at such a high speed. Once the preform neck has fully dropped to near the take-up drum, the fibre is snapped and taped onto the accelerating drum by hand; the configuration settings (within the fibre drawing tower user interface) of the take-up drum are then changed so that both ‘zero’ and ‘span’ are 100 $m.min^{-1}$. This change in configuration causes the drum to rapidly reach a take-up

speed of 468 m.min^{-1}, which is the required take up speed to create such small diameter fibre. Once the take-up drum is fully up to speed, the traverse speed of the drum should be increased to create a gap in the fibre spool, and then decreased to near minimum, to create a solitary spool of continuous diameter fibre.

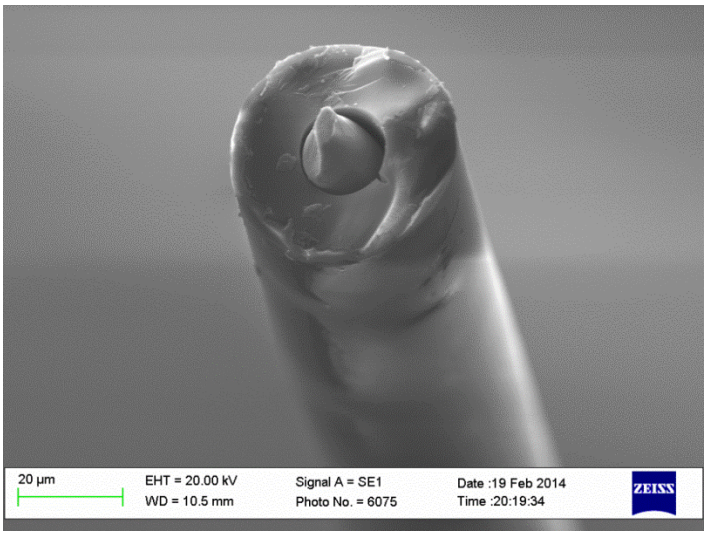

Figure 5.2 SEM image of copper-core borosilicate microfibre

The take-up drum needs to be brought up to speed as fast as possible for a successful fibre draw to take place and this is due to the fast preform feed rate that is being used. If the take-up drum was not immediately brought up to speed, too much preform material enters the furnace hot zone and a large bulb of preform material is drawn down with the fibre and creates a snap. The fast feed rate is necessary to create the required preform neck shape. A long neck region, which allows molten copper to pool, is desired for a continuous metal-core fibre to be drawn. If the neck is not visibly elongated as soon as the fibre is attached to the take-up drum, then a bulb of preform material will be drawn down with the fibre within a few seconds and will cause instability in the preform neck; inducing a fibre snap. The same fibre drawing procedure can also be used for silver or gold metal cores, which do not behave significantly different during the fibre draw to copper. Figure 5.3 shows a bungle of copper, gold and silver borosilicate-encapsulated microwire all drawn under the same conditions.

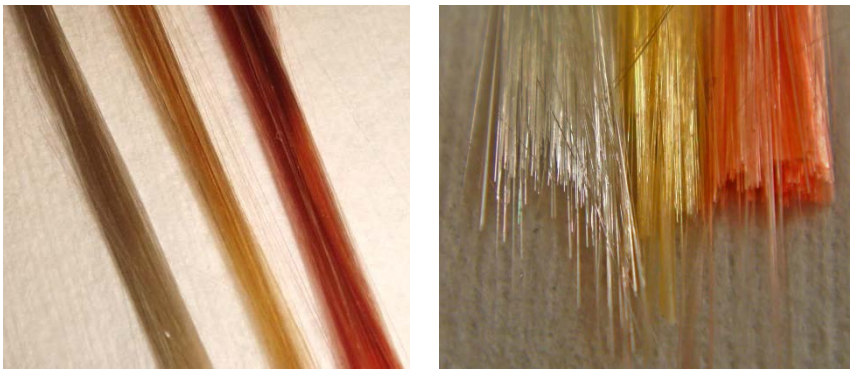

Figure 5.3 From left to right: bundles of silver, gold and copper-core borosilicate microfibre

Uses of such fibres range from electrical to textile-based reinforcement applications. The most simplistic function of glass-encapsulated microwire is to expose the metal core at both ends of a length, and the resultant fibre is a glass-insulated microwire for electrical applications. This particular use is very beneficial within small devices that require electrical links, and would suffer from short-circuiting if bare microwires are to cross paths. Conversely, when the borosilicate glass is etched away from the metal core, an extremely small diameter microwire is revealed, which cannot be produced from the conventional method of extrusion or wire drawing. As well as electrical-based applications, the metal-core fibreglass produced can be incorporated into textile products, creating a metal filament reinforced material suitable for functions such as ballistic protection [102].

Microwires created in this work have shown an extremely high-quality surface finish due to the nature of the fabrication technique; the molten metal is formed into shape through contact of softened glass, which has an extremely smooth surface. To produce bare metal microwire, wet etching in diluted hydrofluoric acid has been used. By submerging a bundle of glass-encapsulated microwire in 20% hydrofluoric acid for 150 minutes, the glass is fully removed and the metal microwire is not damaged. A small bundle is held within a PTFE sieve and fully submerged in diluted hydrofluoric acid, which is contained in a larger PTFE beaker. Around half way through the etching time, the PTFE sieve is agitated to reorder the fibre bundle. This movement allows the hydrofluoric acid to contact all the fibres in the bundle uniformly. If this step is not followed, the fibres contained in the centre of the bundle are not subject to the same etching environment as the fibres on the outside and are therefore not etched to the same extent. Once the etching time has lapsed, the PTFE sieve containing the microwire is slowly transferred into a beaker full of deionised water and then placed in an ultrasonic bath for 10 minutes. The microwire can then carefully be picked up with tweezers and placed in a petri-dish full of methanol. The methanol is then left to evaporate, leaving a bundle of microwire in the petri-dish. Under the mentioned recipe, copper microwire has been created, as shown in Figure 5.4.

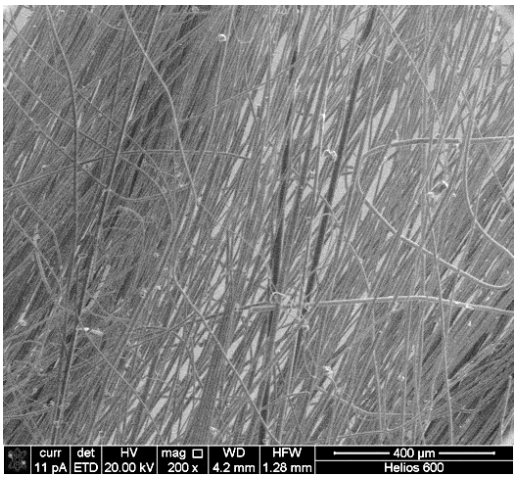

Figure 5.4 SEM image of bare copper microwire

To produce a fibre tip with a flat cross section, various cleaving techniques have been tried. A high quality cleave is necessary for applications such as connecting wires, where a clean connection must be made between the fibre tip and the relevant interface. Cutting the fibres with scissors or scalpel knife revealed rugged fibre tips with randomly protruding or recessed metal cores. Cleaving the fibres with a hand-held ceramic cleaver did not improve the quality of the fibre tip, due to crushing the glass. However, with the use of a ruby fibre scribe, better results were achieved; the glass cleaves well, but the continuous metal core remains intact. Therefore, when the fibre is snapped at the cleave, the glass tip is crushed due to the leverage created around the metal core. The extremely small diameter of the fibres resulted in a mechanical tension cleaver not being able to grip onto the fibre properly, again resulting in a poor cleave. CO_2 (10.6 µm) laser cleaving can produce fibre cleaves of very high standard [103-105], therefore was tested on glass-encapsulated copper microwires. Unfortunately, due to the thermal process of CO_2 laser cleaving, the tips of the fibres were molten. This resulted in bundles of fibres fusing together, or single fibre tips melting into a glassy dome, covering the metal tip (shown in Figure 5.5). Alternative fibre cleaving techniques have been reported, for example, focused ion beam milling [106], which has produced good results, however, this process is extremely time consuming and not suited to cleaving multiple fibres at once. Ultraviolet (193 nm) laser cleaving [107] has been reported on polymer fibres and has been tried on glass-encapsulated copper microwire. A 405 nm, 200 mW laser diode was focused onto multiple fibres, however, the borosilicate glass transmits from around 300 nm – 2 µm, therefore was not affected by the incident laser. Small deformations in the copper were seen as the laser was focused on the microwire, but a higher power laser source is needed to cut through the copper entirely.

High quality fibre cleaving is important for applications such as connecting multiple microwires to a grid array, therefore endeavouring to find a method of cleaving metal core fibres efficiently

is valuable. Polishing bundles of fibre tips has been attempted, however, owing to the density mismatch between the metal core and glass cladding, undercutting was evident, and therefore high calibre results have not yet been achieved.

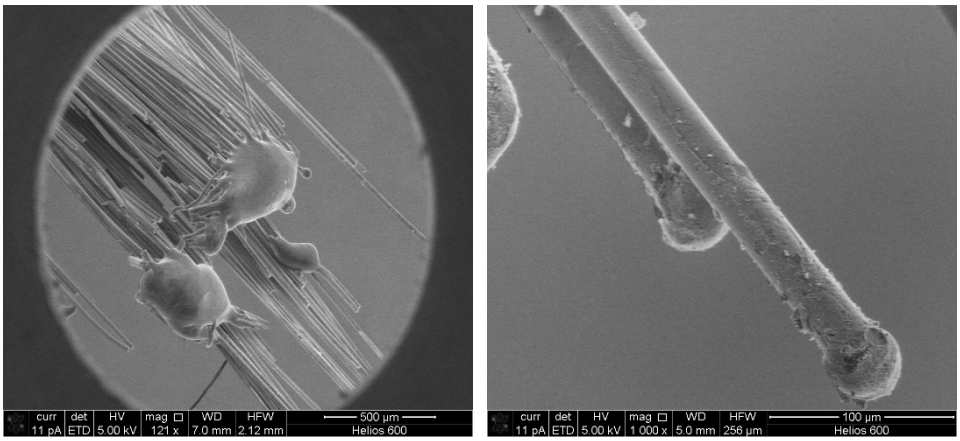

Figure 5.5 Left: fused bundle of glass-encapsulated copper microwires. Right: motlen tips on individual glass-encapsulated copper microwires, taken with SEM

Bundles of glass-encapsulated copper microwire have been inserted into Schott Duran borosilicate tubing with a 6 mm outer diameter and 2.5 mm inner diameter, and re-drawn to create a composite fibre containing multiple copper microwires. Initial trials have produced fibre containing multiple copper microwires, but it can be seen in Figure 5.6 that there are significant gaps between copper microwires. Many of the copper microwires snapped during the fibre draw due to the high temperature used. However, refining the fibre drawing conditions would result in a composite fibre that contains many more lengths of continuous copper microwire. If a fibre were produced containing thousands of uniaxial-aligned microwires or nanowires, the potential to connect thousands of individual connector nodes can be achieved. This application can become particularly useful in devices that require the linking of micro grid arrays.

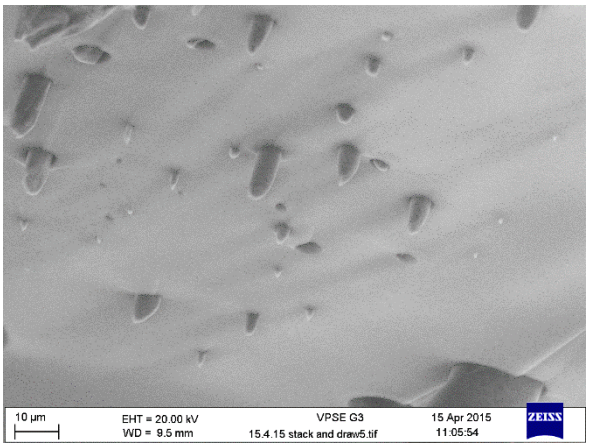

Figure 5.6 SEM image of glass-copper composite fibre cross-section

An overview on the development of glass-encapsulated microwire has been discussed along with resulting fibre drawing parameters necessary to reproduce such fibre. All objectives set by the six month industry-led project were met and multiple core materials have been successfully made into the required dimensions. Further work has been focused on cleaving the fibres to reveal a flat cross section, which is useful in applications such as connecting circuits. Bundles of glass-encapsulated microwire have been stacked and drawn to produce composite fibre containing thousands of copper microwires, and further work will be focused on refining this particular type of fibre.

5.3 Gas Sensing and FLITES

Quantitative sensing of gas species is a subject of great interest in many sectors of industry, research and economics [108]. This includes safety measures via detection of particular toxic or flammable gases [109], atmospheric science; to gain knowledge of various damaging gas species including greenhouse gasses [110], medical diagnosis though the use of breath analysis [111] and an application more related to this work, gas species measurement by optical spectroscopy.

FLITES aims to establish a measurement and imaging system for molecular and particulate species in the extreme environment of an aircraft turbine exhaust plume with penetrating spatial-temporal resolution. The project supports a new phase of low-net-carbon development that is underway in aviation, based on bio-derived fuels and engine combustion efficiency. During the assessment of a new Rolls Royce environmentally friendly engine (EFE) and fuel from Shell, focus will be made on emissions of soot, unburned hydrocarbons (UHC) and NO, which are all regulated by certification authorities. CO_2 is also monitored as a marker, for assessment of individual fuel injection nozzle performance within the EFE.

One of the ORC's roles in the FLITES project is to develop improved infrared transmitting fibre, for the transmission of fibre-laser power of wavelengths within the spectroscopic absorbing regions of interest. These fibres are being developed in parallel within an effort to create a tuneable fibre-laser absorption spectroscopy (TFLAS) system by the team of researchers constituting the FLITES project. Fibre transparency is required at 3.4 – 3.5 and 5.1 μm for the detection of UHC and NO respectively, where 3.4 - 3.5 μm represents a switching window (3.4 μm sits on the UHC absorption peak and 3.45 - 3.5 μm is off).

Gas sensing can be achieved via a number of systems, which include methods based on electrical, acoustic or thermal response [112]. Nevertheless, gas sensors based on optical absorption offer many advantageous factors, including fast response time, minimal drift (the gradual and unpredictable variation of the signal response to a particular gas species when exposed to the same analyte under identical conditions over time [113]) and the potential for zero cross-response from other gases. However, with such great interest in gas sensing from so many sectors, the market has been inundated with commercial gas sensing equipment that can be bought for just a couple of pounds, and more sophisticated devices can reach tens of thousands of pounds in price. In spite of this, there are aspects of the TFLAS system that deem commercially available equipment unsuitable for this project. An output power, orders of magnitude higher than is conventionally available, is required from the fibre-lasers to transmit signal through the gas plume; this is due to the high absorption in such an environment. The delivery of such laser power to and from the gas plume needs to be through an economic medium so that a significant amount of power is not lost through this path; hence, a low loss infrared transmitting optical fibre is required.

Commercially available infrared transmitting optical fibres have been reviewed in an effort to gain knowledge of what is offered, and perhaps more importantly, a benchmark of fibre quality has been revealed as a target to better with GLS fibre made in-house. Some lengths of commercially available As_2Se_3 fibre with core diameter of 100 μm and clad diameter of 170 μm were purchased from CorActive and characterised. This revealed losses much higher than were advertised, although it was noticed that the product "specifications are subject to change without notice", which is far from ideal for such a vital component within the TFLAS system. A cutback loss measurement was carried out on the obtained As_2Se_3 fibre with the use of an FTIR and the result is displayed in Figure 5.7, which shows relatively high losses in comparison to what was advertised (0.5 dB^{-1} over most of this wavelength region).

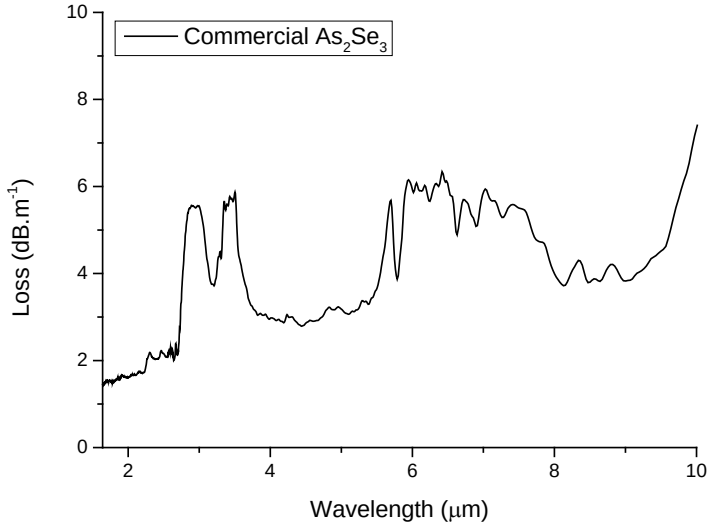

Figure 5.7 Cutback loss measurement on commercial As_2Se_3 fibre using FTIR spectrometer

As was seen in Chapter 3, GLS exhibits low absorption in the wavelength range of interest (3.4 – 5.1 μm), which renders GLS optical fibre an appropriate candidate for the purpose of passive laser-power delivery in the TFLAS system. An ongoing effort to fabricate low loss GLS fibre for FLITES has reached a stage of assurance due to the record low loss bulk GLS, which is being produced for fibre preforms. The current stage of GLS fibre development has been described in Chapter 4, yet there are further developments scheduled specifically for FLITES, including fibre coating, GLS preform extrusion and GLS core-clad structured fibre drawing.

5.4 Other Industrial Led Projects

A number of small industrial projects have been initiated over the course of the work reported in this thesis. Due to the flexible nature of the fibre drawing tower, numerous types of fibre have been fabricated, following interest from industrial organisations.

Ultrafine fibres are used in many applications outside of the optical domain and are utilised for their extremely high specific strength and ductility. This phenomenon becomes apparent due to the minute diameter of the fibre, which inherently defines the material to have fewer molecular defects per unit-length than a larger diameter fibre. A proof of principle fibre draw was carried out in attempt to create fibre of just a few microns in diameter, which can be utilised for applications such as composite materials with ultrafine fibre reinforcement [114]. As a first trial, a 6.2 mm outer diameter, 2 mm inner diameter Schott Duran borosilicate preform was used to create sub-ten micron outer diameter fibre. A vacuum was applied to the preform to collapse the tube, which dramatically reduced the effective diameter of the preform. This was then drawn at

a speed over 400 m.min^{-1}, which produced fibre with an outer diameter below 10 µm and over a kilometre in length, as described in 'Run 289'. An SEM image of a small bundle of fibre tips is shown in Figure 5.8 and it can be seen that there is no sign of a hollow core in the fibre, which is due to the vacuum being applied.

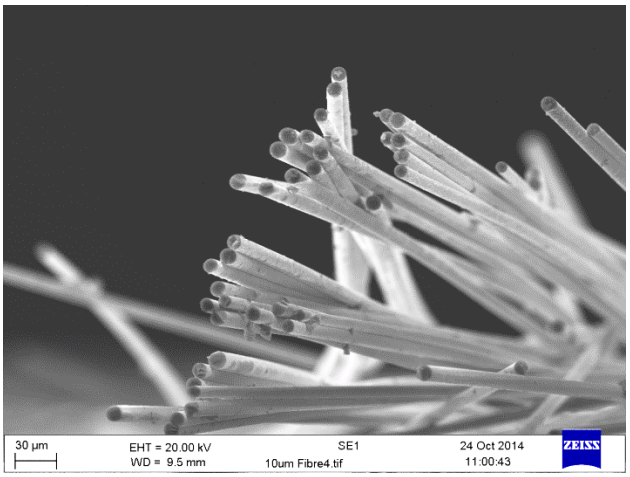

Figure 5.8 SEM image of ultrafine borosilicate fibre tips

The main purpose of the fibre drawing trial was to demonstrate how small a fibre diameter could be achieved with Novel Glass Tower II. For aesthetic reasons, coloured preforms can be used to create fibre of various colours, which will not be affected in terms of performance, but would rather create a more aesthetically pleasing composite material. This small feasibility study has established a foundation for Novel Glass Tower II fibre drawing capabilities, and has effectively promoted this for further industrial interest.

A request to fabricate hollow canes for the spectral broadening of laser pulses, for use in spectroscopic measurements of biological molecules was also given. The cane dimensions requested were around 1100 mm long with an outer diameter of 6.5 mm ± 0.2 mm and an inner diameter of 265 µm ± 5 µm along the entire length of the cane. As described in 'Run 311', Schott Duran borosilicate tubing with an outer diameter of 9 mm and inner diameter of 1.2 mm has been caned at a rate of 40 mm.min^{-1} with a 1.9 mm.min^{-1} feed, resulting in a cane with an inner diameter of exactly 265 µm and an outer diameter of 2 mm. To meet the required outer diameter of 6.5 mm, the cane was simply inserted into a Schott Duran capillary with an outer diameter of 6.5 mm and inner diameter of 2.5 mm. By demonstrating the capabilities available from our equipment, confidence from industrial corporations can quickly be achieved.

A company, who provide gas and particulate analysis for many applications including research and engine testing, requested a mid-infrared transmitting fibre to be made. The application for this fibre is to collect mid-infrared light from a test cell and deliver to a remote detector. The requirements for such a fibre are a large diameter of around 500 µm and transparency from 2.59

– 4.75 µm, both of which can potentially be achieved with GLS fibre. A logical first step towards meeting this objective is to create conventional oxide fibre at the specified diameter due to oxide glasses being relatively simple to draw into fibre. Schott F2 has been drawn into a long length of 500 µm diameter fibre as detailed in 'Run 313', which has provided useful information about the fibre drawing tower capabilities. Initially, a 500 µm diameter fibre seemed too large to fibre draw; instead, caning was considered as a more suitable fabrication method. GLS fibre likely has a different minimum bending radius than Schott F2 fibre, however with the take-up drum having a 500 mm diameter, a large enough bending radius is provided to proficiently accommodate fibres of large diameter. Upon refining the GLS fibre drawing procedure enough to produce conventional 100 – 200 µm diameter fibre, a variation in draw speed should be sufficient to produce 500 µm diameter GLS fibre for this application.

A glass sample in the form of a rod has also been requested, which has a high amount of dielectric loss at microwave frequencies for the use of a calibration reference within a microwave microscope that is under development. Obtaining a small, robust and high-loss material that is uniform, transpired to be a difficult task; however a GLS cane was believed to be able to meet the requirements necessary for this application. GLS canes have been successfully fabricated, the details of which are found in 'Run 288', and have been sent away for testing. The results obtained via email from A. Gregory on the 30th January 2015 were that GLS does not have a great enough loss at the frequency of interest [115], which does not quite fit the requirements needed. However, the ability to produce many materials in the newly developed glass synthesis and melting system described in Chapter 2, and the capability of doping GLS with high levels of many elements, could potentially lead to a suitable material being created in-house.

5.5 Conclusion

Participating in industrial led projects, encouraging the manufacture of novel fibre has demonstrated the relevance of the work reported in this thesis towards the Centre for Innovative Manufacturing in Photonics. As well as investigative studies into the development of novel glass and fibre, manufacturing fibre for projects linking research and industry has bridged a gap that the Centre for Innovative Manufacturing in Photonics aims to provide.

Project goals, progress and results have been illustrated and further work has been discussed. The success of the glass-encapsulated microwire work has led to a second phase of development, and through the encouragement of industrial interest, new limits have been realised in terms of small diameter fibre manufacture. GLS fibre development has been

encouraged through the objective of manufacturing passive laser delivery fibre for FLITES and will continue to be developed for a variety of passive and active mid-infrared fibre applications.

Chapter 6: **Infrared Fibre Development and Further Work**

6.1 Introduction

It has been established that GLS optical fibres have many valuable properties including a wide transparency window and high thermal stability, however, several alternative optical fibre materials exist that can exhibit similar or enhanced properties to that of GLS. Of course, suitability relative to application is a factor when discussing general optical fibre properties, consequently an individual fibre material cannot be singled out as inclusively better than all others. Alternative infrared transmitting fibre materials commercially available include single-crystal sapphire [116], heavy metal fluoride glasses (HMFG) [117], polycrystalline silver halide [118], hollow-core silica [55] and other chalcogenide glass compositions [119]. Furthermore, hollow waveguides offer an alternative fibre geometry and mechanism of guiding infrared light to conventional total internal reflection-based optical fibres [120], which will be discussed along with the other materials mentioned.

Single-crystal sapphire offers a broad transparency range, high melting temperature of 2053 °C and a very high strength and durability. These fibres are most commonly used for sensor applications in chemically hostile or high temperature environments [121]. They are also used in laser power delivery systems, offering the potential of delivering laser power of up to 10 W, withstanding 1 J, 2.94 µm pulses at 10 Hz for up to 20 minutes [122]. Medical power delivery systems exploit the transmission window of sapphire and biocompatibility for use in laser surgery [123]. However, a key drawback associated with single-crystal sapphire fibre is its limited length of up to a few meters; this is due to the challenging fabrication process of growing single crystal fibres.

HMFG possess a transparency range spanning from around 0.3 – 6 µm depending on the glass composition, and much like chalcogenides, HMFG have great compositional flexibility, which allows for tailoring both optical and physical properties. These types of fibre possess a theoretical minimum loss of 0.001 $dB.km^{-1}$ at 3.44 µm [124] (BaF_2-GdF_3-ZrF_4), which if fabricated, could lead to very economic long-haul optical communication systems being developed. Low losses, which have been reported in HMFG fibres [125] contributes towards their suitability for high resolution spectroscopy, temperature measurement and laser power delivery. A 20 W output power laser operating at 2.8 µm, using erbium doped HMFG fibre has been reported by Faucher et al. in 2011 [126], demonstrating high stability of the material.

Polycrystalline silver halide is a fibre material predominantly utilised for its ability to transmit high levels of CO_2 laser power at 10.6 μm (continuously up to 45 W or short pulses up to 250 W [127]), specifically for surgical applications. The suitability of this application is reinforced by the flexibility and nontoxic nature of the resultant fibre. Single crystal silver halide is grown from a melt and can be extruded to form an optical fibre [18]. The extrusion process is carried out at temperatures between 25 and 200 °C [128], requires high pressures of up to 25 kbar [129], and diamond-coated dies that don't react with the chlorine content in the halide [130].

Hollow-core silica fibres provide low loss transmission up to around 4 μm [55] and present very low bending losses [131]. Specifically, hollow-core photonic bandgap fibres are used in gas sensing [132] and have great interaction with gas-filled cores to allow operation down to 50 ppm. Low loss mid-infrared transmission has been reported through hollow-core silica photonic bandgap fibre [133], however, the limited transmission of wavelengths beyond 4 μm presents a major disadvantage compared to other infrared transmitting fibres.

Chalcogenides are an extremely versatile group of glasses that can be formed into optical fibre. The vast glass-forming range accessible from this group of glasses offers a fibre transparency range from 0.4 – 13 μm and a host of optical and physical properties can be manipulated through stoichiometric control. This feature is why chalcogenides are highly valued as an optical fibre material despite strong extrinsic absorption seen in current chalcogenide fibres, resulting from contaminants inherently contained within the raw materials. However, these losses will decrease as more research is invested into the development of high purity chalcogenide materials. Because chalcogenide optical fibres have high transparency beyond 4 μm, they become an excellent candidate for photonic sensors operating in the sensitive gas-absorbing region above 4 μm and for the delivery of infrared laser power.

The infrared transmitting hollow waveguide is a sustainable alternative to conventional solid-core fibre geometry and can be made from plastic, metal, or glass tubes that have a highly reflective coating deposited on the inside surface. This form of fibre comprises of many different materials and as a collective offer many advantages over solid-core optical fibre. Due to having an air-core, these fibres possess no end reflections, high laser power threshold, small beam divergence and are by nature very rugged, however hollow waveguides are extremely sensitive to bending, which varies as 1/R, where R is the bending radius [120]. Nevertheless, they are considered suitable for chemical and temperature sensing as well as CO_2 laser delivery. Losses as low as 0.1 $dB.m^{-1}$ have been reported [134] and the ability to transmit continuous wave laser powers as high as 2.7 kW [135].

Having briefly discussed the capabilities of several types of infrared transmitting fibre, a picture can begin to be built, containing each type of fibre and its suitability in terms of application.

Figure 6.1 clarifies the wavelengths that each type of fibre mentioned is capable of transmitting, with silica fibre as reference. Although there is considerable overlap, many factors influence material selection for specific applications. For example, physical properties like strength, flexibility, thermal stability and obtainable fibre length, or optical properties such as nonlinearities and specific absorption bands.

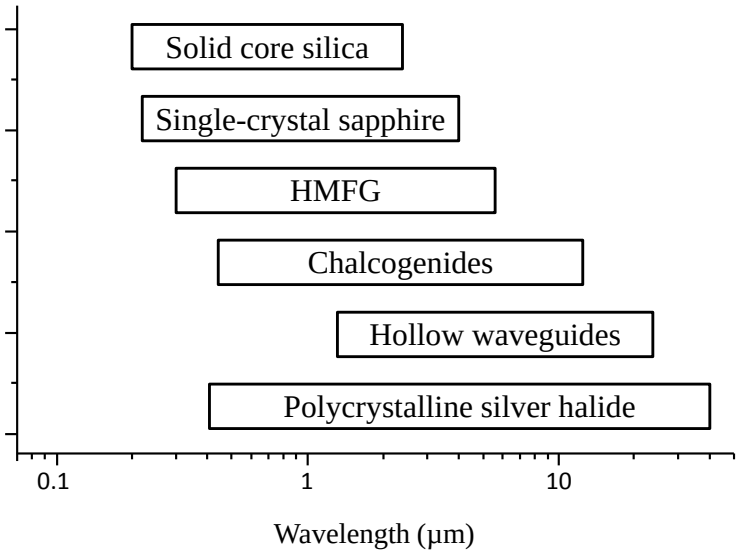

Figure 6.1 Low loss transmission ranges of silica [136], single-crystal sapphire, HMFG [125], chalcogenide [1], hollow waveguide [1] and polycrystalline silver halide [127] optical fibres

6.2 Additional GLS Fibre Study

It has been established that chalcogenide fibres are suitable for the delivery of infrared laser power and for use in photonic sensor devices operating in sensitive gas absorbing regions. GLS has become a particular material of interest due to its availability within the Novel Glass and Fibre Group with high purity. Preform drawing to obtain a single material, multimode fibre has been discussed in Chapter 4; however, additional GLS fibre forms have been pursued in order to create both active and passive GLS fibre structures.

Vacha et al. suggested in 1987 “it may very well be possible to find an oxide glass overcladding material compatible with a fluoride glass, which has a refractive index larger than that of the oxide. This raises the intriguing possibility of making low cost, high strength IR transmitting fibers for short range applications which consist of only a single fluoride core plus an oxide glass clad” [137]. Inspired by this short concluding comment to a Materials Science Forum letter, oxide glasses have been sourced that thermally match GLS in terms of fibre drawing properties. The fibre produced will have the optical transmission of GLS up to around 3 μm

when the oxide cladding will begin to absorb the incident light. There are a few points that can be recognised with this fibre design that offer benefits over conventional GLS preform fibre drawing. The GLS will be confined within a somewhat protective jacket during fibre drawing, which will act as a barrier against hydrolysis, providing the oxide material is dry and clean itself. Therefore, the atmosphere within the furnace during fibre drawing does not need to be completely oxygen free, which makes the drawing process easier, as the extended furnace tube described in Chapter 4 does not need to be in place. Yet, the most attractive attribute that can be realised from this fibre design is that the fibre structure should retain the mechanical properties of the oxide cladding, making the fibre stronger than that of pure GLS. The fibre becomes a lot more user-friendly in terms of robustness, and fibre snaps during the removal of polymer coatings for example becomes considerably easier to avoid.

The method in which these fibres have been made is by firstly selecting suitable oxide glass; beginning with the up-to-date Schott glass library [138], glasses were compared to a single thermal property of GLS at a time, and were dismissed or reserved accordingly. The properties taken into account were the coefficient of thermal expansion, thermal conductivity, T_g and glass softening point. All of these properties are known for GLS, from in-house measurements and literature [139], and are disclosed within the Schott glass catalogue for oxide glasses. Four Schott glasses were deemed appropriate for this application: N-F2, N-KZFS8, N-LAF7 and N-SF8, as shown in Table 6.1. 10.4 mm diameter rods were purchased in 100 mm lengths and a bore was then drilled longitudinally down the centre of each rod using an ultrasonic drill. Bores ranging from 1 – 2 mm in diameter were drilled, resulting in a tube suitable for GLS cladding. The rods were etched in 30 % hydrofluoric acid for exactly 12 minutes each, which removed any residual cutting fluid and improved the surface quality on the inner and outer surface areas of the tube. The tubes were then thoroughly rinsed with deionised water and kept in a vacuum oven for 48 hours at 100 °C prior to use. GLS canes have been fabricated with a diameter just slightly smaller than the inner diameter of the relevant oxide tube. GLS canes that had an increasing taper towards one end were inserted in the Schott glass tubes, so that the cane was held inside. The cane was inserted from the bottom of the tube so that the tight-fitting end was at the bottom, and a light vacuum could be applied from the top of the preform, to collapse any gap between the core and clad. Figure 6.2 shows a preform with a GLSO cane inserted in the core and the resultant fibre that was drawn.

Table 6.1 Selected properties of GLS(O) and Schott glasses

Glass Property	GLS	GLSO	N-LAF7	N-SF8	N-F2	N-KZSF8
T_g (°C)	~575	~560	568	567	569	509
Softening point (°C)	~640	~620	669	678	686	635
C.T.E. ($x10^{-6}$ K^{-1})	~6.4	~10	8.39	9.92	9.1	9.4
Thermal conductivity ($W.(mK)^{-1}$)		~0.43	0.83	1.03	1.05	1.05
Refractive Index	~2.4	~2.5	1.78	1.69	1.62	1.72

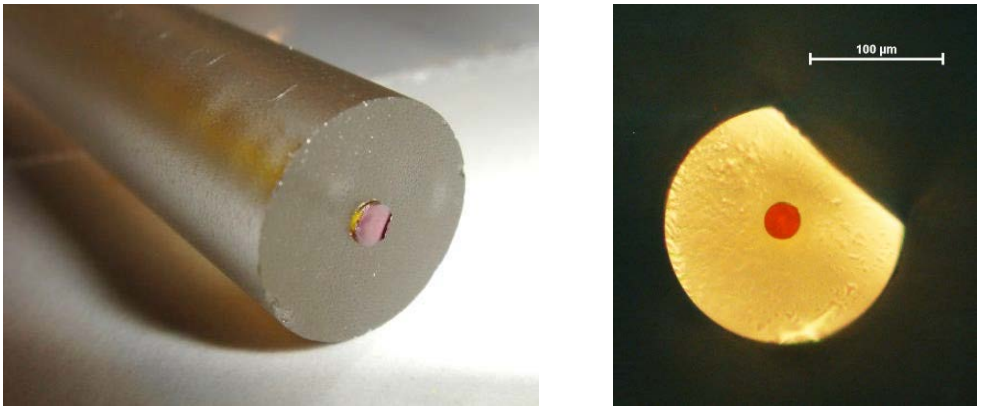

Figure 6.2 'Run 291'. Left: N-SF8 tube with GLSO (LF188) cane inserted. Right: resulting fibre cross-section

Best results have been produced from GLSO core materials rather than GLS; this is due to GLS crystallising within the oxide cladding, and therefore not drawing into fibre. However, GLSO glass canes available from our glass inventory have been used to better effect. Only a few fibre draws of this type have been attempted due to limited availability of GLS and GLSO canes and oxide tubes, although further work will certainly involve the pursuit of fabricating GLS-core, oxide clad fibre. A 25 cm length of fibre from 'Run 291' has been characterised, which revealed a loss of 80 dBm^{-1} at 1550 nm. This measurement was completed with the use of a 1550 nm telecommunications loss measurement set-up and mounting a 25 cm length of the fibre in a capillary and polishing both end faces prior to characterisation. The majority of the loss evident in the measurement is likely due to the core-clad interface, which varies in quality along the fibre length and causes scattering. An example of a non-circular core section from the same fibre draw is shown in Figure 6.3; this flaw can be eradicated over time with refinement of drawing conditions. In addition to fabricating GLS-core, oxide clad fibre for passive applications; a far smaller core diameter can be created by firstly caning the initial preform to a diameter suitable to be inserted in a subsequent oxide glass tube, which would then be drawn

into a fibre, resulting in a GLS core diameter of just a few microns. This small core fibre geometry is suited to nonlinear applications such as supercontinuum generation, rather than passive light transmission.

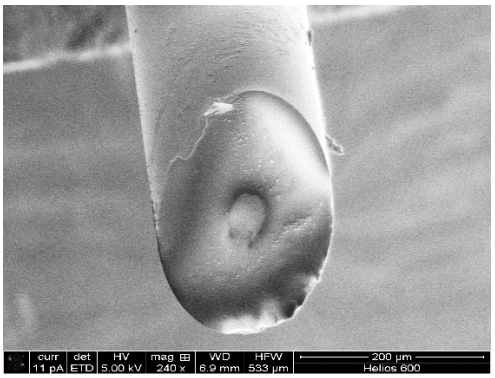

Figure 6.3 SEM image of poor quality core-clad interface from ‘Run 291’

6.3 Ge:Sb:S Preform Manufacture by Chemical Vapour Deposition

As previously discussed, chalcogenide glasses suffer from high extrinsic losses due to their inherent impurity content within the raw materials. On the contrary, the fundamental reason that silica-based optical fibres can achieve such low losses is that the preforms are made from extremely high purity materials, manufactured by a chemical vapour deposition (CVD) technique [140]. CVD is a process, which introduces gaseous reactants and precursors into a heated tube, whereby a chemical reaction takes place. The resultant solid material is deposited onto the interior surface of the tube, which builds up over time to produce a solid rod. The development of this technique has made a huge impact on the optical losses in silica fibre through the combination of using extremely high purity precursors and the removal of waste reaction product, which CVD ensures. The technology behind CVD is a very complex subject involving thermodynamics, fluid dynamics and chemistry amongst many more scientific and engineering disciplines. If ultrahigh purity silica preforms are manufactured by CVD, then the immediate question that comes to mind is, why are chalcogenide glass preforms not made in the same manner? There has been a reasonable amount of published work and discussion on this topic [141-144], though a definitive solution has not yet been realised; mainly due to the low yield rates produced by chalcogenide precursors, the high amount of thermal cycles and the availability of ultrahigh purity precursors at rational financial cost. Nevertheless, a proposal to deposit a thick film of Ge:Sb:S on the interior of borosilicate and soda-lime tubing was tried in an attempt to create a preform that could be drawn under vacuum to create a fibre with a small Ge:Sb:S core. Two separate methods have been carried out in an attempt to create such preforms, both of which are discussed in the following subchapter.

The first method took into account that only a thin deposition would be made, and that upon collapsing the preform to create the fibre, an extremely small core and outer diameter would be created, therefore a thick walled preform tube was designed (Figure 6.4) so that the resulting fibre would be easier to handle. The glass used in this experiment was 16 mm outer diameter soda-lime glass tubing with an 8 mm outer diameter middle section, each with 2 mm thickness. The 16 mm outer diameter tubing is compatible with the 16 mm Chemcon fittings used in the CVD apparatus and the smaller diameter section is what is utilised for the deposition. A small, 25 mm-bore tube furnace was used for these experiments and the preform was positioned so that deposition of the Ge:Sb:S would occur within the smaller diameter section, which would consequently be drawn into fibre.

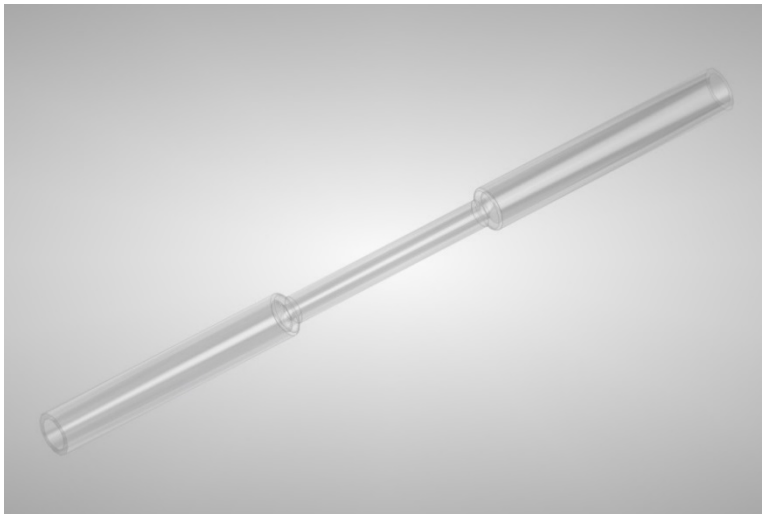

Figure 6.4 Soda-lime glassware for Ge:Sb:S CVD-core preform

The recipe used for this deposition involved taking the furnace up to 400 °C and dwelling for 3 hours with a 200 sccm argon purge in order to dry the tube thoroughly. Liquid $GeCl_5$ and $SbCl_4$ precursors were then introduced into the hollow preform by bubbling 100 and 200 sccm of argon through each precursor respectively. A separate H_2S and argon mix of 50 and 150 sccm respectively was also injected into the preform, which reacts with the liquid precursors to create the final deposited composition. The deposition was 5 hours long and was then purged with argon at a reduced flow rate of 150 sccm whilst slowly reducing in temperature until cool. The result of this first method was that the decreased inner diameter of the middle section created a Venturi effect, whereby the flow increased upon entering the reduced diameter and as a result, very little deposition was made on the middle section of the preform. Ge:Sb:S was deposited on the larger diameter sections of tube though, which was drawn into fibre under no vacuum, detailed in ‘Run 78’. The result of this fibre draw was a hollow fibre with a concentric ring of Ge:Sb:S, around 1 µm thick, on the interior of the soda-lime capillary, as seen in Figure 6.5.

Full details of the CVD can be found in the run sheet ‘CVD_PB_KK_003’, which is stored as a hard copy in the CVD run-sheet folder, kept in the CVD laboratory.

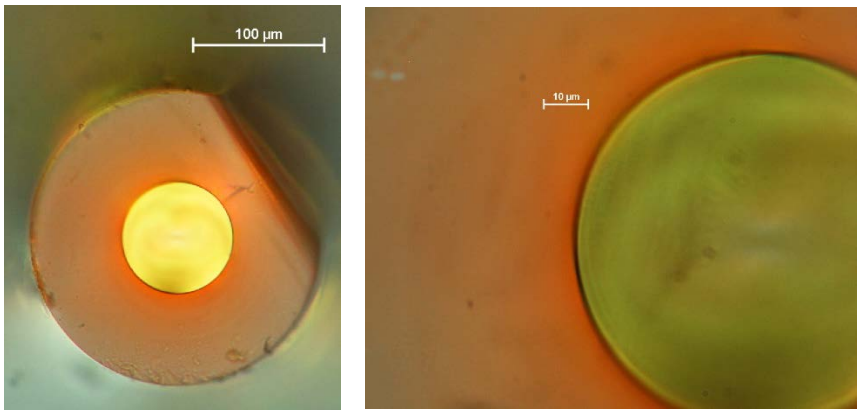

Figure 6.5 Optical microscope images of hollow soda-lime fibre with a Ge:Sb:S coated interior (‘Run 78’)

The second phase of this project utilised a tube furnace longer in length, and modified preform glassware in which to deposit. The preform glassware is shown in Figure 6.6 and it can be noted that the three prongs on the right hand side of the image are where H_2S gas, $GeCl_5$ and $SbCl_4$ vapour (carried by the argon) is injected. The bulb between the injection prongs and tube acts as a mixer so that the three constituents can homogenise before entering the tube in which the vapour deposits. The previous set-up involved attaching separate precursor injection glassware to the preform tube via a plastic Chemcon fitting, which is a cumbersome task within the glovebox and added the possibility of introducing impurities from the plastic fitting into the deposition. Depositions of over 1 g have been successfully carried out twice using this technique, full details of which are contained in CVD run sheets ‘CVD_PB_KK_004’ and ‘CVD_PB_KK_005’. Run 004 took place with borosilicate glassware and 005 with soda-lime, under identical recipes.

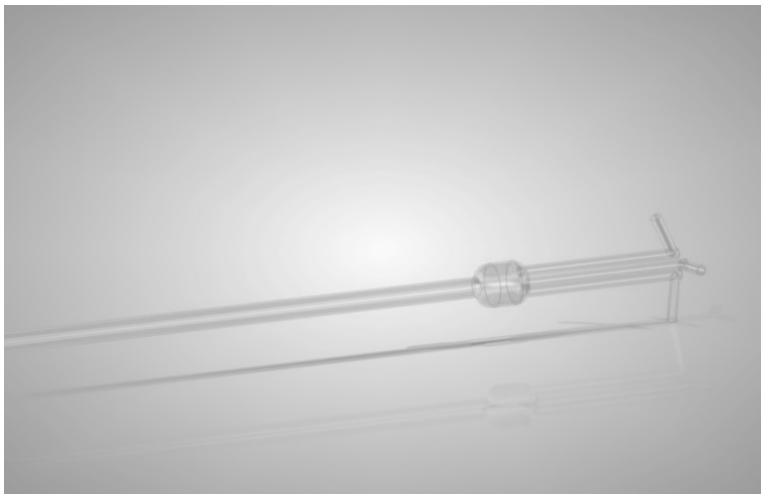

Figure 6.6 Glassware for Ge:Sb:S CVD-core preform

Having produced a glass tube preform with an inner concentric layer of Ge:Sb:S amounting to over 1 g, fibre drawing trials have taken place. ‘Run 293’ and ‘Run 310’ describe the fibre draws in detail, however the most noted attribute of the fibre draws was the low melting point of the Ge:Sb:S compared to the borosilicate or soda-lime. Nevertheless, the Ge:Sb:S would pool at the necking region of the preform during the fibre draw and flow into the core of the fibre being drawn, much like during the metal-core fibre fabrication method. The main difficulty during both fibre draw trials was refining the vacuum strength. Figure 6.7 shows the effect of too high a vacuum, where the entire preform neck has collapsed unevenly and has left two channels for the molten Ge:Sb:S to flow down. The resulting fibre from this consequence is shown in Figure 6.8 where two cores containing Ge:Sb:S can clearly be seen. The composition of the glass preform in which the CVD is performed will be refined in future work. This result is a proof of principle, which can lead to further work taking place. Ideally, the thermal properties of the preform should match the thermal properties of the deposited chalcogenide material, in terms of fibre drawing suitability. Furthermore, the two glasses should not chemically react during the CVD or fibre drawing procedures.

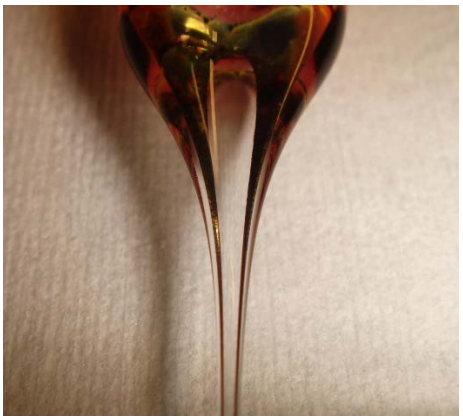

Figure 6.7 Collapse of preform neck due to too high a vacuum

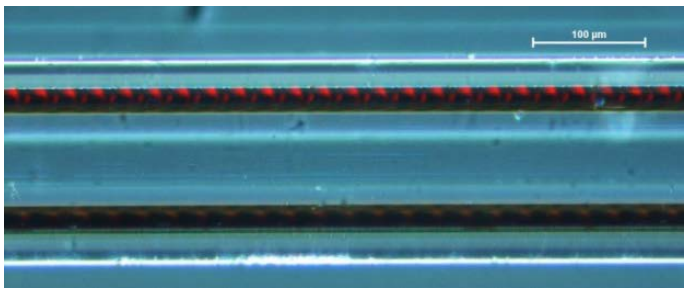

Figure 6.8 Optical microscope image of resulting dual-core produced by high vacuum

Further work towards the objective of creating chalcogenide-core fibre through CVD will firstly involve the refinement of fibre drawing parameters such as vacuum strength. Depositing more material inside the preform tube is predicted to be trivial as the mentioned CVD runs have been relatively short and could be run overnight in order to build up a thicker layer of Ge:Sb:S. This will allow longer fibre draws to take place, as draws are currently cut short due to the core material becoming exhausted after just a short time.

The method behind creating chalcogenide-core preforms using a CVD technique has been described and the benefits of which has been highlighted. Initial results have been promising and suggest that pursuing the concept can eventually deliver fibre with a chalcogenide core of extremely high purity, and hence low optical loss.

6.4 Crucible Drawing

There are many established fibre drawing techniques that are used in both industry and research. Each method possesses its own advantages and is typically selected based on the fibre material to be drawn. Slow fabrication methods like laser heated pedestal growth [145] or a modified micro-Czochralski method [146] are suited to fabricating single crystal fibres. This is because the slow process allows the glass melt to arrange its molecular structure into the lowest energy

(single crystal) state. Preform drawing is not suited for polycrystalline or single crystal preforms due to the fast process in which the fibre is drawn. It is more appropriate for materials that have a large working temperature range, which allows the preform be drawn into a fibre whilst avoiding crystallisation. Due to the relatively small working temperature range that most chalcogenide glasses exhibit, crucible drawing can be employed.

Crucible drawing is a high temperature fibre drawing process whereby the fibre source material is crushed or bulk glass, held within a crucible and heated up to its melting temperature. A simple apparatus is shown in Figure 6.9, which is suited for the crucible drawing of GLS. The tube is held in the centre of a vertical tube furnace, which provides a uniform heat to the entire crucible. A vitreous carbon crucible is fixed inside silica tubing using Fortafix Ceramix TC caulking compound, which creates an airtight seal between the bottom aperture of the silica tubing and the vitreous carbon crucible. The fibre source material is placed inside the vitreous carbon crucible and a purge gas is applied from the top of the silica tubing. Once the fibre source material is molten, the flowing purge gas has no exit, so translates into a positive pressure within the crucible drawing apparatus. After some time, the glass flows through the nozzle of the vitreous carbon crucible and is collected on a fibre take-up drum similar to conventional preform drawing. The viscosity of the glass at the exit of the crucible is around $10^{2.3}$ poise (consistency of treacle), which provides a steady flow that can be manipulated by varying the gas pressure applied to the top of the crucible. An increase in gas pressure results in an increase of effective feed rate and therefore increases the fibre diameter, and a decrease in gas pressure effectively reduces the feed rate. If the viscosity is too high during fibre drawing, the glass will not flow from the aperture of the crucible, and conversely, if the viscosity is too low, the entire supply of fibre material will rapidly flow out of the crucible aperture. Therefore, it is important to refine the drawing conditions in terms of applied pressure and working temperature, relative to the desired fibre diameter and the glass viscosity respectively.

Figure 6.9 GLS crucible drawing apparatus with vitreous carbon nozzle

Due to the relatively small working temperature range that GLS exhibits when preform drawing; crucible drawing has been perused as an alternative fabrication technique. A temperature of over 850 °C is necessary to melt GLS, and initial trials have provided promising results. Small amounts of fibre have been drawn as detailed in 'Run 59' and further developments have been made to the crucible drawing apparatus to accommodate GLS. Firstly, a vitreous carbon crucible has been incorporated into the assembly to create a container that does not react with molten GLS, like silica, which is typically used for arsenic-based chalcogenide crucible drawing. Secondly, a purge system for the tube furnace in which the crucible drawing assembly is contained, has been installed; this is essential to create an oxygen-free atmosphere so that the vitreous carbon crucible and the GLS are protected from oxidation. Further development of the crucible drawing system can involve the introduction of a double crucible apparatus [147] whereby core-clad structured fibres can be drawn. Two concentric crucible nozzles are implicated within this set-up with separate pressures being delivered to each individual crucible. Varying the individual pressures on the concentric crucible inlets can modify core-clad diameter ratios with great accuracy if appropriate pressure regulators are used.

The fibre drawing technique of crucible drawing has been investigated and initial trials have produced small amounts of GLS fibre. An inspiring conclusion made by Dianov, 1997 [148], in a crystallisation study of praseodymium doped GLS quotes "in view of [the crystallisation dynamics] and the high viscosity of Ga-La-S melts, the fabrication of optical waveguides by drawing from the melt is preferred over processing glass rods". There are benefits that this fabrication technique offers over preform drawing; firstly, the intermediate process of forming a preform rod from bulk glass is eliminated. This removes a large processing step within fibre production that can introduce impurities or flaws into the GLS preform. Secondly, an extremely high quality core-clad interface is created during this fabrication technique. Owing to the high

temperature used, the viscosity of the core and clad materials is much lower than preform drawing, this allows for a very smooth surface finish due to the reduced surface tension. The most beneficial feature of crucible drawing GLS over preform drawing is that the risk of crystallisation is dramatically reduced in comparison; this is due to the rapid cooling of the molten glass during the crucible drawing process, which can prevent crystallisation if the cooling rate is sufficiently fast that the glass does not have time to crystallise.

6.5 Optical Fibre Characterisation

Once a fibre has been drawn, the first stage of characterisation is simply visual inspection, whether by eye or using an optical microscope. Although simple, this step presents a useful gauge on how the fibre has been drawn in terms of shape, size and quality. Features such as the presence of air gaps, scattering centres or core diameter uniformity can be investigated through optical microscope imaging. Once a fibre has been confirmed to be of suitable quality through microscope imaging, more thorough techniques are put in place to measure the optical loss of a fibre over its transparency range; or more complex measurements such as modal or dispersion analysis [149, 150] can be put in place.

Although only a handful of fibres have been characterised in terms of optical loss in this work, the ongoing development of preform material and fibre drawing procedure will increase the number of fibres drawn that need to be suitably characterised to determine whether the fibre is suitable for device application. Fibre loss measurements to date have been carried out using a Harrick FiberMate adapter with the FTIR described in Chapter 3. A background scan is taken with the fibre secured in the adapter and subsequent background scans are taken after reducing the length of the fibre by cleaving. The following equation (6.1) is used to determine the optical loss in $dB.m^{-1}$.

$$Loss\ (dB.m^{-1}) = \frac{10 \log \frac{P_1}{P_2}}{l} \qquad (6.1)$$

Where P1 is the power measured through the long length of fibre, in units of Watts. P2 is the power measured through the reduced length of fibre, in units of Watts, and l is the difference in length of fibre removed between measurements, in units of metres. This is known as the cutback technique and is a widely used fibre loss measurement applied in research and industry [151]. Unfortunately, there are a few limitations set by using the FTIR and fibre adapter, which has promoted the motivation to build an upgraded system for fibre characterisation. Firstly, the fibre adapter requires a minimum of around 300 mm of fibre, which is on occasion longer than the length of high quality GLS created in current fibre draws. Secondly, the fibre is secured into the

fibre adapter using SMA fibre connectors with no fine adjustments currently available to tune the signal being transmitted through the fibre. This creates a high amount of variation in signal from the output end of the fibre. Lastly, within the FiberMate are multiple optical components and mirrors that can collect moisture and dust, which can add noise into the measurement. The most accurate way to couple light into a fibre tip is by using free-space coupling with the aid of nano-precision stages and secure fibre clamps. As part of the ongoing fibre development plan, a fibre loss measurement set-up is being assembled to characterise the increasing amount of fibres that are being produced in-house. A resource, which is able to provide accurate fibre loss measurements over a wavelength range that covers the transparency region of any fibre that can be made in-house, is of high importance. Together with a white light and infrared source, a passive fibre characterisation set-up has begun to be assembled. A Meiji Techno FT191 quartz halogen light source, which transmits from around 0.4 – 2 µm and Newport 80007 infrared source with silicon carbide emitter that transmits from 1.7 – 28 µm have been used to conceive the fibre loss measurement system shown in Figure 6.10.

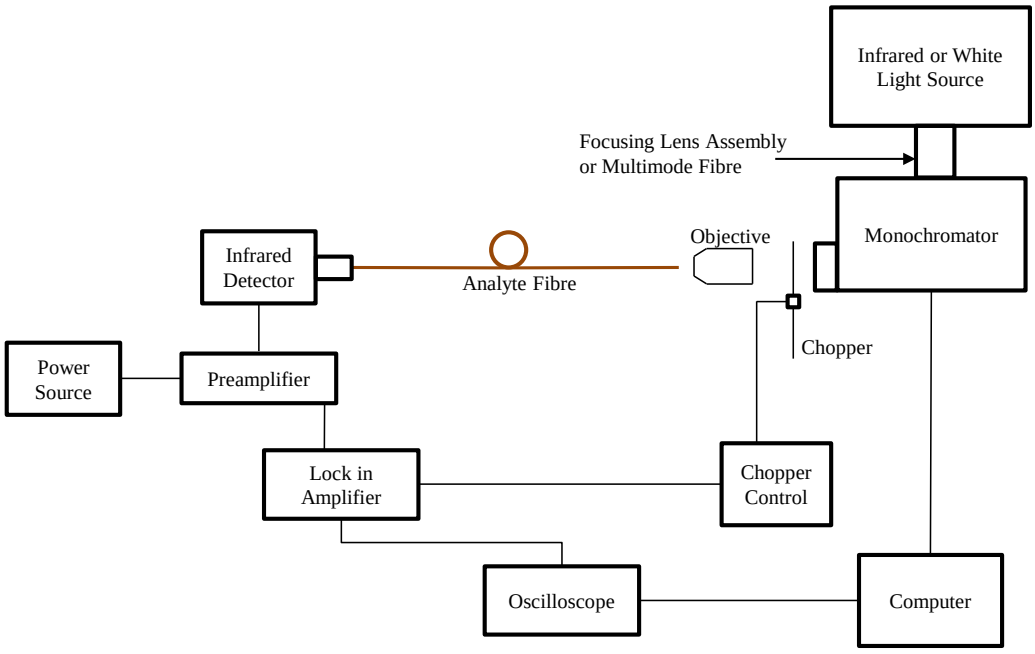

Figure 6.10 Fibre loss measurement set-up

The above fibre loss measurement set-up combines two light sources to cover a wavelength range from 0.4 – 28 µm, which is sufficient to characterise GLS fibre amongst many other types of fibre that can be drawn in-house. The modular assembly is built upon a separate breadboard for easy movement if required. Once the light has exited the end of the fibre, it can either be coupled directly into a photo detector or focused into a fibre, which can transmit the signal to an optical spectrum analyser (OSA), depending on the wavelengths of interest. The components that make up the schematic diagram in the above figure can be re-arranged and components can

be added, to characterise both passive and active fibres and offer a facility with several advantages over the FTIR and FiberMate set-up. Development of the fibre characterisation set-up will continue as future work and will be refined to act as a fibre loss measurement system for GLS fibre, to work in supplement to the FLITES project.

6.6 Conclusion

Although chalcogenide fibre has been established as a sound infrared transmitting medium, alternative fibre materials and structures have been recognised as a possible alternative. Specific properties of each type of fibre have been outlined and suitable applications are acknowledged. A project involving the fabrication of chalcogenide-core preforms via CVD has been summarised along with the advantages that this method offers. An alternative fibre drawing technique, crucible drawing, has been described and initial results have provided reassurance that crucible drawing is a viable method of producing GLS optical fibre. A fibre loss measurement set-up has been designed and upon completion, will become a vital component within the fibre development system to optically characterise fibres manufactured in-house.

Chapter 7: **Summary**

This thesis has covered progress made in numerous research areas including bulk glass manufacture, glass characterisation and the fabrication of several types of fibre for various industrial and academic projects. The work reported in this thesis has been carried out with the ambition to link industry to research and manufacture fibre in accordance with goals set by the Centre for Innovative Manufacturing in Photonics.

The first goal of this work, as listed in the introduction of the thesis, was to design and implement a modular fibre drawing facility for various types of fibre. A modular fibre drawing furnace has been built and utilised for all fibre drawing discussed in this thesis. The all-silica furnace design makes modifications quick and at a low cost. The modular aspect allows for many perform sizes and materials to be drawn on the same fibre drawing tower.

The second goal was to characterise and develop bulk infrared transmitting glass for fibre production. A study on the physical and optical properties of bulk GLS over its entire glass-forming region was completed, which revealed relationships between composition and these properties. Results have been displayed in the form of tables and graphs that can be used as reference when deciding what GLS composition is most suitable for the user's application, in terms of processing and final device form.

Thirdly, develop fibre drawing procedures for improved quality infrared transmitting glass. Progress has been made towards achieving high quality GLS fibre. Small amounts of crystal-free GLS fibre has been drawn, and with continued development of the fibre drawing procedure, optimism towards achieving low loss GLS has been established.

Lastly, to manufacture refined metal-core fibre for various device applications had been set as a goal. With modifications to the fibre drawing tower, continuous lengths of glass-encapsulated microwire is now achievable, alongside an established fibre drawing procedure for this type of fibre. Furthermore, metal-core fibres with a complex cross-section of various materials have been fabricated and procedures for doing so have been reported.

Appendix A GDMS Results

Glow Discharge Mass Spectroscopy

NORTHERN ANALYTICAL LABORATORY, INC.

13 Delta Dr. #4, Londonderry, NH 03053
Phone: (603) 434-8400 FAX: (603) 434-8500
www.northernanalytical.com

SAMPLE NO.	G52889
FILE NO.	2UOSH1
DATE:	04/04/2013

Mr. Paul Bastock La2S3
Optoelectronics Research Centre
University of Southhampton PO # 60357750
Southhampton Hampshire SO17 1BJ #Testbourne

ANALYSIS	ppmw	ANALYSIS	ppmw	ANALYSIS	ppmw
~~H~~		Zn	≤10	Pr	34
Li	0.76	Ga	10	Nd	100
Be	<0.1	Ge	<5	Sm	0.85
B	0.95	As	<0.5	Eu	0.60
~~C~~		Se	<1	Gd	<5
~~N~~		Br	<1	Tb	0.15
~~O~~		Rb	<0.5	Dy	0.45
F	200	Sr	30	Ho	0.15
Na	720	Y	0.20	Er	0.20
Mg	11	Zr	0.050	Tm	0.12
Al	13	Nb	<0.5	Yb	<0.5
Si	575	Mo	0.25	Lu	<0.2
P	7.2	Ru	<0.1	Hf	<0.5
S	Major	Rh	<1	~~Ta~~	<10
Cl*	35	Pd	<1	W	<1
K	14	Ag	<5	Re	<0.1
Ca	800	Cd	<1	Os	<0.1
Sc	<0.1	In	<1	Ir	<0.1
Ti	1.3	Sn	3500	Pt	<1
V	0.10	Sb	1.2	Au	<1
Cr	1.5	Te	≤1	Hg	<1
Mn	11	I	1.7	Tl	<0.1
Fe	24	Cs	<0.1	Pb	3.7
Co	<0.1	Ba	450	Bi	0.17
Ni	0.60	La	Major	Th	<0.05
Cu	1.0	Ce	550	U	<0.05

*** Inhomogenous - lowest value**

Accredited Nadcap™ Materials Testing Laboratory

ISO 9001:2008 AS9100 Registered Firm

ANALYSIS BY: William A. Guidoboni / Sr. Analytical Chemist
Name/Function

APPROVED BY: Richard J. Guidoboni / President
Name/Function

Glow Discharge Mass Spectroscopy

NORTHERN ANALYTICAL LABORATORY, INC.

13 Delta Dr. #4, Londonderry, NH 03053
Phone: (603) 434-8400 FAX: (603) 434-8500
www.northernanalytical.com

SAMPLE NO.	G53355
FILE NO.	2UOSH5
DATE:	13/06/2013

Mr. Paul Bastock La2S3

Optoelectronics Research Centre

University of Southhampton PO # 60366031

Southhampton Hampshire SO17 1BJ Lot # 25

ANALYSIS	ppmw	ANALYSIS	ppmw	ANALYSIS	ppmw
~~H~~		Zn	≤10	Pr	0.12
Li	0.55	Ga	15	Nd	0.20
Be	<0.1	Ge	<5	Sm	0.53
B	1.0	As	<0.5	Eu	0.45
~~C~~		Se	<1	Gd	<0.5
~~N~~		Br	<1	Tb	<0.1
~~O~~		Rb	<0.5	Dy	<0.5
F	<5	Sr	0.44	Ho	<0.1
Na	~2%	Y	3.2	Er	<0.1
Mg	2.5	Zr	0.29	Tm	<0.1
Al	4.3	Nb	<0.5	Yb	<0.5
Si	60	Mo	0.12	Lu	<0.2
P	4.6	Ru	<0.1	Hf	<0.5
S	Major	Rh	<1	~~Ta~~	<10
Cl	20	Pd	<1	W	<1
K	1.5	Ag	<1	Re	<0.1
Ca	15	Cd	<1	Os	<0.1
Sc	<0.1	In	<0.5	Ir	<0.1
Ti	0.37	Sn	<0.5	Pt	<1
V	0.013	Sb	<0.5	Au	<1
Cr	0.72	Te	<0.5	Hg	<1
Mn	0.21	I	<0.1	Tl	<0.1
Fe	2.7	Cs	<0.1	Pb	0.25
Co	<0.1	Ba	0.80	Bi	<0.1
Ni	0.20	La	Major	Th	0.40
Cu	0.40	Ce	0.70	U	<0.05

Accredited Nadcap™ Materials Testing Laboratory

ISO 9001:2008 AS9100 Registered Firm

ANALYSIS BY: William A. Guidoboni / Sr. Analytical Chemist
Name/Function

APPROVED BY: Richard J. Guidoboni / President
Name/Function

Appendix B DSC Standard Operating Procedure

DSC
Set-up and Operation Procedure

Prepared By	Signature	Date
Paul Bastock		1st September 2014

Reviewed By	Signature	Date
Dan Hewak		
Ed Weatherby		
Khouler Kahn		
Chris Craig		

Rev #	Who	Signature	Date
2			
3			
4			
5			
6			

DSC
Set-up and Operation Procedure

Trained Users	Signature	Date
Paul Bastock		
Chris Craig		
Khouler Kahn		
Stanley Tse		
Cui Long		

Checklist Before Starting Up

This standard operating procedure is a guide, and more detailed information can be found in the Pyris Help function, manuals kept in the red ring binder and in the shared drive

	Checklist	Comment	Notes
1	Make sure you have read and signed the risk assessment	Make any amendments necessary for your particular analysis	The risk assessment is kept in the lab's red ring binder and an electronic copy stored on the shared drive
2	Make sure the material being analysed is covered by an up to date COSHH form	If not, create a COSHH and save it on the shared area and also make a hard copy for the red ring binder	A list of COSHH forms already in place are found in the shared area
3	Turn on the helium gas at the wall (Fig 1) and check that there is pressure on the DSC pressure valve (Fig 2)	Before doing this, check "zepler institute facilities" updates to see if there are any current issues with gas supplies. If there is no pressure, check with Ed Weatherby as first contact, then with technical support (Mark Lessey)	The gas should be turned off at the valves after each run to ensure no gas is flowing over a prolonged time and wasted. All gas valves are labeled.
5	Check the status of the process cooling water	This valve is located under the work-bench (Fig 3)	If there are any problems with the water connections or supply, contact technical support immediately.
6	Make sure the platinum furnace lids are in place and are in good condition	If the lid has an indented top or needs to be re-shaped then instructions on how to do this are contained within this SOP	The platinum lids are very delicate and should only be handled with sharp tip tweezers or vacuum tweezers
7			

Appendix B

Starting up the DSC and computer

- Turn on the process cooling water by opening up the valve pictured in Fig 3
- Switch the DSC on via the switch located on the back of the instrument and wait until the 'ready' LED is lit (Fig 4)
- After logging into the computer, make sure it is networked and then open up Pyris Manager software. Hover the mouse at the top of the monitor screen and click the button 'Diamond DSC'
- Open the helium gas valves as pictured in Fig 1 and ensure there is pressure on the pressure gauge on the side of the DSC (Fig 2)
- Open the top of the DSC so as to open it as in Fig 5 and twist the cover to reveal the two furnace compartments.
- Carefully remove the furnace platinum lids using vacuum tweezers like in Fig 6 and re-shape using the tool in Fig 7 if necessary (there are instructions on how to use this tool in its box)

The DSC is now ready to have samples inserted into the furnaces……

Sample preparation and brief software guide

(This is a very short guide on the basics, and full software information can be found in the Pyris software help function)

- A sample must be able to fit within the aluminium pans which are shown in Fig 8. And it must also be weight prior to use so that the weight can be recorded within the Pyris software.
- The sample should be able to fit in the pan and be able to be crimped to create a container with no air gaps like that in Fig 9.
- The left hand furnace is the reference furnace which should contain an empty sample pan and the right hand furnace should contain a sample within a sealed pan.
- To seal a sample within a sample pan, the sample pan crimper (Fig 10) is to be used.
- Once the sample is placed inside a pan and a lid put on top of the sample (like Fig 8 but with a small sample in the pan under the lid) it can then be placed onto the crimper like in Fig 11
- Press down on the top of the crimper and what should result is a crimped pan like in Fig 9. (This is a picture of an empty pan and the sample should be covered in aluminium and have no air gaps.)
- Using vacuum tweezers, place an empty sample pan in the left hand furnace and a loaded sample pan in the right hand furnace, like Fig 12.
- Make sure the pans are concentrically centred to allow the platinum lid to fit back into the furnace and not be touching the aluminium pan like in Fig 13
- Now, replace the platinum lids (Fig 14) for both furnaces and twist the furnace enclosure so that the furnace is covered.
- There is a hole in the DSC lid to allow for the handle of the furnace cover, so if the DSC lid does not close, it is because the enclosure has not been twisted shut.
- Now the Pyris software can be used to write the recipe of the DSC run.
- Fill out the ‘sample info’ tab and notice that within ‘sample info’, the weight needs to be input manually as highlighted in Fig 15
- Fill out the ‘Initial State’ tab (Fig 16a) default settings are:
    - Start the Run: Action occurs immediately
    - Switch the Gas to Helium at 20 ml/min: Action occurs immediately
- Set initial temperature to 40 °C as it is above room temperature so is easy to equilibrate to and initial force to 100mN for standard recipes.
- Under ‘Program’ tab , fill out your recipe. ‘Add Step’ adds a step after the highlighted item, whereas ‘Insert Step’ inserts a step before the highlighted item. End condition of ‘Go To: 40 °C’ is usually used. Then click done.
- Click on the ‘View Program’ tab to review your recipe and conditions.
- Click ‘Start/Stop’ to begin the run (Fig 16b)
- Once the DSC is running, you can select which curves to view under the ‘Curves’ drop down option at the top of the ‘Instrument Viewer’
- You can right click on the axes to re-scale them, but the default scales are often most useful.

Appendix B

Saving and Analysing DSC Data

- Once a run has finished, click File > Save All
- The file can then be opened with 'Pyris Data Analysis'
- Once opened the file can be exported as a text file through File > Export Data > ASCII format… and plotted in alternative software
- Within the Data Analysis, values can be easily calculated by selecting Calc > ___. The use of these 'calc' functions are intuitive and help is found within the Pyris software if needed.

- This guide has briefly detailed how to use the hardware and how to start a simple run.

- A fully detailed procedure for re-calibrating the instrument can be found in the red ring-binder and also in the shared drive.

Figures

1.

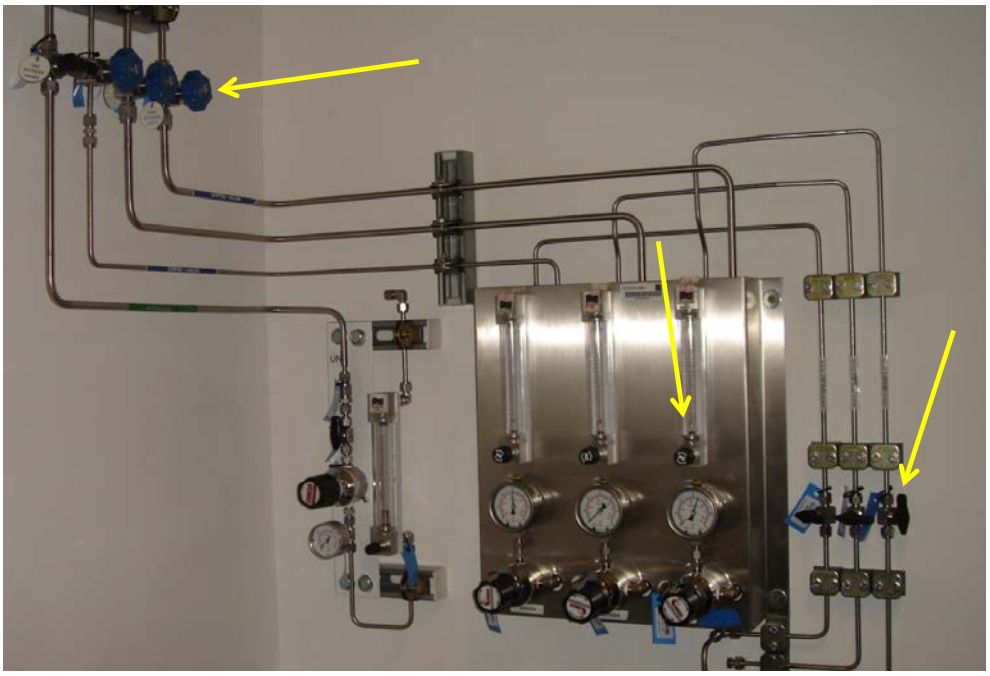

2.

Pressure gauge on the right hand side of the DSC should read around 3 – 6 psi

3.

Ensure these valves are open

By-pass

4.

5.

Use the small handle to rotate the furnace enclosure to reveal the 2 furnaces

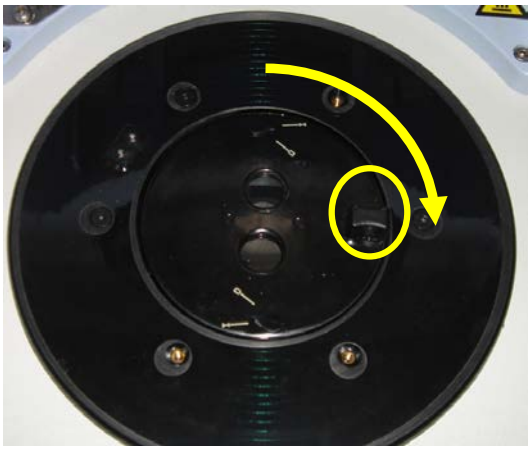

6.

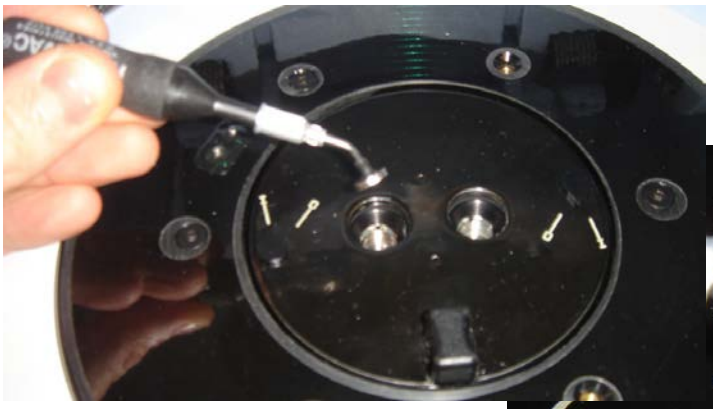

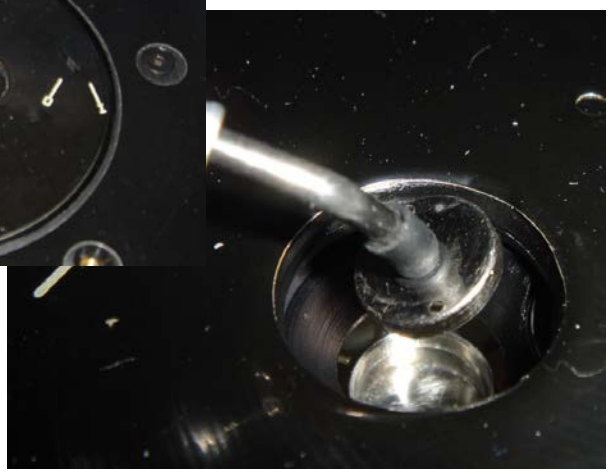

7.

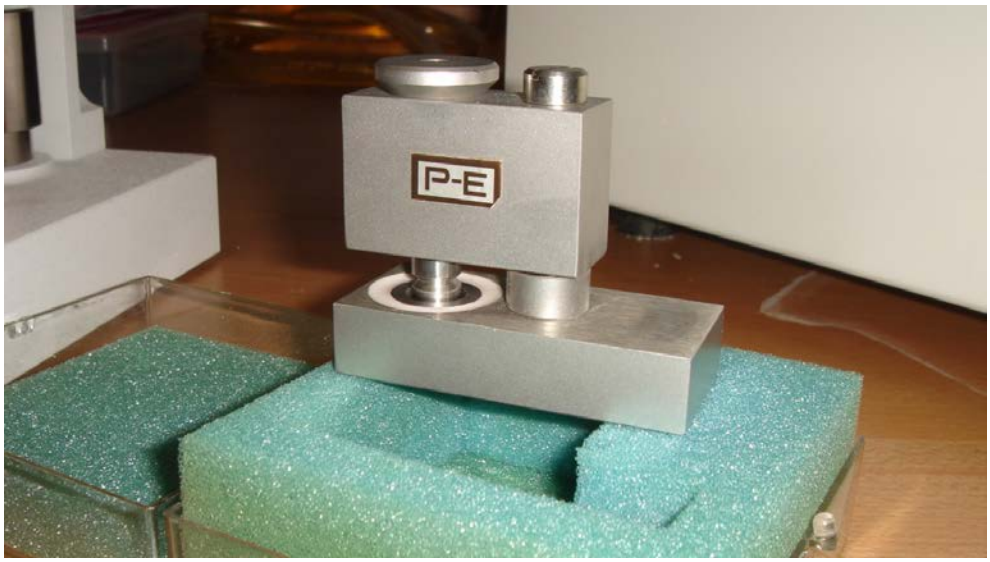

8.

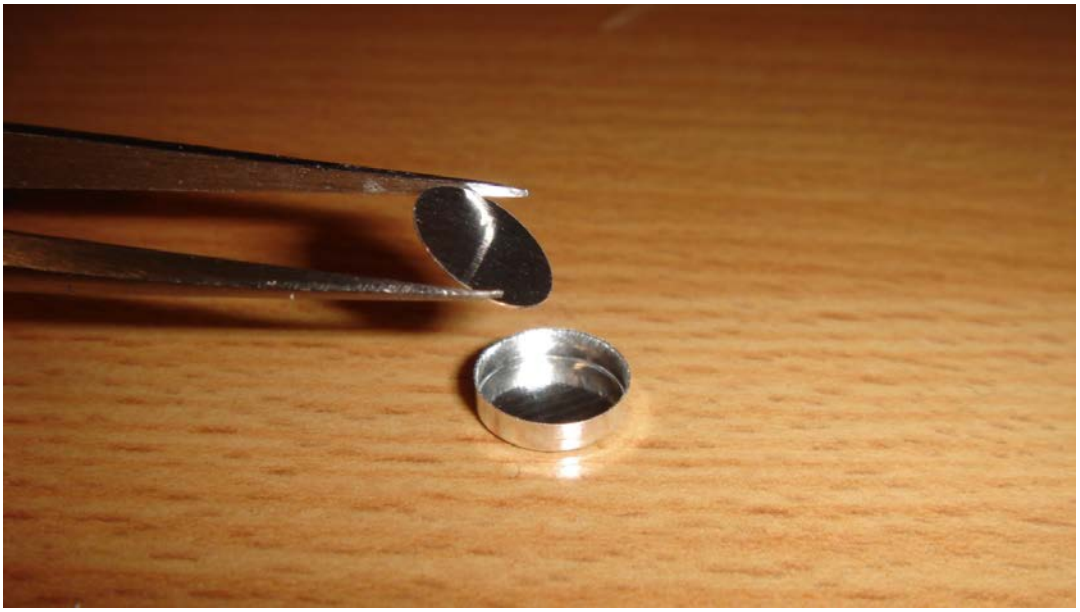

9.

10.

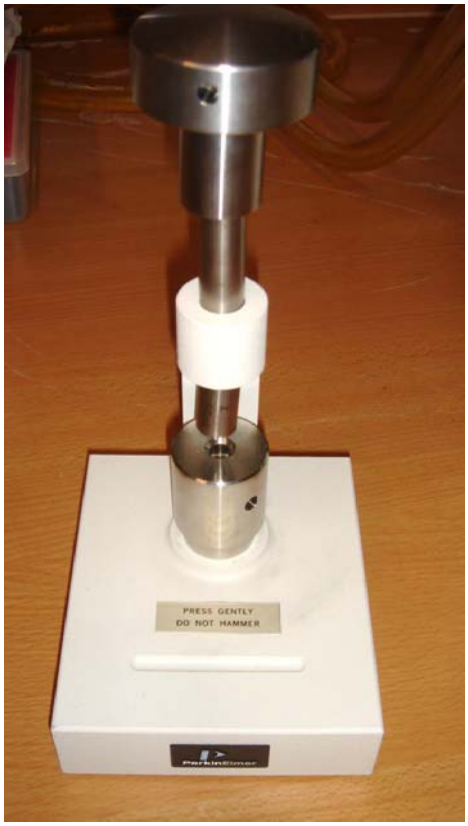

11.

12.

13.

14.

15.

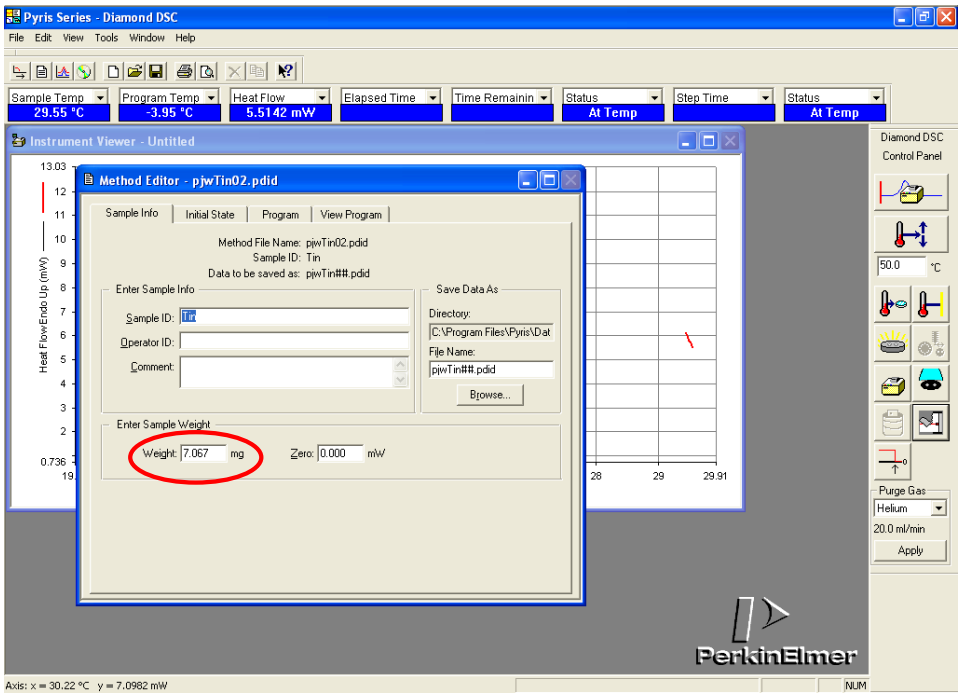
Pyris Series - Diamond DSC
File Edit View Tools Window Help
Sample Temp 29.55 °C
Program Temp -3.95 °C
Heat Flow 5.5142 mW
Elapsed Time
Time Remainin
Status At Temp
Step Time
Status At Temp
Instrument Viewer - Untitled
Method Editor - pjwTin02.pdid
Sample Info
Initial State
Program
View Program
Method File Name: pjwTin02.pdid
Sample ID: Tin
Data to be saved as: pjwTin##.pdid
Enter Sample Info
Sample ID: Tin
Operator ID:
Comment:
Save Data As
Directory: C:\Program Files\Pyris\Dat
File Name: pjwTin##.pdid
Browse...
Enter Sample Weight
Weight: 7.067 mg
Zero: 0.000 mW
Heat Flow Endo Up (mW)
Diamond DSC Control Panel
50.0 °C
Purge Gas
Helium
20.0 ml/min
Apply
PerkinElmer
Axis: x = 30.22 °C y = 7.0982 mW
NUM

16.

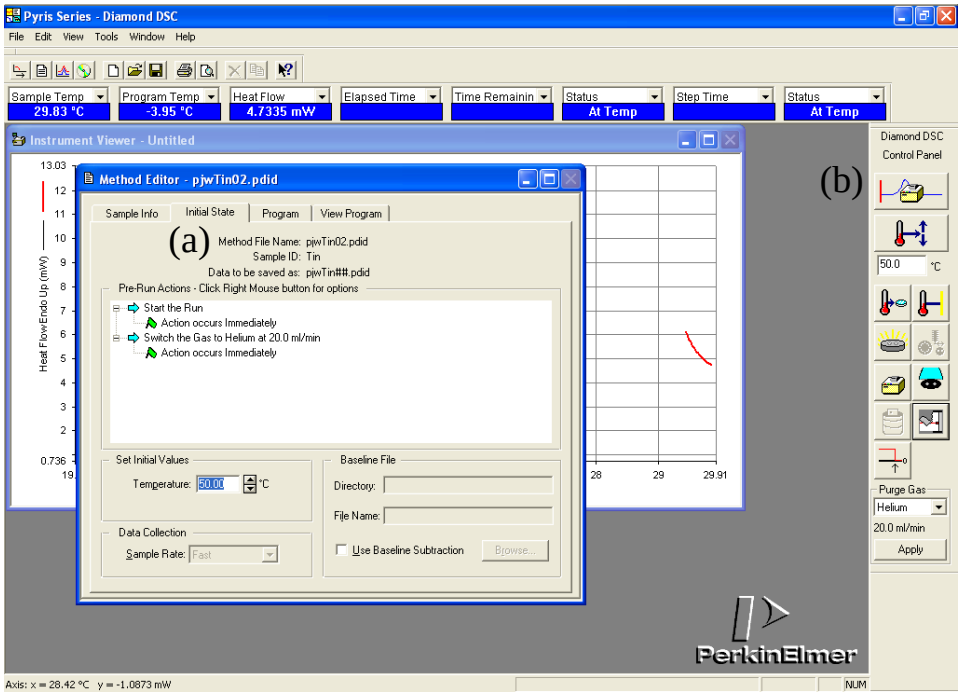
Pyris Series - Diamond DSC
File Edit View Tools Window Help
Sample Temp 29.83 °C
Program Temp -3.95 °C
Heat Flow 4.7335 mW
Elapsed Time
Time Remainin
Status At Temp
Step Time
Status At Temp
Instrument Viewer - Untitled
Method Editor - pjwTin02.pdid
Sample Info
Initial State
Program
View Program
(a)
Method File Name: pjwTin02.pdid
Sample ID: Tin
Data to be saved as: pjwTin##.pdid
Pre-Run Actions - Click Right Mouse button for options
Start the Run
Action occurs Immediately
Switch the Gas to Helium at 20.0 ml/min
Action occurs Immediately
Set Initial Values
Temperature: 50.00 °C
Baseline File
Directory:
File Name:
Data Collection
Sample Rate: Fast
Use Baseline Subtraction
Browse...
(b)
Heat Flow Endo Up (mW)
Diamond DSC Control Panel
50.0 °C
Purge Gas
Helium
20.0 ml/min
Apply
PerkinElmer
Axis: x = 28.42 °C y = -1.0873 mW
NUM

Appendix C TMA Standard Operating Procedure

TMA
Set-up and Operation Procedure

Prepared By	Signature	Date
Paul Bastock		1st September 2014

Reviewed By	Signature	Date
Dan Hewak		
Ed Weatherby		
Khouler Kahn		
Chris Craig		

Rev #	Who	Signature	Date
2			
3			
4			
5			
6			

TMA
Set-up and Operation Procedure

Trained Users	Signature	Date
Paul Bastock		
Chris Craig		
Khouler Kahn		
Stanley Tse		
Cui Long		

Checklist Before Starting Up

This standard operating procedure is a guide, and more detailed information can be found in the Pyris Help function, manuals kept in the red ring binder and in the shared drive

	Checklist	Comment	Notes
1	Make sure you have read and signed the risk assessment	Make any amendments necessary for your particular analysis	The risk assessment is kept in the lab's red ring binder and an electronic copy stored on the shared drive
2	Make sure the material being analysed is covered by an up to date COSHH form	If not, create a COSHH and save it on the shared area and also make a hard copy for the red ring binder	A list of COSHH forms already in place are found in the shared area
3	Turn on the gas at the wall for the gas you plan to use during the thermal analysis and check that there is pressure/flow	Before doing this, check "zepler institute facilities" updates to see if there are any current issues with gas supplies. If there is no pressure, check with Ed Weatherby as first contact, then with technical support (Mark Lessey)	The gas should be turned off at the valves (Fig 1) after each run to ensure no gas is flowing over a prolonged time and wasted. All gas valves are labeled.
5	Make sure all the connections to the TMA are securely in place	The power connections can come out easily, so they are held in place with cable ties and laser table posts (Fig 2)	There is only one gas purge control between the TG/DTA and the TMA, so make sure the communication cable is plugged into the TMA
6	Make sure the correct probe and cylinder are in place.	Directions on how to change the probes and cylinders are within the TMA Module which is kept in the Red ring-binder in the laboratory.	A list of probes and cylinders are in this SOP and their uses are described.
7	Before starting a run, confirm whether the sample can be prepared into a suitable form	A sample must be a small shape which has a known volume like a rod, fibre or cube	The sample should have sharp edges and the volume of the sample should be accurately known. The sample also has size restraints set by the probe and cylinder dimensions.

Starting up the TMA and computer

- Turn on the required gas supply (Fig 1)
- Turn on the gas purge MFC box (Fig 3), this is controlled by the Pyris software, so the flow meters will read 0
- Turn on the by pressing the green button on the front of the TMA (Fig 3)
- Watch the LCD panel, and wait for the following message to appear before doing anything else “LINKwaitFOR MB2 … Muse Ver.2.0”
- Open the TMA by pressing and holding down ‘Open’ (Fig 3)
- Make sure the correct probe and cylinder are installed, otherwise, see TMA Module for advice on how to change them
- Depending which probe/cylinder is used, position the equipment in it’s ‘zero’ position. This usually involves resting the probe on the bottom of the cylinder.
- After logging into the computer, make sure it is networked and then open up Pyris Manager software. Hover the mouse at the top of the monitor screen and click the right button (‘Diamond TMA’)
- The LCD screen on the TMA should now read “1 ISO.” on the top line with a temperature on the second line.
- Click Yes to initialise the probe as shown in Fig 4
- If you are using a purge gas, click ‘Apply’ under the ‘Purge Gas’ (Fig 5a) dialog box and make sure either Argon, Nitrogen or Oxygen is selected as your preference. Once it has been applied, make sure the flow meter is reading a value (say 200 ml/min) on the MFC box, and that the correct gas is flowing as per labels on the MFC box.
- In the main control panel, type in 40 °C under the ‘Go to Temperature’ (Fig 5b) button then press ‘Go to Temperature’ (Fig 5c). This brings the furnace temperature to the ‘Initial Temperature’ which is defined later.

The TMA is now ready for use……

TMA Probes and Cylinders

- There are a variety of probes and cylinders to accommodate thermal analysis covering glass transition temperatures, coefficient of thermal expansion, young's modulus, creep, stress relaxation, tensile properties and softening points of materials. There are many other properties which the equipment can interoperate if used in the correct manner.

- An example experiment of each probe type has been displayed in the below table and each probe/cylinder is kept in its labelled container.

Probe	Relevant Cylinder	Material	Example of Use
Knife Edge	Flat bottom (with 3-point bending accessory)	Silica	3-point bending
Penetration (large and small)	Flat bottom	Silica	Softening
Flat tip	Flat bottom	Silica or Alumina	CTE
Conical point	Flat bottom	Silica	Indentation
Elongation kit	Slotted	Silica and Stainless Steel	Elongation

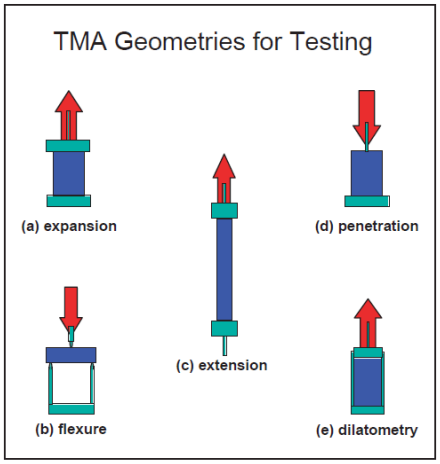

Appendix C

Sample preparation and brief software guide

(This is a very short guide on the basics, and full software information can be found in the Pyris software help function)

- A sample with known dimensions should be used, for example a rod or cube. The Pyris software uses the sample volume in the calculations it makes so it is necessary to have a well prepared sample.
- Once a sample has been prepared which can fit within its relevant probe/cylinder, it can then be inserted into the TMA.
- The elongation set-up is slightly different to conventional measurements and a sample prepared and sitting in the TMA is shown in Fig 6
- It is a good idea to apply a small amount of force (100 mN, Fig 5d) to ensure there is good contact between probe and cylinder if appropriate. This ensures for a true zero reading
- Click on the 'Read Zero' button (Fig 5e)
- Open the TMA furnace by pressing and holding the down button on the front of the TMA
- To insert the sample into the TMA, click on Sample Load (Fig 7) and input the distance in mm which you want the probe to move to allow room for you to insert the sample.
- Click on 'Move Tube' to open gap and 'Close Gap' to move the probe down into position with the sample in place.
- Visually check that the sample is in securely in position before closing the furnace, and repeat the process if necessary as it is crucial that the samples stays in position throughout the TMA run.
- Now close the TMA furnace by pressing and holding the up button on the front of the TMA
- Read Height can now be pressed and the sample height will automatically be updated. Sample width and depth or diameter is to be typed in manually.
- The 'initial state' within the sample editor offers a few TMA programs to be used. 'Force Linear Program' is standard, however, depending on the experiment which is being carried out, other programs may be more suitable.
- Fill in the user information in the 'sample info' tab. It is best to save to the desktop then transfer results to the network afterwards.
- Fill out the 'Initial State' tab (Fig 8) default settings are:
    - Start the Run: Action occurs immediately
    - Switch the Gas to Nitrogen at 200 ml/min: Action occurs immediately
- Set initial temperature to 40 °C as it is above room temperature so is easy to equilibrate to and initial force to 100mN for standard recipes.
- Under 'Program' tab , fill out your recipe. 'Add Step' adds a step after the highlighted item, whereas 'Insert Step' inserts a step before the highlighted item. End condition of 'Go To: 40 °C' is usually used. Then click done.
- Click on the 'View Program' tab to review your recipe and conditions.
- Click 'Start/Stop' to begin the run
- Once the TMA is running, you can select which curves to view under the 'Curves' drop down option at the top of the 'Instrument Viewer'
- You can right click on the axes to re-scale them, but the default scales are often most useful.

Saving and Analysing TMA Data

- Once a run has finished, click File > Save All
- The file can then be opened with 'Pyris Data Analysis'
- Once opened the file can be exported as a text file through File > Export Data > ASCII format… and plotted in alternative software
- Within the Data Analysis, values can be easily calculated by selecting Calc > ___. The use of these 'calc' functions are intuitive and help is found within the Pyris software if needed.

- This guide has briefly detailed how to use the hardware and how to start a simple run.

- A fully detailed procedure for re-calibrating the instrument can be found in the red ring-binder and also in the shared drive.

Figures

1.

Oxygen: clear line
Nitrogen: blue line
Argon: green line
(from left to right)

2.

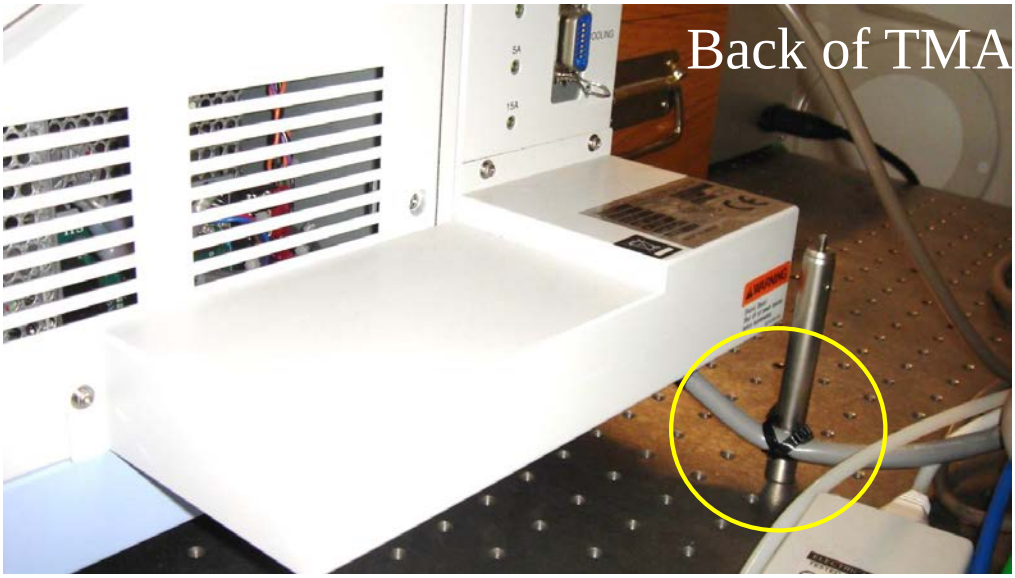

3.


AIR COOLING UNIT A
NITROGEN
GAS I
OXYGEN
GAS II

4.

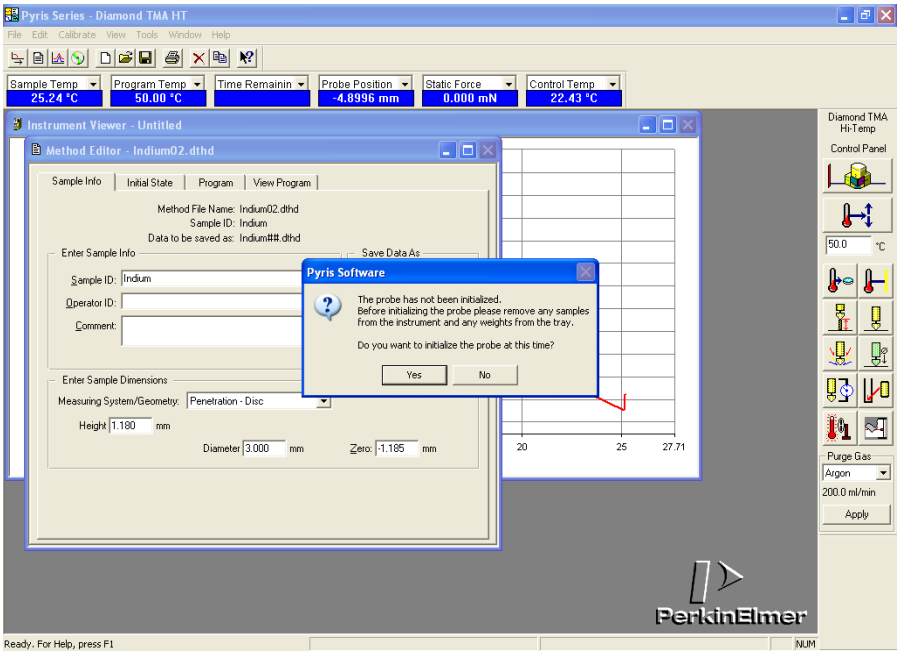
Pyris Series - Diamond TMA HT
Instrument Viewer - Untitled
Method Editor - Indium02.dthd
Sample Info
Initial State
Program
View Program
Method File Name: Indium02.dthd
Sample ID: Indium
Data to be saved as: Indium##.dthd
Enter Sample Info
Sample ID: Indium
Operator ID:
Comment:
Save Data As
Enter Sample Dimensions
Measuring System/Geometry: Penetration - Disc
Height 1.180 mm
Diameter 3.000 mm
Zero: -1.185 mm
Pyris Software
The probe has not been initialized.
Before initializing the probe please remove any samples from the instrument and any weights from the tray.
Do you want to initialize the probe at this time?
Yes
No
Diamond TMA Hi-Temp
Control Panel
Purge Gas
Argon
200.0 ml/min
Apply
PerkinElmer
Ready. For Help, press F1
NUM

5.

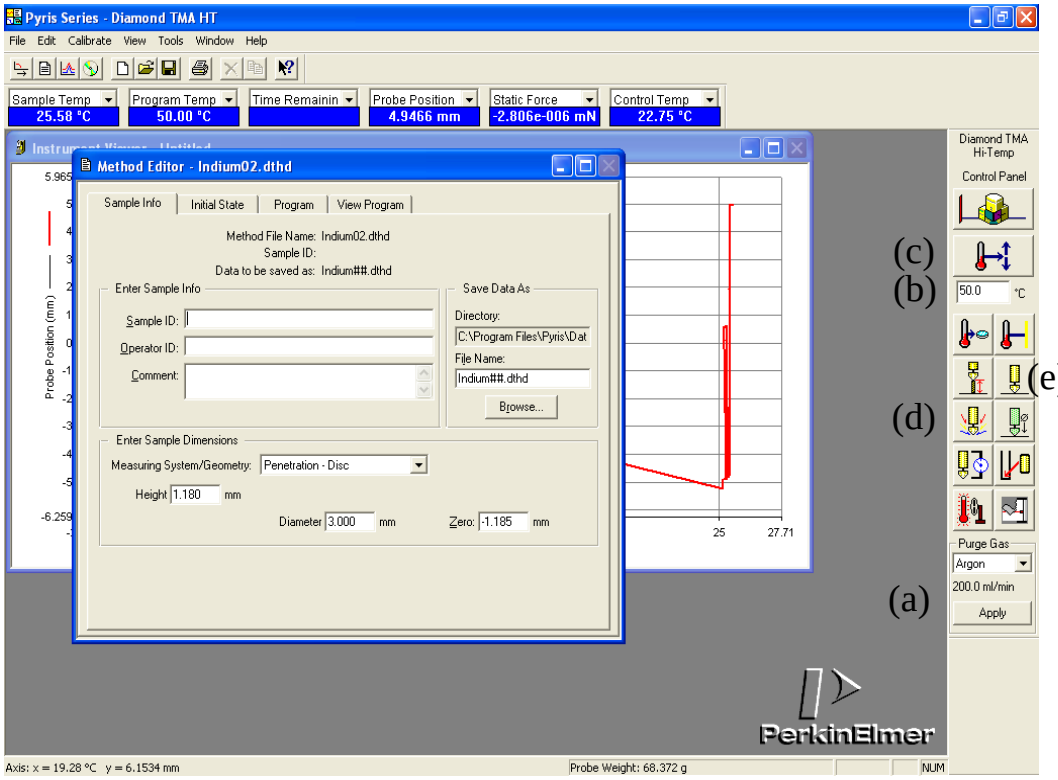
Pyris Series - Diamond TMA HT
File Edit Calibrate View Tools Window Help
Sample Temp 25.58 °C
Program Temp 50.00 °C
Time Remainin
Probe Position 4.9466 mm
Static Force -2.806e-006 mN
Control Temp 22.75 °C
Method Editor - Indium02.dthd
Sample Info
Initial State
Program
View Program
Method File Name: Indium02.dthd
Sample ID:
Data to be saved as: Indium##.dthd
Enter Sample Info
Sample ID:
Operator ID:
Comment:
Save Data As
Directory:
C:\Program Files\Pyris\Dat
File Name:
Indium##.dthd
Browse...
Enter Sample Dimensions
Measuring System/Geometry: Penetration - Disc
Height 1.180 mm
Diameter 3.000 mm
Zero: -1.185 mm
Probe Position (mm)
25
27.71
Diamond TMA Hi-Temp
Control Panel
50.0 °C
Purge Gas
Argon
200.0 ml/min
Apply
(a)
(b)
(c)
(d)
(e)
PerkinElmer
Axis: x = 19.28 °C y = 6.1534 mm
Probe Weight: 68.372 g
NUM

6.

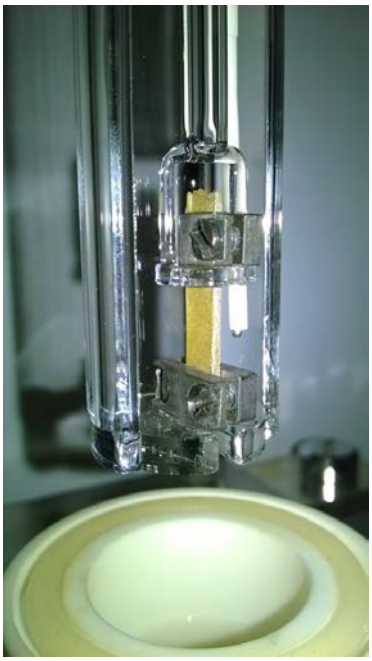

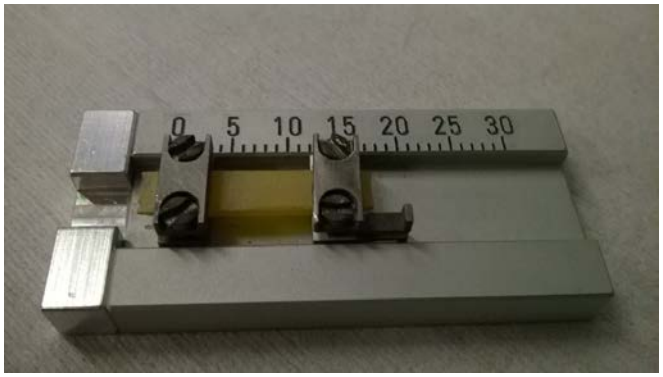
0 5 10 15 20 25 30

7.

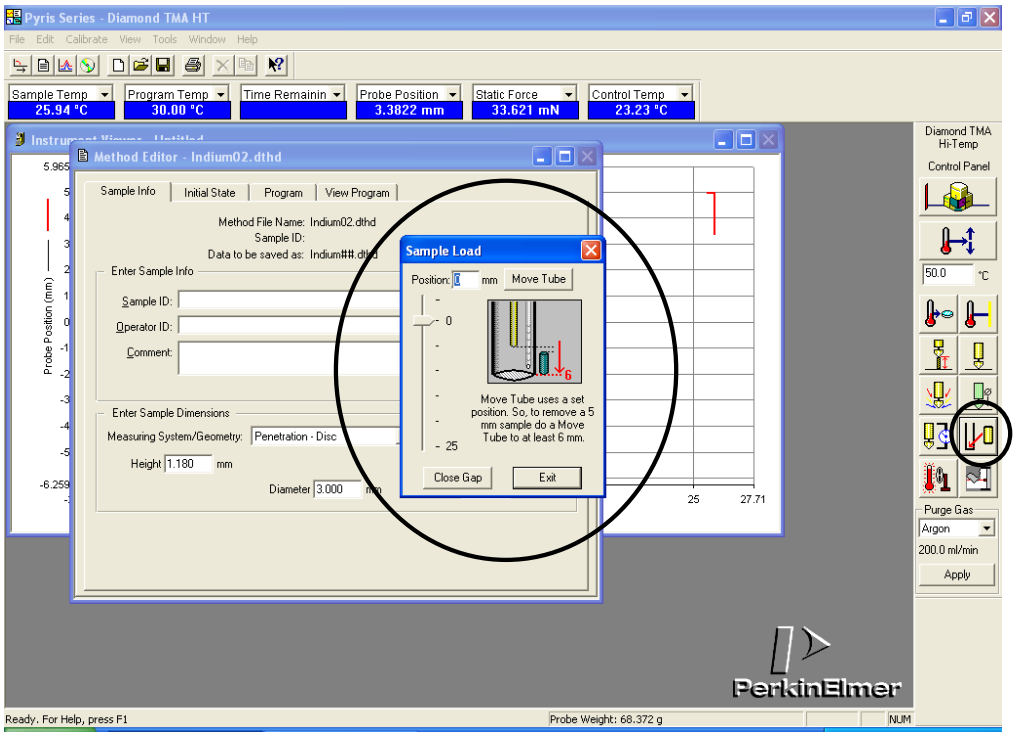
Pyris Series - Diamond TMA HT
Method Editor - Indium02.dthd
Sample Load
Move Tube uses a set position. So, to remove a 5 mm sample do a Move Tube to at least 6 mm.
Close Gap
Exit
Diamond TMA Hi-Temp Control Panel
Purge Gas
Argon
200.0 ml/min
Apply
PerkinElmer
Ready. For Help, press F1
Probe Weight: 68.372 g

8.

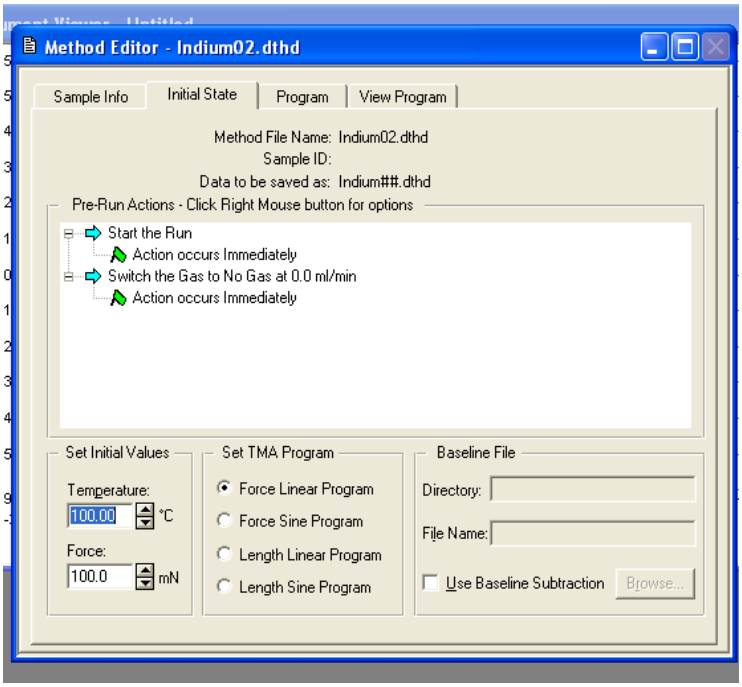
Method Editor - Indium02.dthd
Sample Info
Initial State
Program
View Program
Method File Name: Indium02.dthd
Sample ID:
Data to be saved as: Indium###.dthd
Pre-Run Actions - Click Right Mouse button for options
Start the Run
Action occurs Immediately
Switch the Gas to No Gas at 0.0 ml/min
Action occurs Immediately
Set Initial Values
Temperature:
100.00
°C
Force:
100.0
mN
Set TMA Program
Force Linear Program
Force Sine Program
Length Linear Program
Length Sine Program
Baseline File
Directory:
File Name:
Use Baseline Subtraction
Browse...

Appendix D TG/DTA Standard Operating Procedure

TG/DTA
Set-up and Operation Procedure

Prepared By	Signature	Date
Paul Bastock		1st September 2014

Reviewed By	Signature	Date
Dan Hewak		
Ed Weatherby		
Khouler Kahn		
Chris Craig		

Rev #	Who	Signature	Date
2			
3			
4			
5			
6			

TG/DTA
Set-up and Operation Procedure

Trained Users	Signature	Date
Paul Bastock		
Chris Craig		
Khouler Kahn		
Stanley Tse		
Cui Long		

Checklist Before Starting Up

This standard operating procedure is a guide, and more detailed information can be found in the Pyris Help function, manuals kept in the red ring binder and in the shared drive

	Checklist	Comment	Notes
1	Make sure you have read and signed the risk assessment	Make any amendments necessary for your particular analysis	The risk assessment is kept in the lab's red ring binder and an electronic copy stored on the shared drive
2	Make sure the material being analysed is covered by an up to date COSHH form	If not, create a COSHH and save it on the shared area and also make a hard copy for the red ring binder	A list of COSHH forms already in place are found in the shared area
3	Turn on the gas at the wall for the gas you plan to use during the thermal analysis and check that there is pressure/flow	Before doing this, check "zepler institute facilities" updates to see if there are any current issues with gas supplies. If there is no pressure, check with Ed Weatherby as first contact, then with technical support (Mark Lessey)	The gas should be turned off at the valves (Fig 1) after each run to ensure no gas is flowing over a prolonged time and wasted. All gas valves are labeled.
4	Check that the extract system works and the extract line is securely in place	Check "zepler institute facilities" updates for this information	The extract is flexible, so make sure it is fixed in place well
5	Make sure all the connections to the TG/DTA are securely in place	The power connections can come out easily, so they are held in place with cable ties and laser table posts (Fig 2)	There is only one gas purge control between the TG/DTA and the TMA, so make sure the communication cable is plugged into the TG/DTA
6	Make sure there is sufficient powder on the 2 platinum thermocouples/balances	The alumina prevents and crucibles from sticking to the platinum thermocouples/balances	If you need more alumina powder then it can be found in the chemical storage cupboard
7	Make sure you have 2 identical crucibles for analysis	Both reference and sample crucibles need to be the same in order to get an accurate result	There is a selection of crucibles available, however, users must purchase their own specialty crucibles if needed (eg. Platinum) Make sure the crucibles you use are suitable and don't react with your sample at elevated temperatures. Also ensure that you are purging the chamber with necessary gas regarding both crucible and sample

Appendix D

Starting up the TG/DTA and computer

- Turn on the required gas supply (Fig 1)
- Turn on the gas purge MFC box (Fig 3), this is controlled by the Pyris software, so the flow meters will read 0
- Turn on the TG/DTA by pressing the green button on the front of the TG/DTA (Fig 3)
- Watch the LCD panel, and wait for the following message to appear before doing anything else "LINKwaitFOR MB2 … Muse Ver.2.0"
- Open the TG/DTA by pressing and holding down 'Open' (Fig 3)
- Make sure there is sufficient alumina powder on the crucible holder so as to prevent sticking. Fig 4 shows an adequate amount.
- Load your 2 empty crucibles using tweezers (Fig 5), BE EXTREMELY CAREFUL NOT TO PUT TOO MUCH FORCE ON THE ARMS, AND MAKE SURE NOT TO KNOCK THEM. *Knocking the arms or applying any force, or a weight much more than 20 mg requires a full recalibration!!* It is best to drop the crucible from a very small height to avoid applying any more force on the arms.
- Close the TG/DTA by pressing and holding down 'Close' (Fig 3)
- After logging into the computer, make sure it is networked and then open up Pyris Manager software. Hover the mouse at the top of the monitor screen and click the left button ('Diamond TG/DTA')
- The LCD screen on the TG/DTA should now read "1 READY" on the top line with a voltage and temperature on the second line.
- If you are using a purge gas, click 'Apply' under the 'Purge Gas' (Fig 7a) dialog box and make sure either Argon, Nitrogen or Oxygen is selected as your preference. Once it has been applied, make sure the flow meter is reading a value (say 200 ml/min) on the MFC box, and that the correct gas is flowing as per labels on the MFC box.
- In the main control panel, type in 40 °C under the 'Go to Temperature' (Fig 7b) button then press 'Go to Temperature' (Fig 7c). This brings the furnace temperature to the 'Initial Temperature' which we will define later.

The TG/DTA is now ready for use……

Sample preparation and brief software guide

(This is a very short guide on the basics, and full software information can be found in the Pyric software help function)

- Fill in the user information in the ‘sample info’ tab. It is best to save to the desktop then transfer results to the network afterwards (Fig 7d).
- Click on the ‘Zero Weight’ button (Fig 7e), then ‘Sample Weight’ (Fig 7f), if the weight does not come up as 0 mg, then continue clicking on zero and sample weight until 0 mg is displayed. It may not display as 0 mg at first due to vibrations from loading the crucibles.
- Fill out the ‘Initial State’ tab (Fig7g), default setting are:
    - Start the Run: Action occurs immediately
    - Switch the Gas to Nitrogen at 20 ml/min: Action occurs immediately
- Set initial temperature to 40 °C as it is above room temperature so is easy to equilibrate to.
- Under ‘Program’ tab (Fig 7h), fill out your recipe. ‘Add Step’ adds a step after the highlighted item, whereas ‘Insert Step’ inserts a step before the highlighted item. End condition of ‘Go To: 40 °C’ is usually used. Then click done.
- Click on the ‘View Program’ tab to review your recipe and conditions.
- Once you are happy, open the TG/DTA by pressing ‘Open’ on the front on the TG/DTA. And carefully remove the sample crucible (on the right, Fig 6)
- Place the crucible on the silver plate on top of the TG/DTA (Fig 6) and carefully load your ~10 mg sample into the crucible. Make sure there is no part of the sample over the top of the crucible as this can lead to the sample melting on to the thermocouple arms and destroy them.
- Load the full crucible back onto the sample holder as previously described
- Press and hold down the ‘Close’ button again until the furnace no longer goes any further back.
- Click on the ‘Sample Info’ tab within the Pyris software and keep an eye on the sample weight. Now click on the ‘Sample Weight’ button (Fig 7f). Keep clicking this every few seconds until the value settles. There is usually some vibration from loading the sample which needs to settle. It can take up to a few minutes for the weight to fully settle.
- You should now see a value of around 10 mg in the ‘Weight: ‘ box.
- Click ‘Reset Monitor’, ‘Zero DTA’ and ‘Start/Stop’ in that order to start the run (Fig 8 a-c respectively)
- Once the TG/DTA is running, you can select which curves to view under the ‘Curves’ drop down option at the top of the ‘Instrument Viewer’ (Fig 8d)
- ‘Weight’ and ‘Heat Flow’ are standard.
- You can right click on the axes to re-scale them, but the default scales are often most useful.

Appendix D

Saving and Analysing TG/DTA Data

- Once a run has finished, click File > Save All
- The file can then be opened with 'Pyris Data Analysis'
- Once opened the file can be exported as a text file through File > Export Data > ASCII format… and plotted in alternative software
- Within the Data Analysis, onset temperatures like T_g, T_x and T_m can be easily calculated by selecting Calc > Onset. Once selected, click and drag from a small distance before the peak where the curve is linear, to an x-value relative to near the top of the peak as shown in Fig 9. Then click Calculate and line the resulting arms up with the linear approach to the peak and the initial slope of the peak, as shown in Fig 10
- To straighten a curve, the Slope tool can be used. Click and drag to cover the section of the curve which you would like to define a new slope to (Fig 11) and then drag the arm to the slope which you wish to define for the selected curve length. The entire curve will pivot from the root of this arm (Fig 12)

- Most other functions are relatively intuitive and detailed guidelines on how to use more advanced functions can be found in the software help function.

- This guide has briefly detailed how to use the hardware and how to start a simple run.

- A fully detailed procedure for re-calibrating the instrument can be found in the red ring-binder and also in the shared drive.

Figures

1.

Oxygen: clear line
Nitrogen: blue line
Argon: green line
(from left to right)

2.

Power cable held by laser table post here

3.

MFC on left and TG/DTA on right

On/off button

On/off button

Open and Close

4.

5.

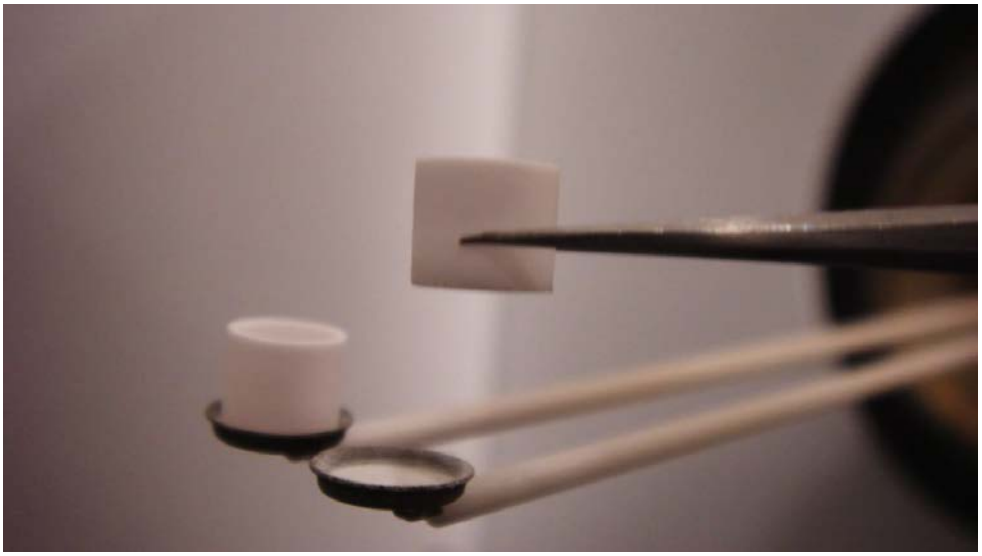

6.

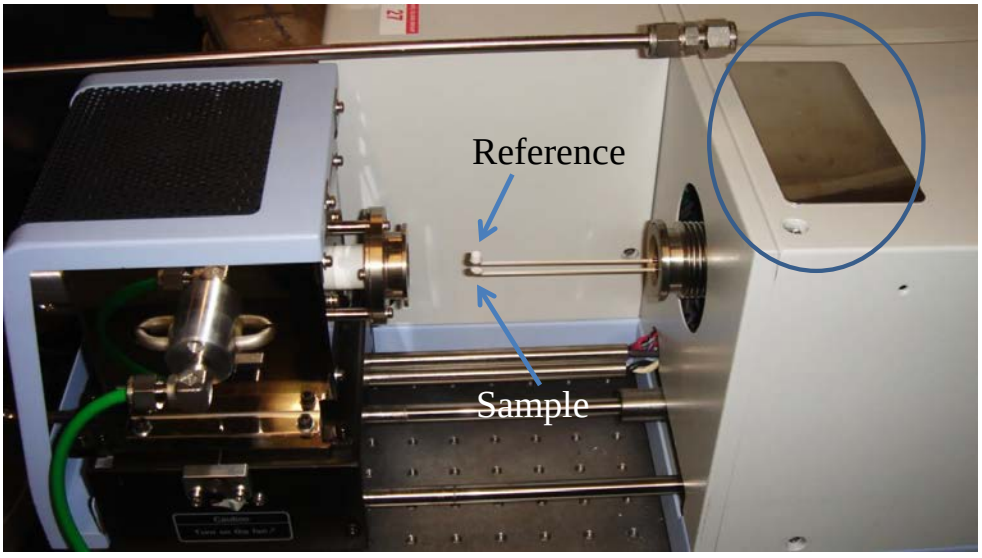

7.

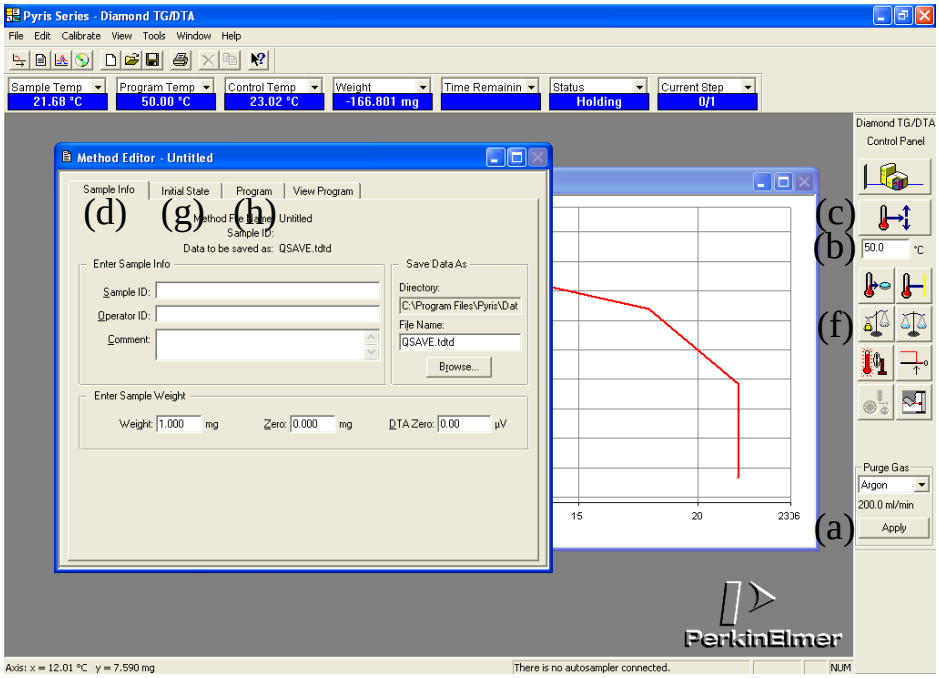
Pyris Series - Diamond TG/DTA
File Edit Calibrate View Tools Window Help
Sample Temp 21.68 °C
Program Temp 50.00 °C
Control Temp 23.02 °C
Weight -166.801 mg
Time Remainin
Status Holding
Current Step 0/1
Method Editor - Untitled
Sample Info
Initial State
Program
View Program
(d)
(g)
(h)
Data to be saved as: QSAVE.tdtd
Enter Sample Info
Sample ID:
Operator ID:
Comment:
Save Data As
Directory:
C:\Program Files\Pyris\Dat
File Name:
QSAVE.tdtd
Browse...
Enter Sample Weight
Weight: 1.000 mg
Zero: 0.000 mg
DTA Zero: 0.00 µV
Diamond TG/DTA Control Panel
(c)
(b)
50.0 °C
(f)
(e)
Purge Gas
Argon
200.0 ml/min
Apply
(a)
PerkinElmer
Axis: x = 12.01 °C y = 7.590 mg
There is no autosampler connected.
NUM

8.

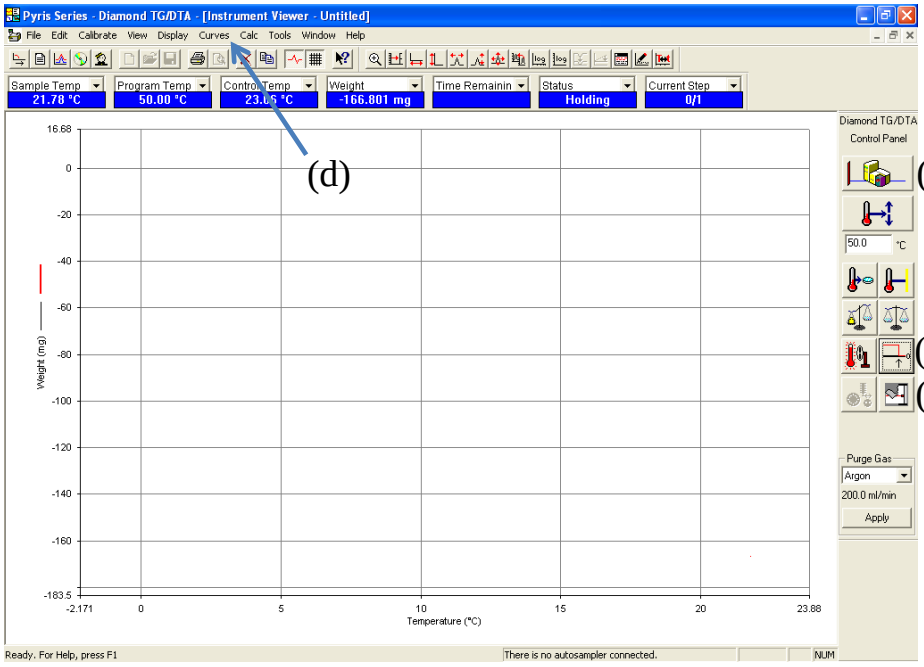
Pyris Series - Diamond TG/DTA - [Instrument Viewer - Untitled]
File Edit Calibrate View Display Curves Calc Tools Window Help
Sample Temp 21.78 °C
Program Temp 50.00 °C
Control Temp 23.06 °C
Weight -166.801 mg
Time Remainin
Status Holding
Current Step 0/1
(d)
Weight (mg)
Temperature (°C)
Diamond TG/DTA Control Panel
(c)
(b)
(a)
Purge Gas
Argon
200.0 ml/min
Apply
Ready. For Help, press F1
There is no autosampler connected.
NUM

9.

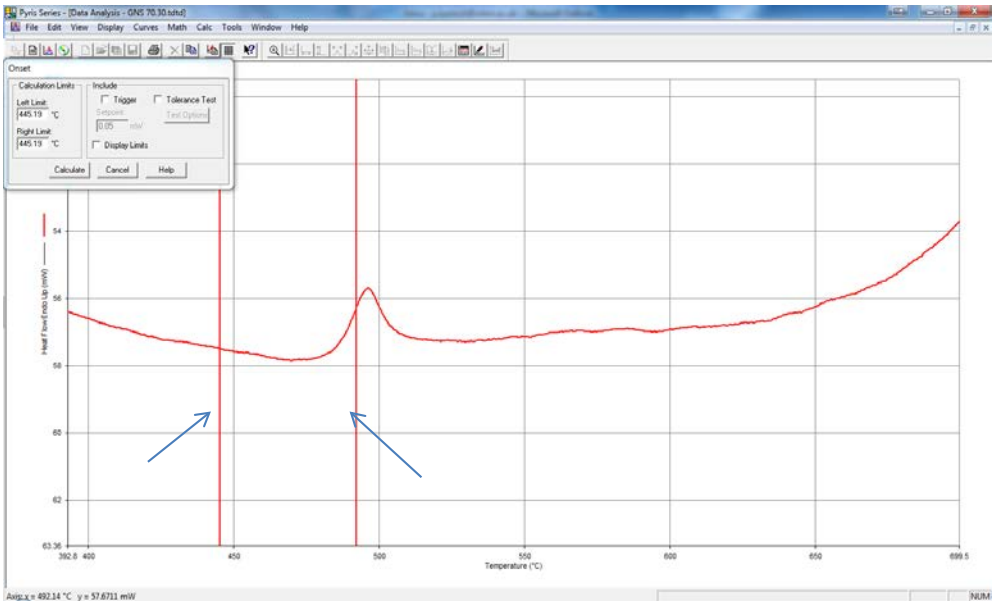
Onset
Calculate
Cancel
Help
Temperature (°C)

10.

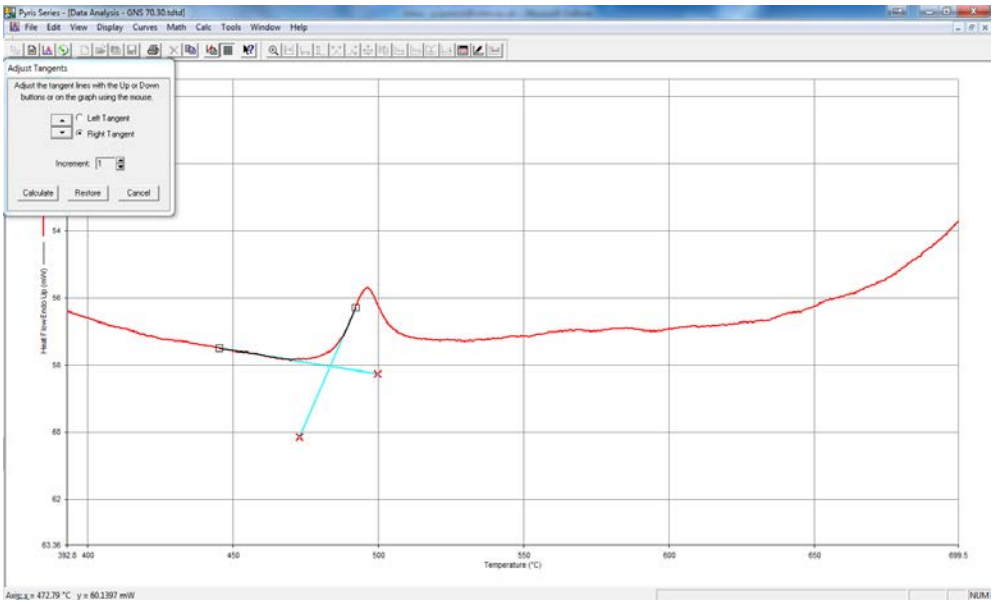
Adjust Tangents
Left Tangent
Right Tangent
Calculate
Restore
Cancel
Temperature (°C)

11.

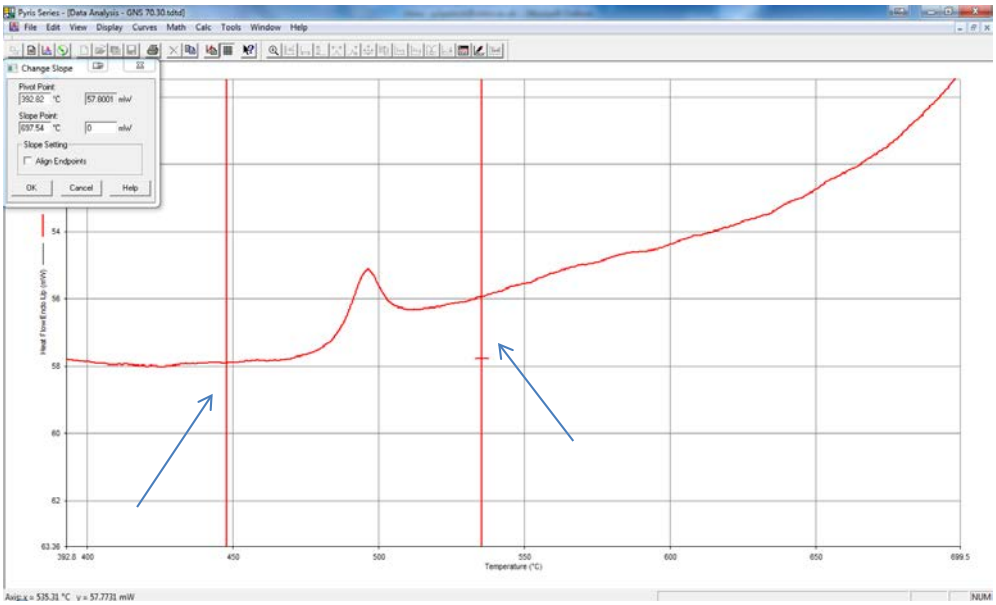
Change Slope
Pivot Point:
392.82 °C
57.8001 mW
Slope Point:
697.54 °C
0 mW
Slope Setting
Align Endpoints
OK
Cancel
Help
Heat Flow Endo Up (mW)
54
56
58
60
62
63.36
392.8
400
450
500
550
600
650
699.5
Temperature (°C)

12.

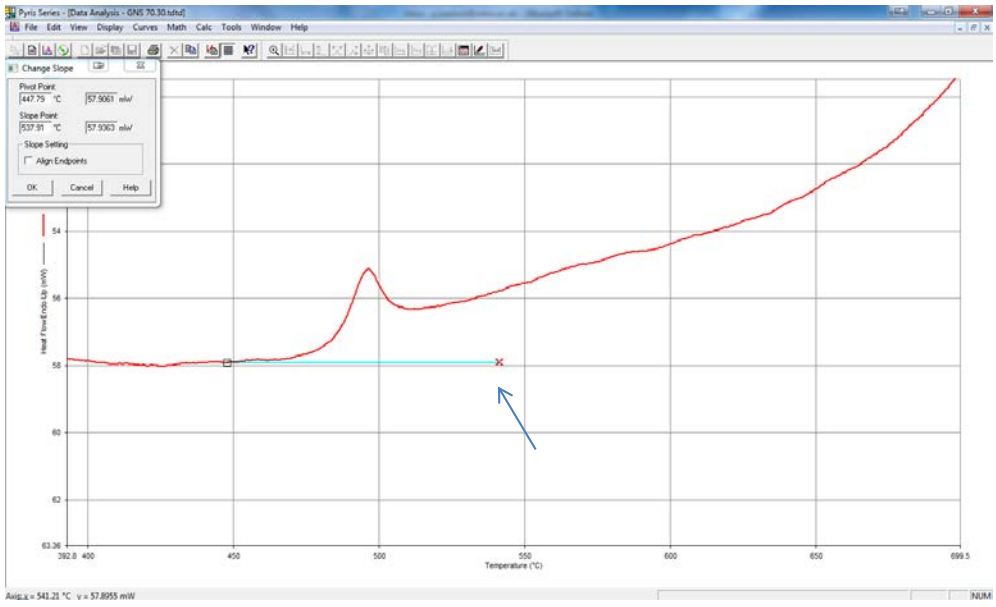
Change Slope
Pivot Point:
447.79 °C
57.9063 mW
Slope Point:
537.91 °C
57.9363 mW
Slope Setting
Align Endpoints
OK
Cancel
Help
Heat Flow Endo Up (mW)
54
56
58
60
62
63.36
392.8
400
450
500
550
600
650
699.5
Temperature (°C)

Appendix E Novel Glass Fibre Drawing Tower II Standard Operating Procedure

Novel Glass Tower 2
Set-up and Operation Procedure

Prepared By	Signature	Date
Paul Bastock		1st September 2014

Reviewed By	Signature	Date
Dan Hewak		
Ed Weatherby		
Khouler Kahn		
Chris Craig		

Rev #	Who	Signature	Date
2			
3			
4			
5			
6			

Novel Glass Tower 2
Set-up and Operation Procedure

Trained Users	Signature	Date
Paul Bastock		
Chris Craig		
Khouler Khan		
Cal Smith		
Henry Stenhouse		

Tower Checklist Before Powering On, For Experienced User

This standard operating procedure is a guide, and more detailed information can be found in the tower manuals kept in the red ring binder and in the shared drive

	Checklist	Comment	Notes
1	Turn on the cooling water system and make sure you get at least 7 litre/min flow	If the flow is too low, check filters (Fig 1) and flow meters (Fig 2).	DI water needs changed annually and filters to Remote Head and Generator need cleaned quarterly
2	Turn on the gas at the wall for the gas you plan to use during the fibre draw and check that there is pressure/flow	Before doing this, check emails to see if there are any current issues with gas supplies. If there is no pressure, check with Ed Weatherby as first contact, then with technical support (Mark Lessey)	The gas should be turned off at the valves (Fig 3) after each run to ensure no gas is flowing over a prolonged time and wasted. All gas valves are labeled.
3	Make sure the fibre draw is included in the risk assessment	Risk assessment is saved in the shared area. Modify if need-be and get signed by relevant personnel.	
4	Check all gas detection units	Check for any warnings or errors on the display panels.	No gas detection units are currently installed but will be in the near future.
5	Check that the extract system works	Switch on the extract (Fig 4) and make sure it is operating correctly and is fixed in a suitable position for the fibre draw.	The extract is flexible, so make sure it is fixed in place well
6	Check the time	The lab needs to be vacated by 6pm unless you have an out of hours risk assessment completed and signed.	Make sure you have enough time to do your full run and allow 30 minutes for the coil to cool down with chilled water and the susceptor is to be purged till it is at a reasonable temperature, <100oC
7	Network the computer	The network run file is found on the temp drive and is called “Soton-drives-for-home-and-labs.hta"	Use your most up to date login credentials, as oppose to lab credentials. If there is no network coverage, check the Ethernet cable is plugged in (Fig 5); reset the computer; then try serviceline x25656 if there is still no coverage.
8			

Furnace Set-Up Before Any Fibre Draw

- All glassware is made by the glassblowers in Chemistry (Paul Frampton and Lee Mulholland) who are happy to make more glassware for the furnace, just pay them a visit! (Tel: 02380593321)
- Make sure that the glassware is aligned properly and fixed in place so that it will not move during the fibre draw. This is a general precaution. If something is not aligned, simply alter the glassware or brackets so that it is aligned. The furnace is modular and is designed to be adjusted whenever necessary. Do not try and make-do with the current set-up if it's not perfect. Modify anything that needs to be.
- Make sure that the control thermocouple is firmly and fully slotted into the susceptor!! The position of the thermocouple must be kept constant so previous run's temperatures are relative. It may fall down slightly if it has not been checked for a long period of time. There is usually a small cable-tie holding it in place
- Use any glassware in the cupboard and use relevant susceptor. There are many different sizes of susceptor, glassware and RF coils to accommodate a large range of preforms.
- An additional inverted susceptor holder can be used in conjunction with the one in place to create a larger purged zone in the furnace which is useful when drawing glasses susceptible to oxidation. Details of this particular furnace modification and others are found in Paul Bastock's thesis with 3-D drawings.
- Make sure all purge line Chemcon fittings are firmly tightened
- Make sure the cane puller is move into, or out of position depending if you wish to use it.

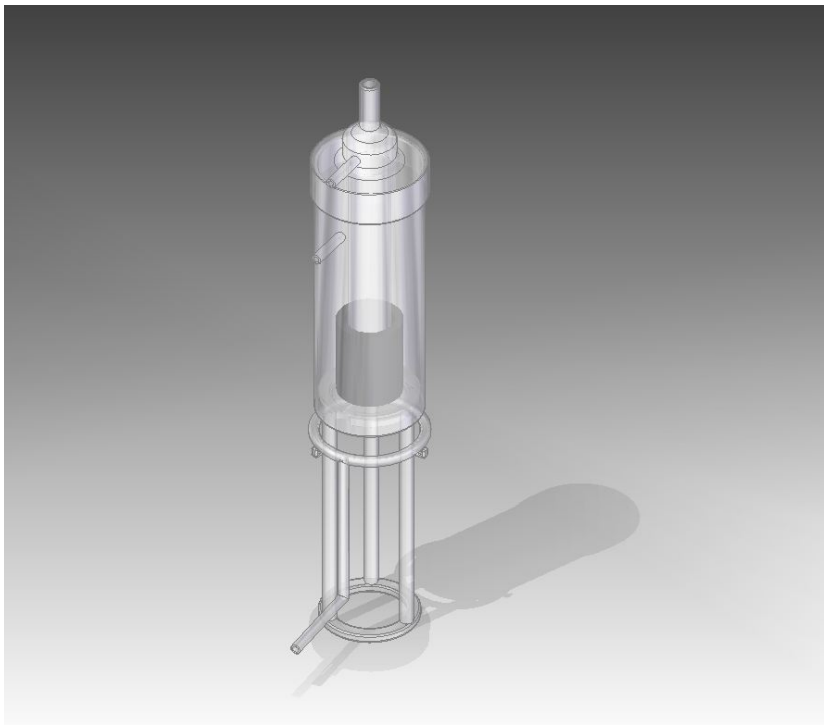

Steps to Turning on the System Ready for a Fibre Draw

- Turn on the water supply in the order pictured and make sure the paper towel is in place to stop overflowing and spillage (Fig 6+7)
- Turn on the gas supply to the gasses you intend to use (Fig 3) and open relevant flow meters and valves (Fig 8) the susceptor purge is usually around 4 l/min for graphite, and 1 l/min for stainless steel
- If you wish to use oxygen during fibre drawing, the valve must be opened in the software (Fig 29) and the "N2 to Solenoid" (Fig 3) must be open too
- Turn on the power switch on the corridor wall (53-51-20-L2-6) (Fig 9)
- Switch on the tower by pressing the green 'On' button on the tower (Fig 10)
- Wait till the alarm sounds then press the '24V' button (Fig 10)
- Login credentials are Username: 3 ; Password: 3 or you can simply press 'Start'
- If you need to use the tower with no limits on temperature etc, then use Username: 4 ; Password: 4.
- Press the green 'Activate' button on the touch screen to make the tower active. (Fig 11)
- Turn on the 'Flexitune' and 'Extract' switches behind the tower (Fig 4)
- Switch the Flexitune generator on under the stairs (Fig 12)
- You can now begin using the tower for fibre drawing.

Preform Set-up

- Once your preform has been properly cleaned and prepared, you can attach it to the preform holder using Ni:Cr wire (Fig 13)
- Add an optional weight onto the bottom end of the preform (Fig 14) to encourage a sharp neck during the initial drop.
- If you wish to use a vacuum or pressure during fibre drawing, then PTFE thread tape can be used so seal the preform to the preform holder (Fig 15) make sure you use plenty of tape to ensure a tight seal. This is the current method, and a new method can be designed if need-be for the modular fibre drawing tower.

Fibre Drawing Procedure

Vacuum/Pressure or Purge Line use

- To set up for a vacuum draw, you must turn the vacuum pump on (Fig 16+22) and also make sure the valve in Fig 17 (D) is set to the relevant option.
- Looking at Fig 17:
  - A – Pressure gauge in psi
  - B – Pressure bleed valve
  - C – Pressure throttle (Argon)
  - D – Pointing upwards = Pressure engaged ; Pointing downwards = Vacuum engaged
  - E – Vacuum bleed valve
  - F – Vacuum throttle
  - G – Vacuum gauge in mBar
- You must ensure the pressure flow meter has significant flow (Fig 8) when using the pressure option.
- The pressure/vacuum line to preform holder is transparent, whilst the purge line to preform holder is green (Fig 18) and can be interchanged simply by loosening the chuck in Fig 18
- The preform holder is simply connected to either line via the 6mm Chemcon Fitting
- The purge line is connected to the MFCs via the Swagelok fitting in Fig 19 and the vacuum/pressure line is fixed into the pressure/vacuum panel and should not be removed.
- The cooling ring (Fig 20) can also attached to the MFC's in Fig 19. A splitter can be added if the cooling ring and purge line need to be used at the same time.

Assembling Furnace/Preform

- Once the furnace is in the configuration/position you want. It is easiest to load the preform/preform holder from below. So have the loaded preform holder ready with attached weight etc if necessary and pass it through from the exit of the furnace all the way up to the preform feed chuck and connect preform holder to 6mm Chemcon fitting tightly. Make sure it is connected correctly by dis-assembling the Chemcon fitting fully and reassembling with the preform holder in place. It needs to be tight enough to hold the entire weight of the preform + weight + tension during fibre drawing.

Heating up the Furnace

- Press "Furnace" on the home page in Fig 11 and you will see the screen in Fig 21.
- Press the numerical button beside the "Run" button and you'll be able to input the desired temperature.
- The ramp rate at which the furnace will increase in temperature can be altered under settings, but 100oC/min is currently used.

Fibre Drawing

- Press "Fibre Draw" on the Furnace screen and you'll see Fig 22
- Pressing "SlowDown" in the "Preform" section activates the feed and will come down at the rate of the number under "Set" in mm/min
- Pressing "Run" in the "Capstan" section will start the take-up drum at the rate of the number under "Set" in m/min
- The "Pot" function toggles the use between the control panel and the dials in Fig 23

Appendix E

Fibre Drawing Procedure

Tips for fibre drawing

- Have a metal bowl ready to catch the falling preform neck
- Immediately throw the preform neck into the hot-glass bin unless it's to be kept for examination
- Have lots of tabs of electrical tape stuck closely to the take-up drum so they can be easily reached when trying to attach fibre to take-up drum
- Have the take-up drum running well before the preform is expected to neck so the fibre can immediately be stuck to the rotating drum
- As soon as the preform is visually necking, start the preform feed!
- Once the fibre is attached to the drum, then move the diameter gauge into position (Fig 24) it can then be positioned using the "unislides" and the diameter control interface detailed in Fig 25.
- Use the run sheet templates to note down as much information before, during and after the fibre draw as possible! Found here:

S:\Chalcogenides\Shared Files\Fabrication\Fibre\Fibre Drawing Run&Data Sheets

- Use the fibre drawing calculators prepared by Paul Bastock, found here:

S:\Chalcogenides\Shared Files\Fabrication\Fibre\Fibre Calculators

- A single mode fibre calculator matlab script is also found here, written by Paul Bastock
- When a new susceptor or furnace configuration is being used, calibrate the furnace. This is done by setting up an empty preform holder and securing the 'Monitor Thermocouple' into the centre of it. Position the preform so that the tip of the thermocouple is directly in line with the bottom of the furnace and take a temperature reading every 2mm-or-so until the top of the furnace is reached. Example furnace calibrations can be found here: S:\Chalcogenides\Shared Files\Fabrication\Fibre\Fibre Drawing Run&Data Sheets

Re-Spooling

- Once fibre has been drawn, It is best to re-spool as soon as possible to avoid any damage which can be caused to the fibre when it is on the take-up drum
- Position the re-spooler like that in Fig 26 and remove the blank plug fin Fig 27 and replace with the re-spooler cable. This will trip the Tower, but just press the 24V button and then the green “Activate” button on the home screen to re-activate the Tower, as in “Steps to Turning on the System Ready for a Fibre Draw”
- From the software home screen (Fig 11) press “Respooler” and you’ll see Fig 28.
- Press “Enable” under the “respooler” section, and within a few seconds, press the green button on the front of the respooler (Fig 29) and this will activate it, ready for use.
- Press “Pot On” in the “Capstan” section
- Take the END of the fibre draw and tape it onto the polystyrene bobbin.
- Make sure the 2 dials (Fig 23) are set to a low, or 0, position.
- Make sure the translator on the take-up drum is disengaged (Fig 30) and the one on the respooler is at a suitable level (the numbers relate to distance between each wind)
- Make the fibre tight by rotating the bobbin slightly, and press “Run” on both the “Capstan” and “Respooler” sections.
- Once the respooling has begun, you can increase the speed and make sure the torque is sufficiently high so the fibre isn't loose on the bobbin.

Appendix E

Software Operation and Tips

- The software is mostly self-explanatory, and additional information can be found in manuals kept in the Red Ring Binder or here :

S:\Chalcogenides\Shared Files\Labs and Equipment\Tower lab 1055\Fibre Drawing Tower Manuals

Mass Flow Controllers

- Press MFCs (Fig 21) within the fibre drawing page and the available gasses are displayed with their respective flow rates.
- To use oxygen, the shot-valve must be opened by pressing the button in Fig 31
- If the gas isn't coming through, turn the flow rate up to 5 to speed up the process, and wait till it comes through, then reduce to the desired flow rate.

Calibration

- If there is an offset, or a lag, between set and actual temperature and the thermocouple is firmly in place, then the "PID Temperature Control" (Fig 32) can be modified to resolve this. By changing the "Gain (DegC / % pwr)", a more controlled temperature can be achieved.

- The max power limit is usually kept at 100% but for low temperature fibre draws (<500oC) then reduce the power limit significantly to have a controlled temperature.

Cane Pulling

- The same steps are followed as “Fibre Drawing Procedure” for cane pulling, although you must ensure the cane puller is in position before starting the draw. Detailed in Fig 33
- Once the neck has dropped on the preform, cleave the neck off and place the fibre between the 2 rollers in Fig 34 and tighten using the wheel labelled in the figure.
- The rollers should touch the fibre/cane and have enough grip to pull the glass but not too much so as to crush it!!
- During caning, the temperature should make the glass soft enough so that it will deform when pulling on it (caning) but not high enough so that the glass drops down by itself. The cane should be tight throughout the whole cane-draw and should not have any flex in it.

Figures

1.

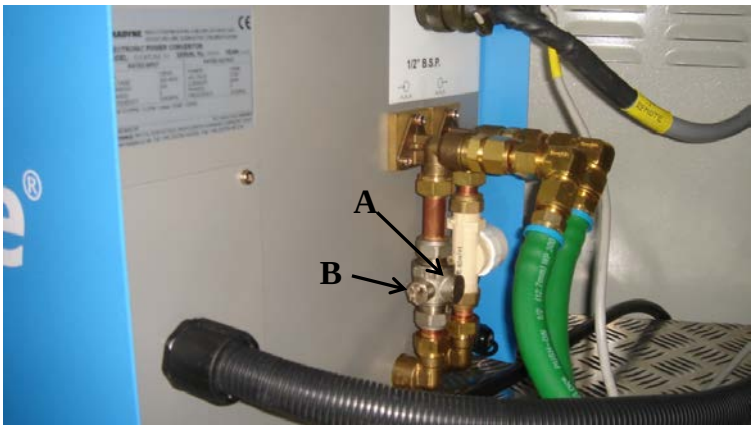

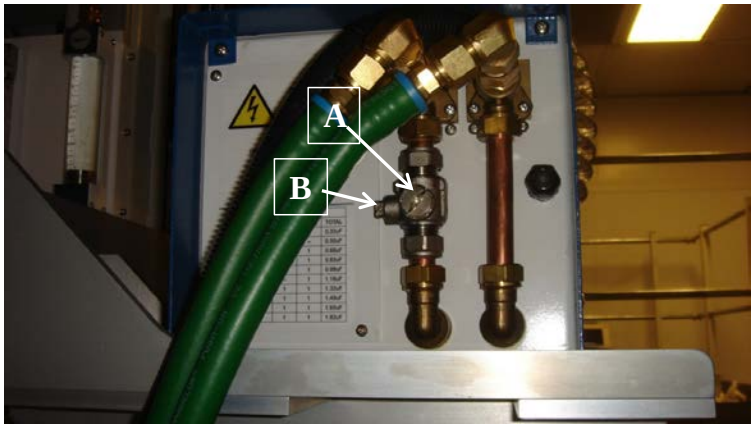

Open “A” with screwdriver to expose filter holder, and then turn “B” clockwise to expose filter. Remove filter with pliers
Top figure is power generator located under stairs.
Bottom figure is of remote read which the copper coil is connected to.

2.

Three flow meters should read ~4 litres/min
Large flow meter should read around 7-8 litres/min

3.

Gas panel located behind Tower 2's control unit. Each gas valve is labelled.

4.

3-Phase power supplies (located behind Tower 2) to various bits of equipment. Each of which are clearly labelled

5.

Make sure the network cable (yellow cable coming out of floor) is plugged in behind the hot-press and also into the computer here…

6.

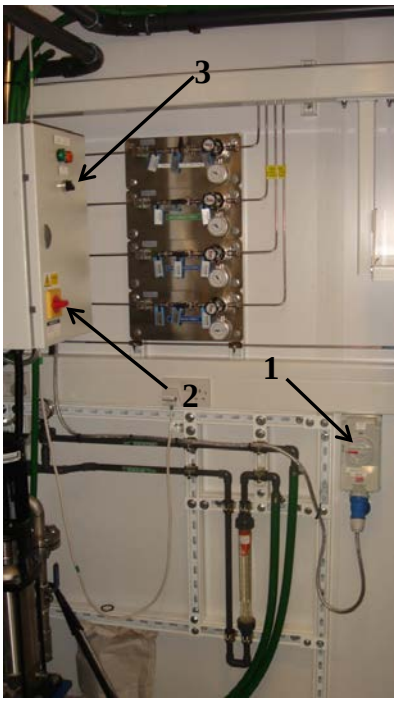

Switch water supply on in order shown and switch off in reverse order.
This is to the right of the stairs, underneath Tower 1's platform.

7.

Water can sometimes spurt out of this fixing when first turned on. (Window side of Tower 2) Keep paper towels there as temporary precaution.

8.

Gas panel (Window side of Tower 2) with flow meters for susceptor purge and preform pressure (labelled)

9.

Main power switch to Tower 2 (wall to the left of Tower 2 when looking straight at it)

10.

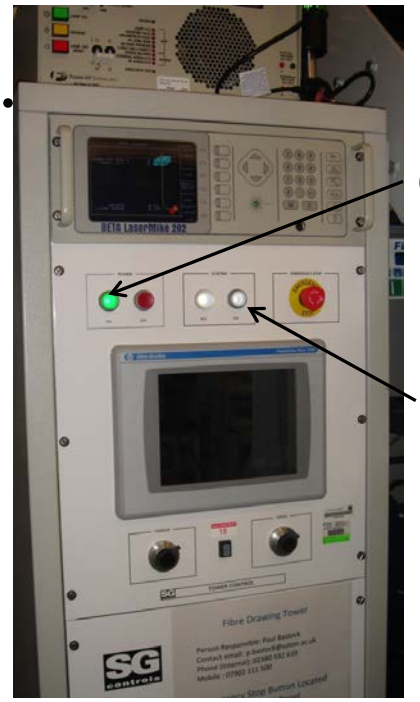

Tower 2 control unit

11.

Press here

12.

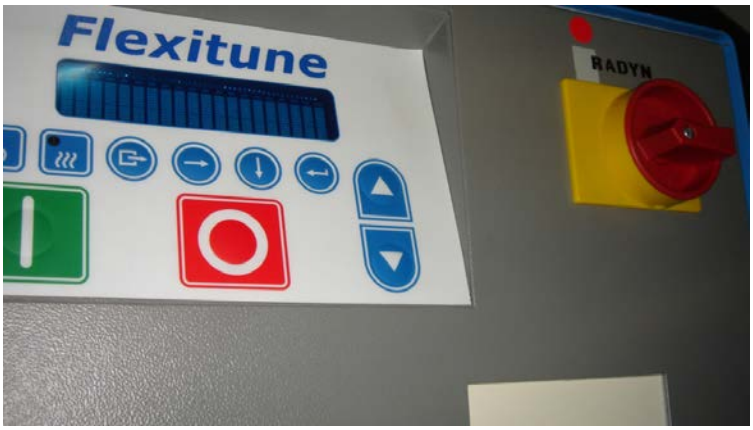

Twist red switch and wait till the LCD screen has stopped displaying words and reads the following message…

13.

14.

15.

16.

Vacuum pump located under stairs.
Power switch is left on, and located here

17.

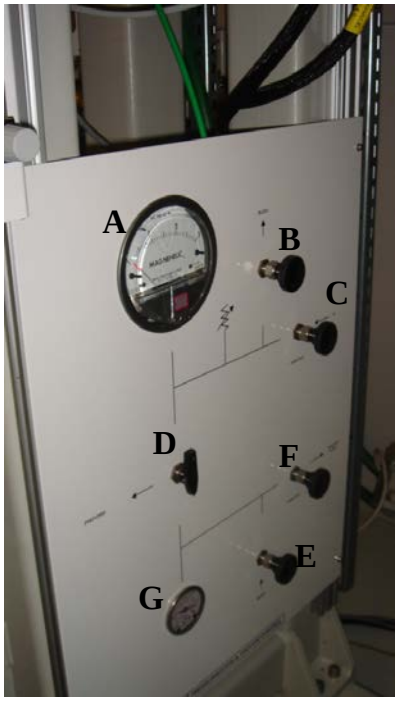

Vacuum/pressure panel located on the bottom right of Tower 2
A – Pressure gauge in psi
B – Pressure bleed valve
C – Pressure throttle (Argon)
D – Pointing upwards = Pressure engaged ; Pointing downwards = Vacuum engaged
E – Vacuum bleed valve
F – Vacuum throttle
G – Vacuum gauge in mBar

18.

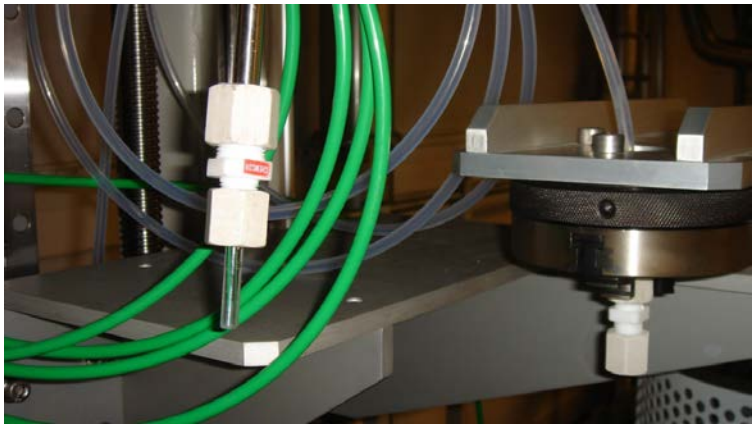

Chuck on very top of Tower 2. This is the feed system and can be used for any preform holder including crucible drawing

19.

Connection from MFCs which can be used for any gas. (On top of MFC box on the right of Tower 2)

20.

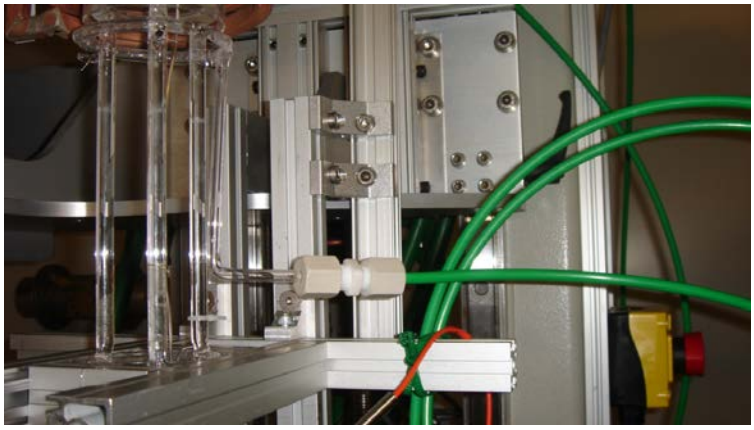

Glass cooling ring used to rapidly cool fibre on exit of furnace. Can't be used with extended furnace though

21.

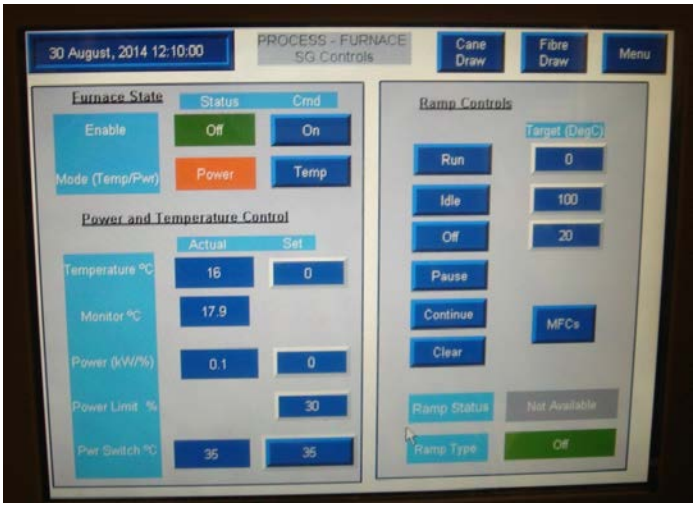

Furnace page on software

22.

Fibre drawing page on software.

23.

Dials on front of Tower 2 which can be used to set fibre drawing speed and used for re-spooling

24.

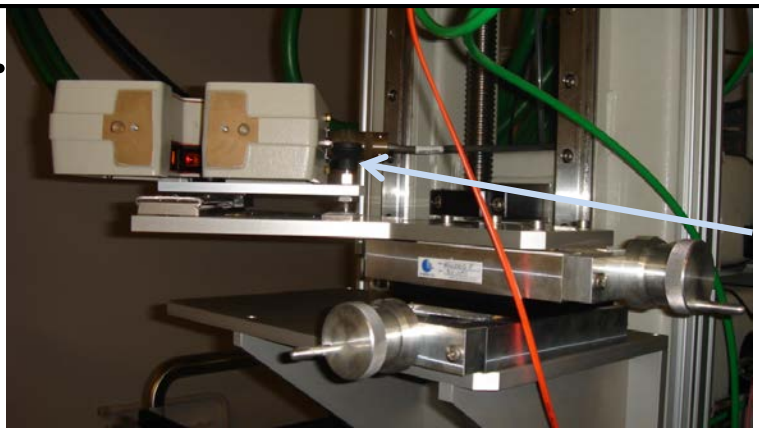

The diameter gauge can slide in and out of position by lifting the small black pull-handle. Once clicked into position, the uni-slides can be used to centre the fibre within the gauge.

25.

Turn the diameter gauge on by pressing “Run/Stop” and display the visual centring aid by pressing the right button 3 times from the home screen.

26.

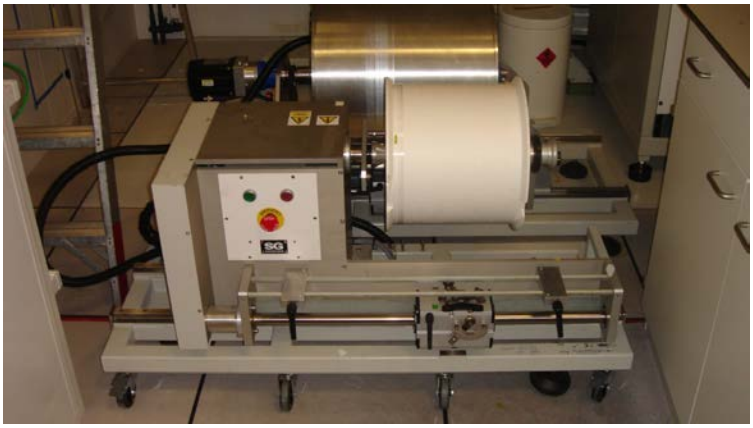

Position the respooler so that the bobbin is as parallel to the take-up drum and as close as you can make it. Best place to stand is between the desk and Tower 2 control unit.

27.

This socket is on the bottom left of Tower 2

28.

Respooler page on software

29.

Respooler page on software

30.

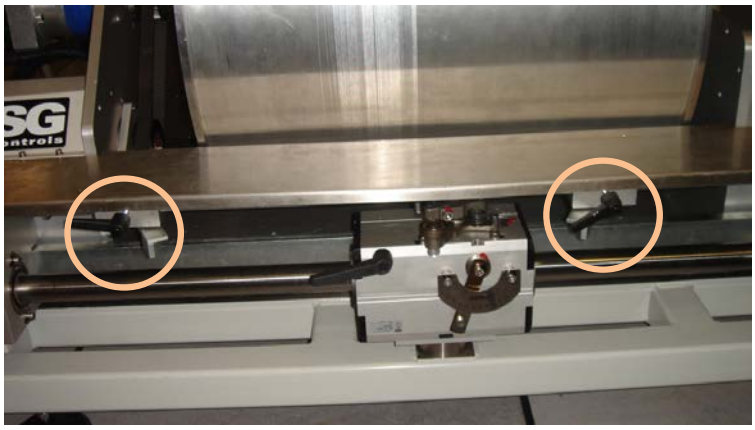

Translator is in the disengaged position here. Move the black handle to a vertical position to engage. The 2 blocks (circled) are the translation limits which can be adjusted. The numerical setting is the spacing between winds

31.

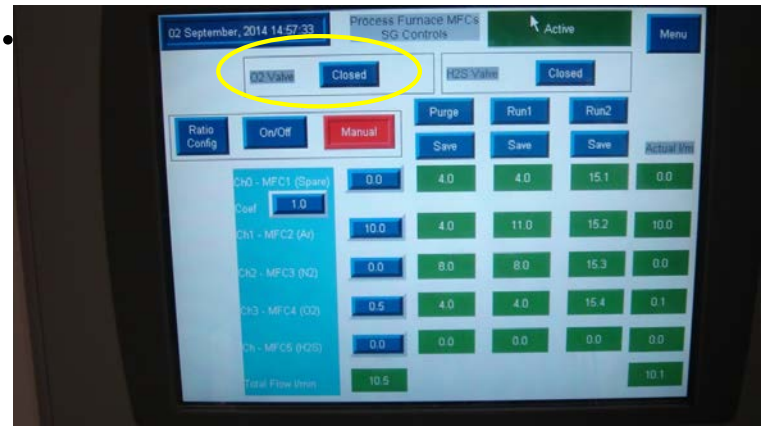

MFCs Software page.
To open the O2 valve, the N2 must also be on to activate the shot-valve

32.

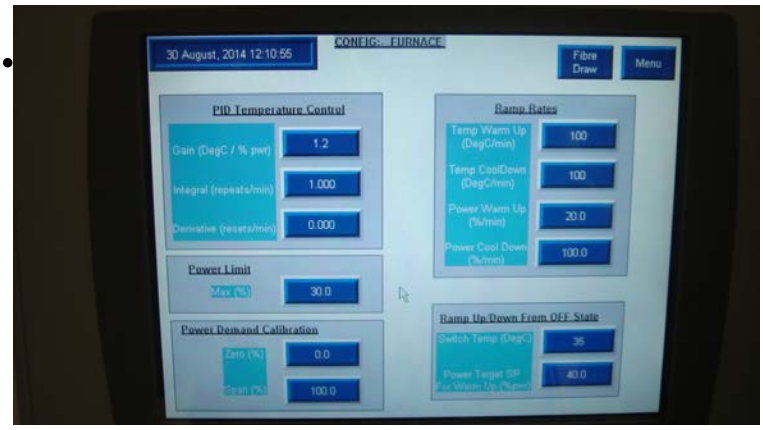

The Gain should only be changed slightly, by 0.1 at a time, and then check to see if the lag has improved.

33.

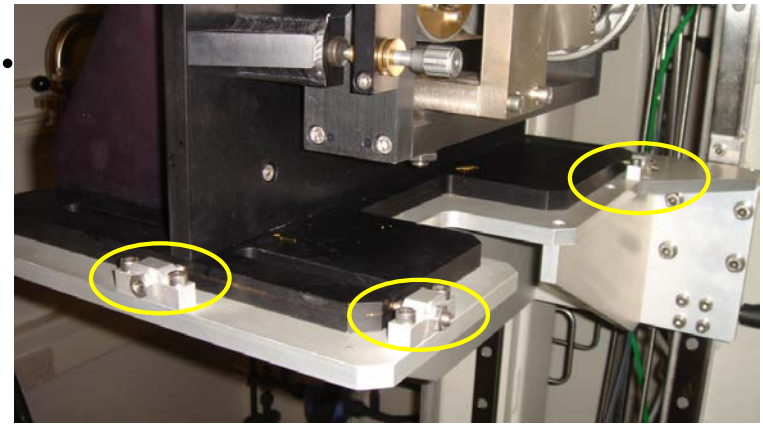

The cane puller is positioned by the circled, adjustable guides. It is simply slid to the left, out of the way for fibre drawing.

34.

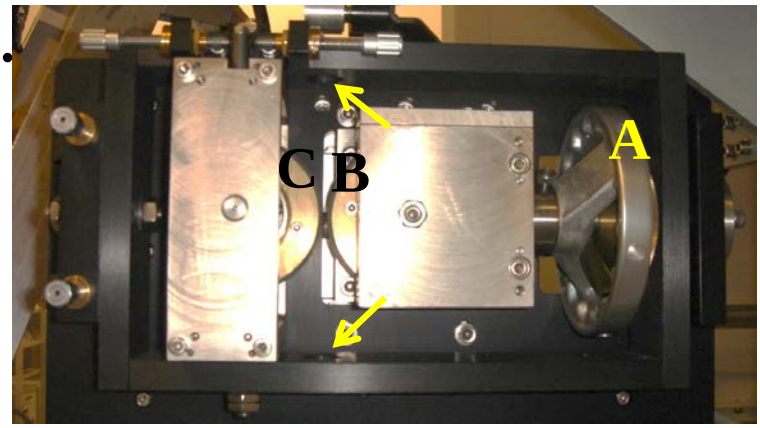

Cane puller detailed.
A – Wheel to close gap between 2 rollers
B – Driving roller
C – Free-wheel roller
Arrows pointing to inlet and exit for cane/fibre

Appendix F List of Fibre Draws (Details Found on Novel Glass and Fibre Group Shared Drive)

Run1 NPK52A Test	Run74 AR-GLAS with GeSbS	Run257 AR-GLAS + GeSbS
Run2 NPK52A Test	Run75 N-LAF7 with Long and Stanley	Run258 Duran with LF354 Core
Run3 F2	Run76 N-SF8 + CIGS&ZnS	Run259 Sodalime + GeSx
Run4 Temperature Profile	Run77 14um N-LAF7	Run260 LD1552
Run5 F2 Structure 1	Run78 AR-GLAS + SbS	Run261 Copper Core Duran
Run6 F2 Structure 1 TC Fault	Run79 AR-GLAS cane	Run262 LD1455 Crucible Draw
Run7 F2 Structure 1	Run80 14um N-LAF7	Run263 LD1552
Run8 F2 Structure 1	Run81 AgCl Crucible Draw	Run264 Duran with LF354 Core
Run9 F2 Structure 1 Cane	Run83 AgCl Crucible Draw	Run265 N-LAF7
Run10 F2 Structure 5 + Al	Run84 AR-GLAS cane	Run266 PBG46 Cane
Run11 F2 Cane	Run85 AR-GLAS cane	Run267 PBG58
Run12 F2 Structure 5 Cane	Run87 PBG14-1	Run268 PBG57 Cane
Run13 Structure 5 Cane + Sn	Run88 PBG14-3	Run269 N-KZFS8
Run14 Shape 2 Cane Tin Solder	Run89 PBG13	Run270 Gold core borosilicate
Run15 Shape 2 Cane Zinc	Run90 GLS Slice for Heriot Watt	Run271 PBG 64 tube trial (2.10)
Run16 Stack run 11	Run91 LD1455 Crucible Draw	Run272 PBG 64 tube (2.10) and PBG 57 core (2.16)
Run17 PMMA Crucible	Run92 IG2 Fibre and cane	Run273 PBG 34 tube (2.16) and PBG 57 core (2.16)
Run18 PMMA Crucible ii	Run93 GLS Slice for Heriot Watt	Run274 PBG 34 tube (2.16) and PBG 57 core (2.16)
Run19 Shape 3 fibre, tin core	Run94 LD455 Crucible Draw	Run275 PBG 34 tube (2.16) and PBG 57 core (2.16)
Run20 Shape 1, Tin Core	Run95 IG6 Fibre and cane	Run276 Cane PBG 56 rod (2.16)
Run21 Shape 3 with Tin full	Run96 IG6 Fibre and cane	Run277 N-SF8
Run22 Shape 5 tin core	Run97 PTFE Tape Test	Run278 N-F2
Run23 Shape 3 tin core cane	Run98 Gas_Temp Core Calibration	Run279 IG6 Crucible Draw
Run24 Shape 2 tin core cane	Run99 Gas_Temp Surface Calibration	Run280 N-F2 Cane
Run25 Shape 5 tin core cane	Run100 to 101 Meon	Run281 N-SF8 Cane
Run26 Shape 2 tin core cane	Run102 PBG core_cladd draw 1 tower 1	Run282 NdSilicate Cane
Run27 Shape 3 tin core cane	Run103 PBG core_cladd draw 2 tower 1	Run283 LD1641A
Run28 Shape 2 zinc	Run104 PBG core_cladd draw 3 tower 1	Run284 LD1641B
Run29 shape 2 zinc	Run105 PBG core_cladd draw 4 tower 1	Run285 LD1641C
Run30 Shape 3 Tin cement	Run106 Canning of PBG 25 tower 1	Run286 LD1641D
Run31 Shape 5 tin cement	Run107 N-LaF7 + GeSe + BiTe	Run287 LD1641 + N-F2 Clad
Run32 Shape 1 tin core w.cement	Run108 LD1455 Crucible Draw	Run288 LD1642E
Run33 AR-GLAS cane	Run109 to 110 Meon	Run289 10um Fibre
Run34 AR-GLAS cane	Run111 PBG suspended core caning 1 tower 1	Run290 LD1641 + N-SF8
Run35 AR-GLAS cane	Run112 PBG suspended core draw 1 tower 1	Run291 LF188 + N-SF8
Run36 F5 tin shape	Run113 N-SF8 + GST	Run292 NdSilicate
Run37 Shape 3 tin core F5	Run114 to 116 Meon	Run293 Boro + GeSbS CVD
Run38 Shape 5 tin core F5	Run117 Graphite susceptor temp calib	Run294 IG5 Crucible Draw
Run39stack and draw of run 38	Run118 LD1552	Run295 IG5 Crucible Draw
Run40 shape 1 f5 cane	Run119 Unknown GLS(O)	Run296 Copper Core Duran
Run41 shape 5 f5 cane	Run120 to 122 Meon	Run297 Copper in Duran
Run42 redraw run 38	Run123 Polymer tube (PEI)	Run298 Copper in Duran
Run43 shape 3 tin core f5.xls	Run124 IG6 Fibre 900um	Run299 Copper in Duran
Run44 redraw of 43	Run125 to 133Meon	Run300 Copper in Duran
Run45 shape 2, F2 neck	Run134 PBG suspended core draw 2 tower 1	Run301 Silver in Duran
Run46 shape 1 f5 tin	Run135 Meon	Run302 Gold in Duran
Run47 shape 3 f5 cane	Run136 PBG41 canning	Run303 LD1641 F
Run48 NSF8 neck	Run137 Meon Tower 1	Run304 Silver Stack and Draw
Run49 shape 5 f5 cane	Run138 Meon Tower 1	Run305 Copper Stack and Draw
Run50 shape 3 f5 cane	Run139 to 205 Meon	Run306 LD1641 F Re-Draw
Run51 49 stack and draw	Run206 Graphite Susceptor Temp Calibration	Run307 Furnace Calibration
Run52 ld462 drop	Run207 Cane Q246	Run308 Furnace Calibration
Run52ii ld462 core, nsf8 clad	Run208 Large coil calibration	Run309 F2 Practice
Run53 neck sodalime	Run209 Large coil calibration	Run310 Soda+CVD GeSbS
Run54 AgCl+Sodalime	Run210 Large coil calibration	Run311 Borosilicate 265um ID
Run55 reattempt 54	Run211 Polymer (PEI)+AsSe fibre draw	Run312 LD1455 Crucible Draw
Run56 reattempt 52	Run212 Polymer (PEI) tube draw	Run313 500um F2
Run57 reattempt 54	Run213 Polymer (PEI) tube draw	Run314 Si_Ca_Al
Run59 GLS crucible practice	Run216 to 241Meon	Run315 N-SF8 + Au Fibre
Run60 NKZFS8	Run242 LD1554	Run316 N-SF8 + Au
Run61 Reattempt of Run 52	Run243 N-SF8 with gold	Run317 N-SF8 + Au Fibre 2
Run62 Reattempt of Run 52	Run244 Duran with LF354 Core	Run318 Cu Microwire Stack and Draw
Run63 ChG core NSF8	Run245 Duran with LD1455 Core	Run319 265um ID Duran Cane for Ultrafast
Run64 GG400 and AgCl	Run247 F2	Run320 265um ID Duran Cane for Ultrafast 2
Run65 GG400 Drop	Run248 F2	Run321 Gold core Duran
Run66 Thread Tape Test	Run249 Ar-GLAS + GeSx	Run322 Gold core Duran
Run67 N-F2 500+100um	Run250 N-SF8	Run323 Gold core Duran
Run68 N-SF8 + Gold	Run251 Meon	Run324 Gold core Duran
Run69 GG400 + AgCl	Run252 LD1554	Run325 Copper in 4-bore capillary
Run70 GG400 Neck pre AgCl	Run253 LD1554	Run326 Copper in 4-bore capillary
Run71 GG400 Hollow drop pre-AgCl	Run254 LD1554	Run327 Gold in 4-bore capillary
Run72 N-SF8 with ChG sputtered fibre core	Run255 LD1554	Run328 N-SF8 with GST Layer
Run73 GLSO Crucible Draw	Run256 LD1552	Run329 N-SF8 with GeSe + Ag Layer

Appendix G Fibre Drawing Furnace Engineering Drawings

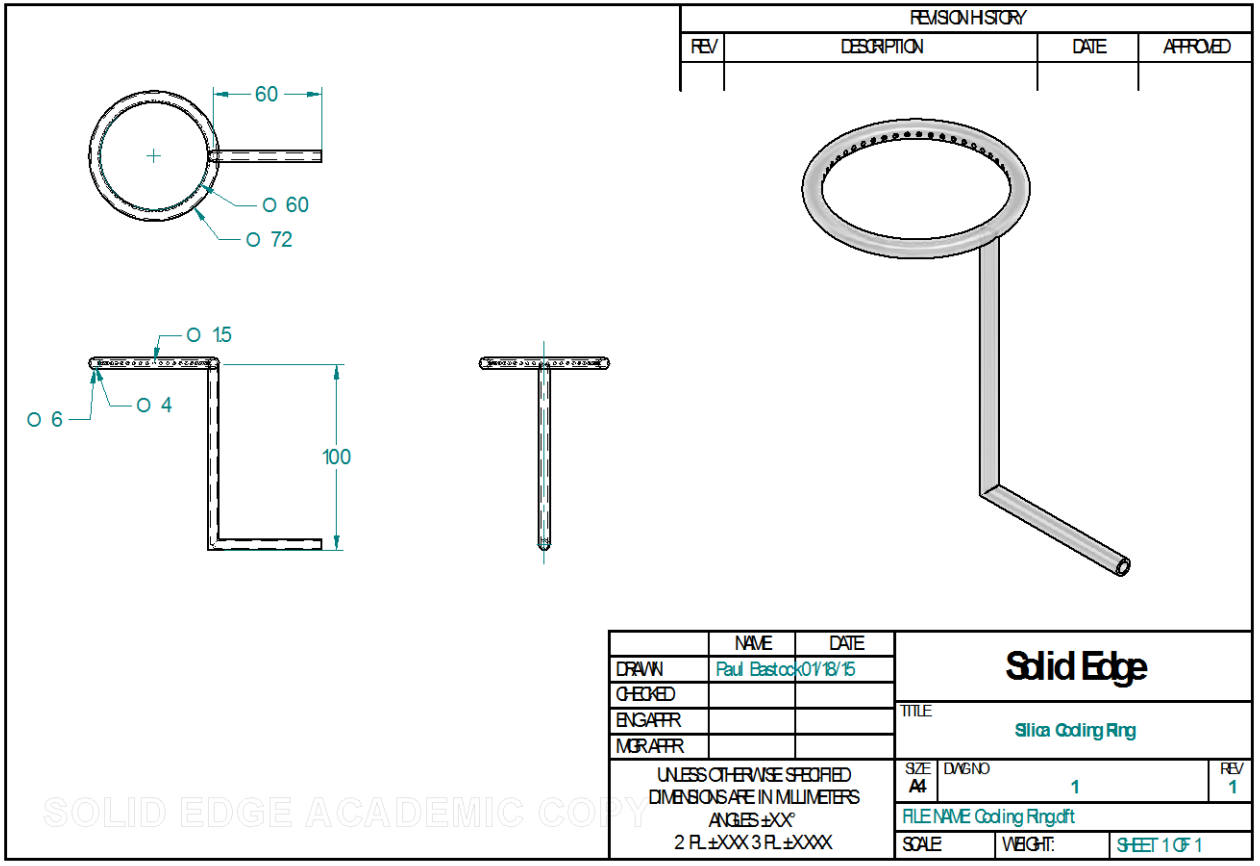

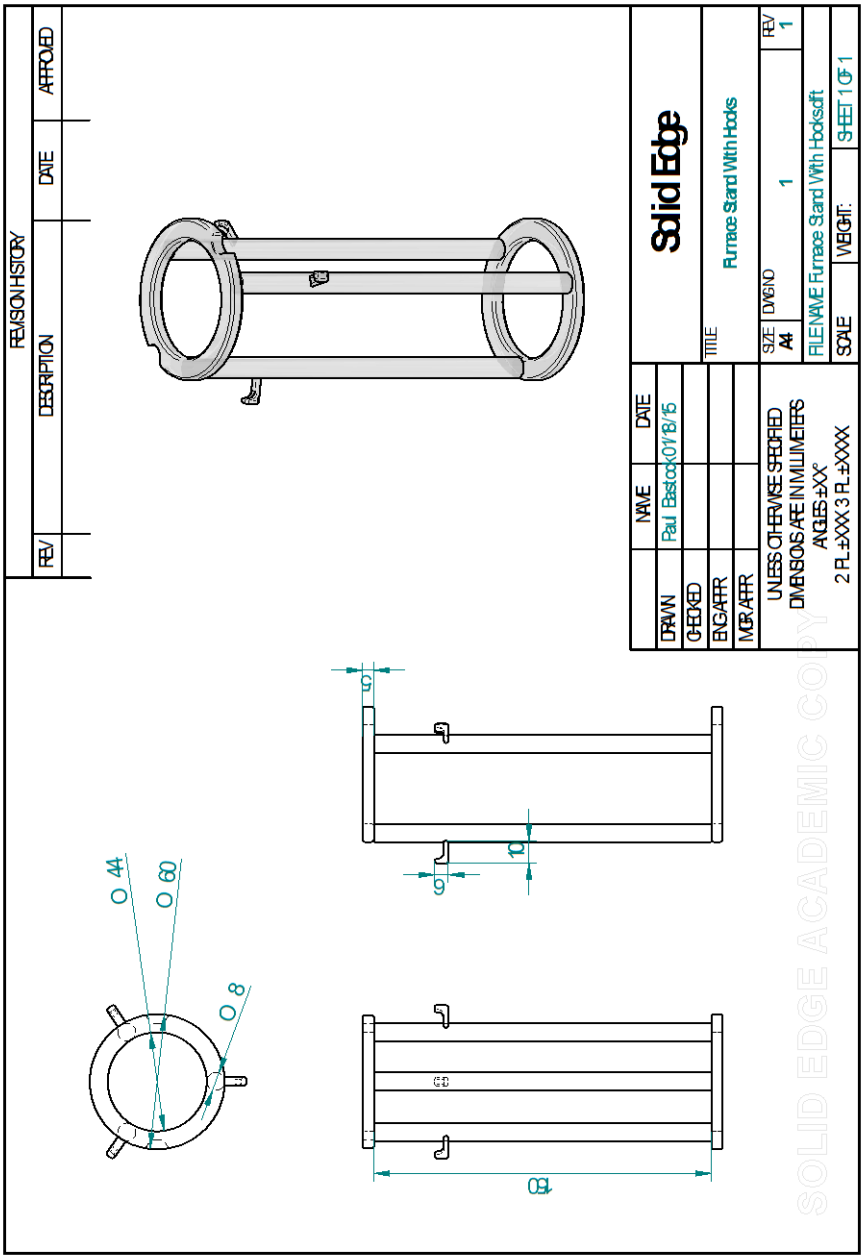
REVISION HISTORY
REV
DESCRIPTION
DATE
APPROVED
Solid Edge
TITLE
Furnace Stand With Hooks
NAME
DATE
DRAWN
Paul Bastock
01/8/15
CHECKED
ENG APPR.
MFG APPR.
UNLESS OTHERWISE SPECIFIED
DIMENSIONS ARE IN MILLIMETERS
ANGLES ±XX°
2 PL ±XXX 3 PL ±XXXX
SIZE
A4
DWG NO
1
REV
1
FILENAME Furnace Stand With Hooks.dft
SCALE
WEIGHT:
SHEET 1 OF 1
SOLID EDGE ACADEMIC COPY
Ø44
Ø60
Ø8
5
10
6
180

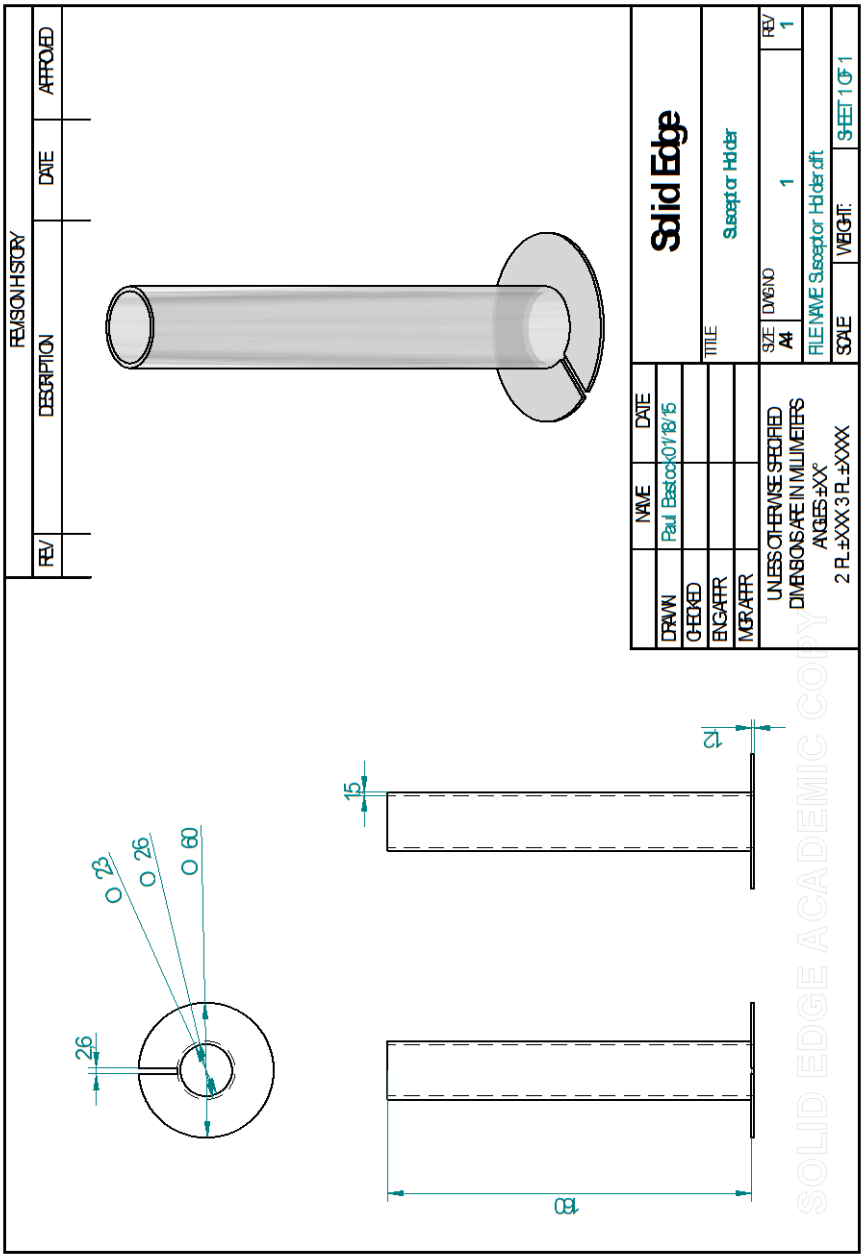
REVISION HISTORY
REV
DESCRIPTION
DATE
APPROVED
Solid Edge
TITLE
Susceptor Holder
NAME
DATE
DRAWN
Paul Bastock
01/18/15
CHECKED
ENG APPR.
MFG APPR.
UNLESS OTHERWISE SPECIFIED
DIMENSIONS ARE IN MILLIMETERS
ANGLES ±XX°
2 PL ±XXX 3 PL ±XXXX
SIZE
A4
DWG NO
1
REV
1
FILE NAME Susceptor Holder.dft
SCALE
WEIGHT:
SHEET 1 OF 1
SOLID EDGE ACADEMIC COPY
Ø23
Ø26
Ø60
26
15
2
80

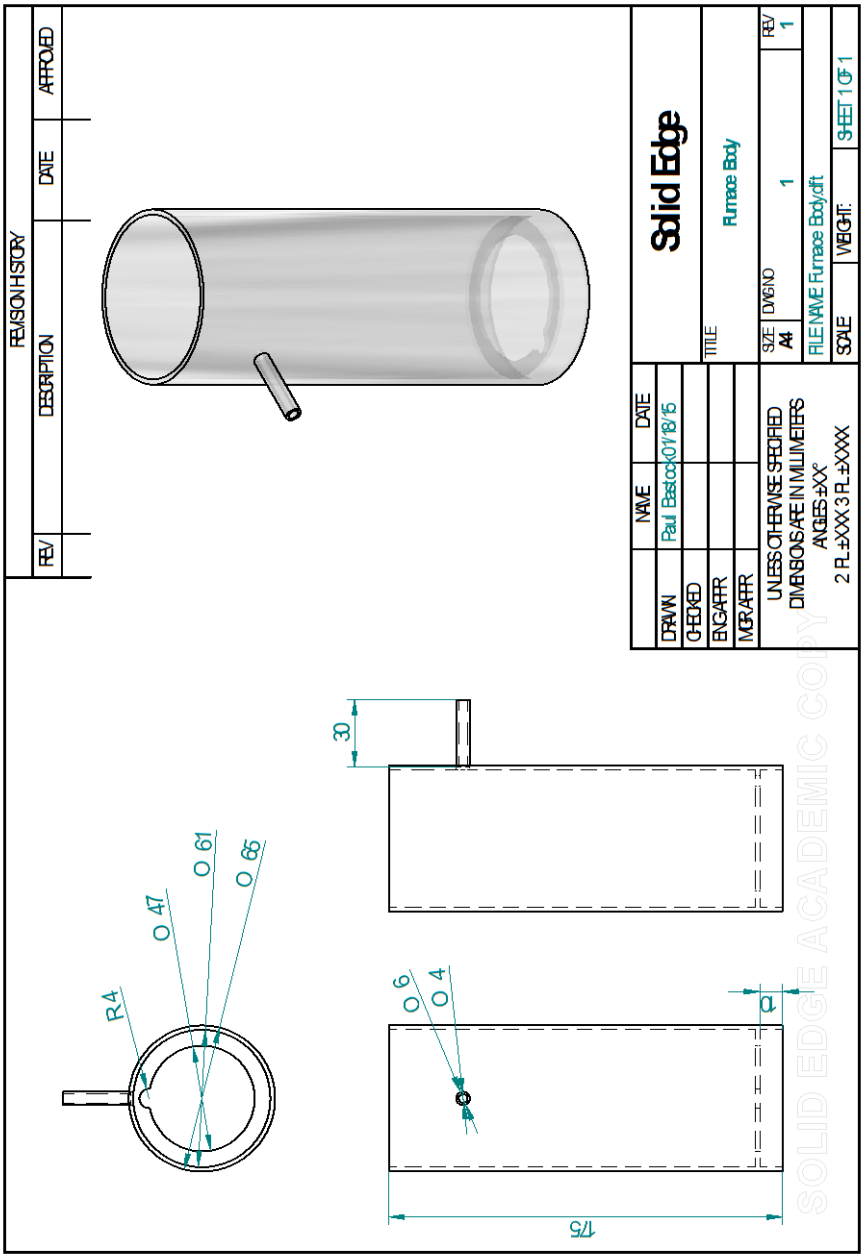
REVISION HISTORY
REV
DESCRIPTION
DATE
APPROVED
Solid Edge
Furnace Body
NAME
DATE
DRAWN
Paul Bastock
01/18/15
CHECKED
ENG APPR.
MFG APPR.
UNLESS OTHERWISE SPECIFIED
DIMENSIONS ARE IN MILLIMETERS
ANGLES ±XX°
2 PL ±XXX 3 PL ±XXXX
SIZE
A4
DWG NO
1
REV
1
FILE NAME Furnace Body.dft
SCALE
WEIGHT:
SHEET 1 OF 1
30
175
R4
Ø 47
Ø 61
Ø 65
Ø 6
Ø 4
d
SOLID EDGE ACADEMIC COPY

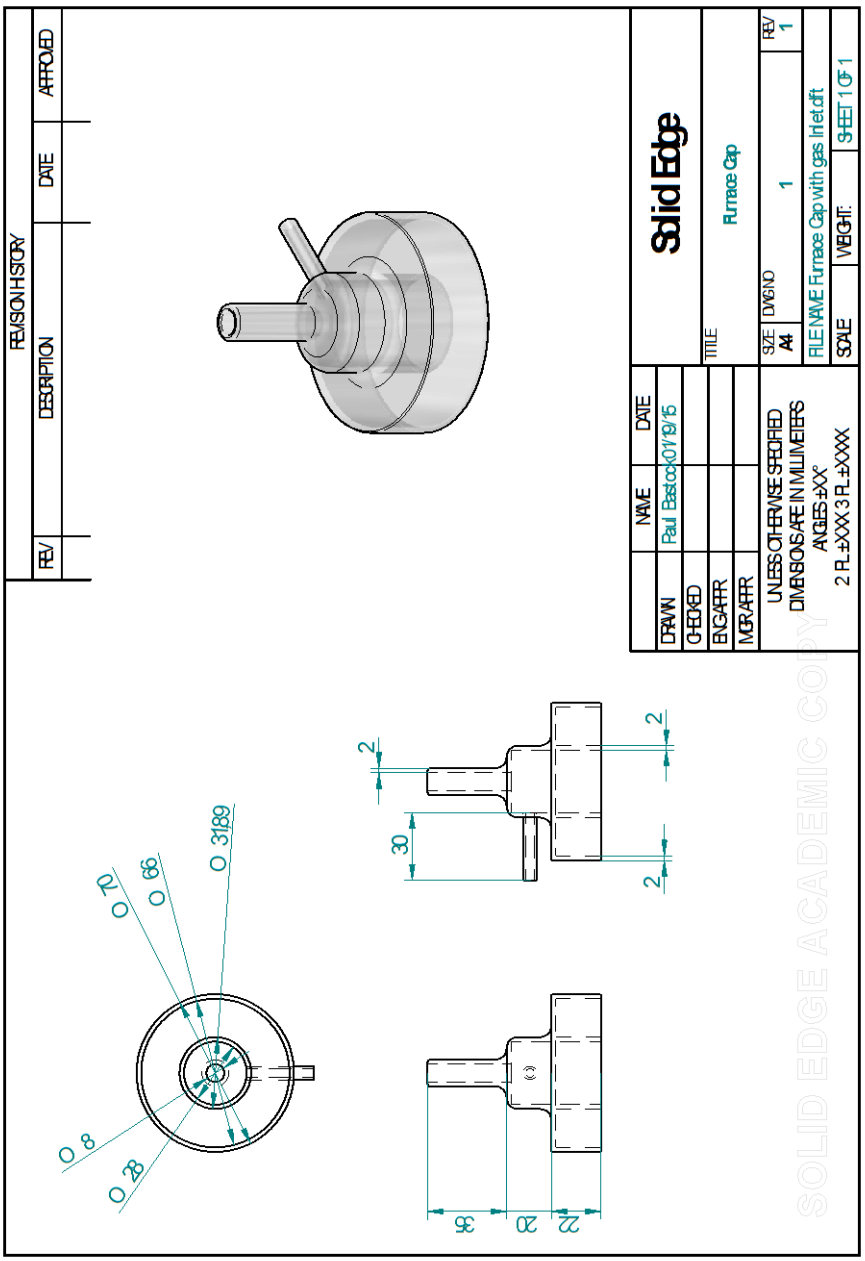
REVISION HISTORY
REV
DESCRIPTION
DATE
APPROVED
NAME
DATE
DRAWN
Paul Bastock
07/9/15
CHECKED
ENG APPR.
MFG APPR.
UNLESS OTHERWISE SPECIFIED
DIMENSIONS ARE IN MILLIMETERS
ANGLES ±XX°
2 PL ±XXX 3 PL ±XXXX
Solid Edge
TITLE
Furnace Cap
SIZE
A4
DWG NO
1
REV
1
FILE NAME Furnace Cap with gas Inlet.dft
SCALE
WEIGHT:
SHEET 1 OF 1
SOLID EDGE ACADEMIC COPY
O 3189
O 72
O 66
O 8
O 28
2
30
2
2
35
30
22

Appendix H Fibre Drawing Parameter Calculator

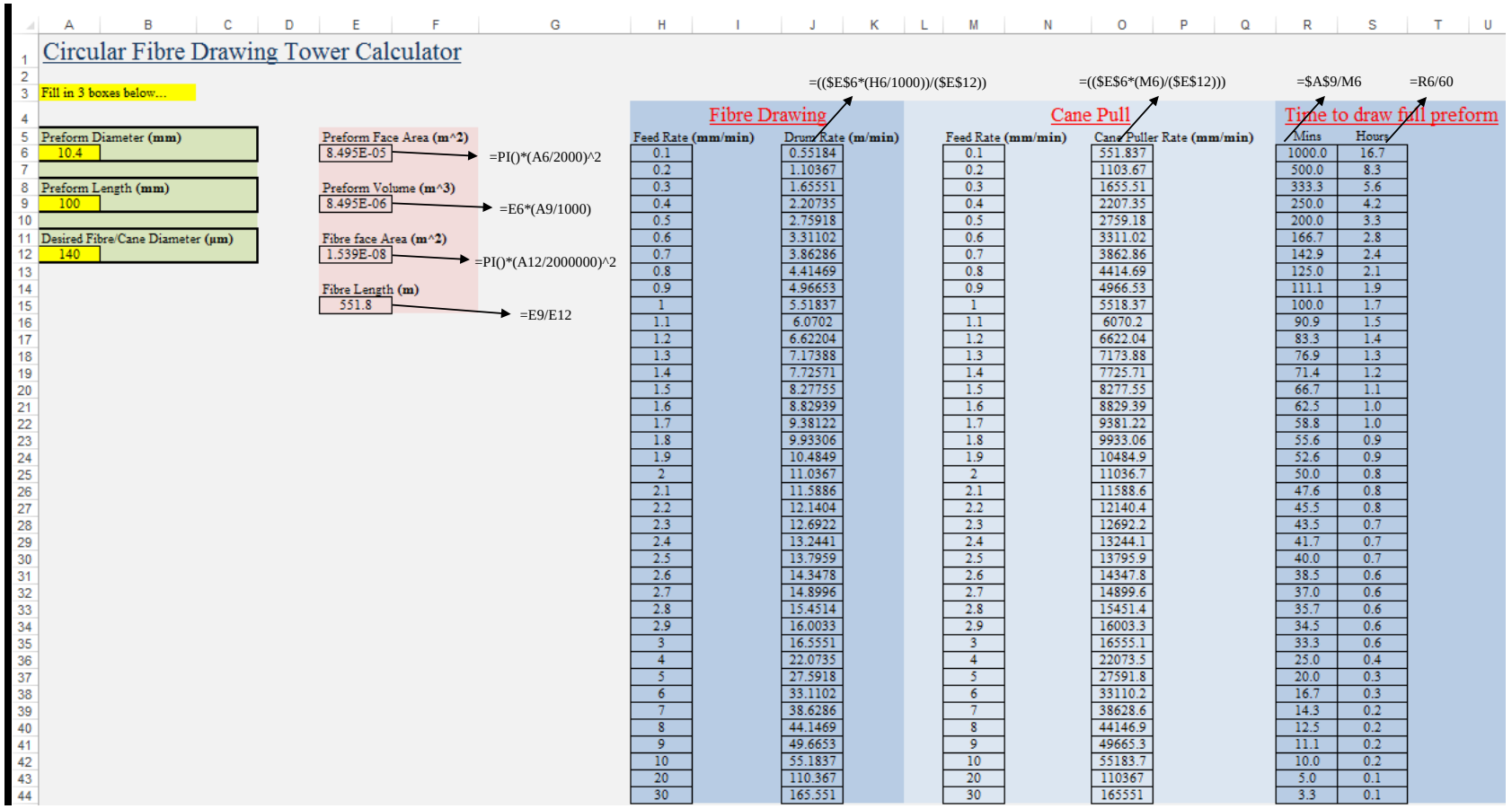

Circular Fibre Drawing Tower Calculator

Fill in 3 boxes below...

Preform Diameter (mm)	10.4
Preform Length (mm)	100
Desired Fibre/Cane Diameter (µm)	140

Preform Face Area (m^2)	8.495E-05	=PI()*(A6/2000)^2
Preform Volume (m^3)	8.495E-06	=E6*(A9/1000)
Fibre face Area (m^2)	1.539E-08	=PI()*(A12/2000000)^2
Fibre Length (m)	551.8	=E9/E12

=((E6*(H6/1000))/(E12)) =((E6*(M6)/(E12))) =A9/M6 =R6/60

Fibre Drawing		Cane Pull		Time to draw full preform	
Feed Rate (mm/min)	Drum Rate (m/min)	Feed Rate (mm/min)	Cane Puller Rate (mm/min)	Mins	Hours
0.1	0.55184	0.1	551.837	1000.0	16.7
0.2	1.10367	0.2	1103.67	500.0	8.3
0.3	1.65551	0.3	1655.51	333.3	5.6
0.4	2.20735	0.4	2207.35	250.0	4.2
0.5	2.75918	0.5	2759.18	200.0	3.3
0.6	3.31102	0.6	3311.02	166.7	2.8
0.7	3.86286	0.7	3862.86	142.9	2.4
0.8	4.41469	0.8	4414.69	125.0	2.1
0.9	4.96653	0.9	4966.53	111.1	1.9
1	5.51837	1	5518.37	100.0	1.7
1.1	6.0702	1.1	6070.2	90.9	1.5
1.2	6.62204	1.2	6622.04	83.3	1.4
1.3	7.17388	1.3	7173.88	76.9	1.3
1.4	7.72571	1.4	7725.71	71.4	1.2
1.5	8.27755	1.5	8277.55	66.7	1.1
1.6	8.82939	1.6	8829.39	62.5	1.0
1.7	9.38122	1.7	9381.22	58.8	1.0
1.8	9.93306	1.8	9933.06	55.6	0.9
1.9	10.4849	1.9	10484.9	52.6	0.9
2	11.0367	2	11036.7	50.0	0.8
2.1	11.5886	2.1	11588.6	47.6	0.8
2.2	12.1404	2.2	12140.4	45.5	0.8
2.3	12.6922	2.3	12692.2	43.5	0.7
2.4	13.2441	2.4	13244.1	41.7	0.7
2.5	13.7959	2.5	13795.9	40.0	0.7
2.6	14.3478	2.6	14347.8	38.5	0.6
2.7	14.8996	2.7	14899.6	37.0	0.6
2.8	15.4514	2.8	15451.4	35.7	0.6
2.9	16.0033	2.9	16003.3	34.5	0.6
3	16.5551	3	16555.1	33.3	0.6
4	22.0735	4	22073.5	25.0	0.4
5	27.5918	5	27591.8	20.0	0.3
6	33.1102	6	33110.2	16.7	0.3
7	38.6286	7	38628.6	14.3	0.2
8	44.1469	8	44146.9	12.5	0.2
9	49.6653	9	49665.3	11.1	0.2
10	55.1837	10	55183.7	10.0	0.2
20	110.367	20	110367	5.0	0.1
30	165.551	30	165551	3.3	0.1

List of Publications

B.Gholipour, P.Bastock, C.Craig, K.Khan, D.Hewak, C.Soci “Amorphous metal-sulphide microfibers enable photonic synapses for brain-like computing” Advanced Optical Materials 2015 Vol.3(5) pp.635-641

B.Gholipour, D.M.Nguyen, L.Cui, V.Nalla, K.Wu, H.Wenchao, P.Bastock, K.Khan, C.Craig, D.W.Hewak, N.I.Zheludev, C.Soci “Beyond the crunch with specialty fibers” Chicheley Hall, London 13-14 May 2015 (Communication networks beyond the capacity crunch - further discussion. The Royal Society)

B.Gholipour, J.Y.Ong, P.Bastock, C.Craig, K.Khan, D.Hewak, C.Soci “Chalcogenide fiber transistors” 8th International Conference on Materials for Advanced Technologies (ICMAT 2015) Suntec, Singapore 28 Jun - 3 Jul 2015 (Materials Research Society of Singapore)

B.Gholipour, J.Y.Ong, P.Bastock, C.Craig, K.Khan, D.W.Hewak, C.Soci “Broadband all-optical fiber transistors” CLEO/Europe-EQEC Munich 21-25 Jun 2015

L.Cui, B.Gholipour, P.Bastock, K.Khan, C.Craig, D.W.Hewak, C.Soci “Planar fabrication assisted fiber nanowire manufacturing” CLEO/Europe-EQEC Munich 21-25 Jun 2015

P.Bastock, C.Craig, K.Khan, E.Weatherby, J.Yao, D.Hewak “Properties of Gallium Lanthanum Sulphide Glass” CLEO 2015, San Jose, USA, 10 – 15 May 2015

B.Gholipour, P.Bastock, C.Craig, K.Khan, D.Hewak, C.Soci, “Amorphous Metal-Sulphide Microfibers Enable Photonic Synapses for Brain-Like Computing”, Advanced Optical Materials, 15 Jan 2015

P.Bastock, C.Craig, J.Yao, K.Khan, D.Hewak, “Manufacturing gallium lanthanum sulphide glass”, Manufacturing the Future Glasgow 23 Sep 2014 [Poster]

D.W.Hewak, C.C.Huang, J.Yao, K.Khan, P.Bastock, F.Al-Saab, B.Gholipour, J.Maddock, E.Weatherby, C.Craig, K.F.MacDonald, N.I.Zheludev, Y.G.Fedorenko, M.A.Hughes, R.M.Gwilliam, K.P.Homewood, R.J.Curry, “Preparation of chalcogenide materials for next generation optoelectronic devices”, Advanced Architectures in Photonics '14 Prague, Czech Republic 21-22 Sep 2014

D.W.Hewak, K.C.C.Huang, K.Khan, P.Bastock, C.Craig, E.Weatherby, “Manufacturing high purity chalcogenide glass”, Society of Glass Technology Annual Meeting (Theme: From Ancient Glass to Modern Techniques) University of Durham, UK 10-12 Sep 2014

Publications

C.H.Tse, Z.G.Lian, P.Bastock, C.Craig, D.Hewak, F.Poletti, Q.J.Wang, “Fabrication of lead-gallium-bismuth (PGB) optical fibre for mid-infrared nonlinearity applications”, Sixth International Conference on Optical, Optoelectronic and Photonic Materials and Applications (ICOOPMA '14) Leeds 27 Jul – 1 Aug 2014

B.Gholipour, P.Bastock, K.Khan, C.Craig, D.W.Hewak, N.I.Zheludev, C.Soci, Duc Minh Nguyen, “Chalcogenide Microfiber Photonic Synapses”, CLEO '14 San Jose, CA, USA 8-13 Jun 2014 [Poster]

B.Gholipour, V.Nalla, P.Bastock, K.Khan, C.Craig, D.W.Hewak, N.I.Zheludev, C.Soci, “Plasmonic Nanowire Continuum Light Source”, CLEO '14 San Jose, CA, USA 8-13 Jun 2014

B.Gholipour, D.M.Nguyen, C.Long, V.Nalla, P.Bastock, K.Khan, C.Craig, D.W.Hewak, N.I.Zheludev, C.Soci “Multimaterial fiber nanomanufacturing: from photodetectors to nonlinear light sources”, SPIE Photonics North Montréal, May 28-30 2014

B.Gholipour, V.Nalla, P.Bastock, K.Khan, C.Craig, D.Hewak, N.I.Zheludev, C.Soci, “Highly collimated broadband emission from plasmonic nanowire embedded in fiber”, 5th International Conference on Metamaterials, Photonic Crystals and Plasmonics (META 14) Singapore 20 May 2014

P.Bastock, C.Craig, D.Hewak, “The fabrication of metal core microfibre”, EPSRC Ultra Precision Conference Cranfield, UK 6 May 2014

B.Gholipour, P.Bastock, K.Khan, C.Craig, D.W.Hewak, N.I.Zheludev, C.Soci, “Chalcogenide optical axons and photonic synapses”, IPS Meeting 2014 Singapore 26 Feb 2014

B.Gholipour, P.Bastock, C.Craig, K.Khan, W.Zilong, D.Hewak, N.I.Zheludev, C.Soci, “Photodarkening in chalcogenide fibers: observation and applications”, 4th Asian Spectroscopy Conference (ASC 2013) Singapore 15 Dec 2013

P.Bastock, C.Craig, E.Weatherby, K.Khan, D.W.Hewak, “Advancing the applications of chalcogenide glass for infrared power transmission”, SPIE Security & Defence (Technologies for Optical Countermeasures) Dresden, Germany 23-26 Sept 2013

P.Bastock, K.Khan, D.Hewak, “Innovative manufacturing of high purity mid-infrared glass”, Manufacturing the Future Cranfield University, UK 17 Sep 2013 [Poster]

P.Bastock, K.Khan, D.Hewak, “Fabrication of novel glass fibre”, International Conference on Photorefractive Effects, Materials and Devices Winchester, UK 4 Sep 2013 [Poster]

P.Bastock, K.Khan, D.Hewak “Non-circular glass metal composite fibre”, ISNOG 2012 St Malo France 1-5 July 2012 [Abstract]

References

1. Harrington, J.A., *Infrared fibers and their applications*. 2004: SPIE press Bellingham.
2. Brady, D.J., *Gallium lanthanum sulphide based glasses for mid-infrared optical fibres*. 1999, University of Southampton.
3. Nagayama, K., et al., *Ultra-low-loss (0.1484 dB/km) pure silica core fibre and extension of transmission distance.* Electronics Letters, 2002. **38**(20): p. 1168-1169.
4. Sanghera, J., et al., *Fabrication of long lengths of low-loss IR transmitting As 40 S (60-x) Se x glass fibers.* Lightwave Technology, Journal of, 1996. **14**(5): p. 743-748.
5. Taylor, G., *A method of drawing metallic filaments and a discussion of their properties and uses.* Physical Review, 1924. **23**(5): p. 655.
6. Donald, I. and B. Metcalfe, *The preparation, properties and applications of some glass-coated metal filaments prepared by the Taylor-wire process.* Journal of materials science, 1996. **31**(5): p. 1139-1149.
7. Gumennik, A., et al., *All-in-Fiber Chemical Sensing.* Advanced Materials, 2012. **24**(45): p. 6005-6009.
8. Sorin, F., et al., *Exploiting collective effects of multiple optoelectronic devices integrated in a single fiber*. Nano Letters, 2009. **9**(7): p. 2630-2635.
9. Heo, J., et al., *Remote fiber-optic chemical sensing using evanescent-wave interactions in chalcogenide glass fibers.* Applied optics, 1991. **30**(27): p. 3944-3951.
10. Zhang, X., H. Ma, and J. Lucas, *Applications of chalcogenide glass bulks and fibres.* J. Optoelectron. Adv. Mater, 2003. **5**(5): p. 1327-1333.
11. Kosolapov, A.F., et al., *Demonstration of CO2 laser power delivery through chalcogenide-glass fiber with negative-curvature hollow core.* Optics Express, 2011. **19**(25): p. 25723-25728.
12. Sanghera, J. and I. Aggarwal, *Active and passive chalcogenide glass optical fibers for IR applications: a review.* Journal of Non-Crystalline Solids, 1999. **256**: p. 6-16.
13. Pollnau, M. and S.D. Jackson, *Mid-infrared fiber lasers*, in *Solid-State Mid-Infrared Laser Sources*. 2003, Springer. p. 225-261.
14. Gholipour, B., et al. *Plasmonic Nanowire Continuum Light Source*. in *CLEO: 2014*. 2014. San Jose, California: Optical Society of America.
15. Tyagi, H., et al., *Plasmon resonances on gold nanowires directly drawn in a step-index fiber.* Optics letters, 2010. **35**(15): p. 2573-2575.
16. Farrington, A.M., N. Jagota, and J.M. Slater, *Simple solid wire microdisc electrodes for the determination of vitamin C in fruit juices.* Analyst, 1994. **119**(2): p. 233-238.
17. Chiriac, H. and T.A. Óvári, *Amorphous glass-covered magnetic wires: preparation, properties, applications.* Progress in materials Science, 1996. **40**(5): p. 333-407.
18. Ishiwatari, H., M. Ikedo, and F. Tateishi, *An optical cable for a CO2 laser scalpel.* Lightwave Technology, Journal of, 1986. **4**(8): p. 1273-1279.
19. Wolfbeis, O.S., *Fiber-optic chemical sensors and biosensors.* Analytical Chemistry, 2004. **76**(12): p. 3269-3284.
20. Lezal, D., et al., *Preparation and characterization of sulfide, selenide and telluride glasses.* Journal of Non-Crystalline Solids, 2003. **326**: p. 47-52.
21. Carter, S.F., P.W. France, and J.R. Williams, *Absorption due to gases dissolved in glasses based on ZrF4.* Physics and Chemistry of Glasses, 1986. **27**(1): p. 42-47.
22. Weber, M., *Science and technology of laser glass.* Journal of Non-Crystalline Solids, 1990. **123**(1): p. 208-222.
23. Lindstrom, R.E., *Process for fractionating lanthanide mixtures containing cerium.* 1969, Google Patents.
24. Becker, J.S. and H.-J. Dietze, *Inorganic trace analysis by mass spectrometry.* Spectrochimica Acta Part B: Atomic Spectroscopy, 1998. **53**(11): p. 1475-1506.
25. Deline, V., et al., *Mechanism of the SIMS matrix effect.* Applied Physics Letters, 1978. **33**(9): p. 832-835.

References

26. Hoffmann, V., et al., *Glow discharge mass spectrometry.* Analytical and bioanalytical chemistry, 2005. **381**(1): p. 173-188.
27. King, F.L., J. Teng, and R.E. Steiner, *Special feature: Tutorial. Glow discharge mass spectrometry: Trace element determinations in solid samples.* Journal of Mass Spectrometry, 1995. **30**(8): p. 1061-1075.
28. Barshick, C., D. Duckworth, and D. Smith, *Inorganic mass spectrometry: fundamentals and applications*. 2000: CRC Press.
29. Shibata, S., T. Manabe, and M. Horiguchi, *Preparation of Ge-S glass fibers with reduced OH, SH content.* Japanese Journal of Applied Physics, 1981. **20**(1): p. L13.
30. Hrubý, A., *Evaluation of glass-forming tendency by means of DTA.* Czechoslovak Journal of Physics B, 1972. **22**(11): p. 1187-1193.
31. Jones, D.R. and M.F. Ashby, *Engineering Materials 2: An Introduction to Microstructures, Processing and Design*. 2005: Butterworth-Heinemann.
32. Gabbott, P., *Principles and applications of thermal analysis*. 2008: John Wiley & Sons.
33. Bureau, B., et al., *Recent advances in chalcogenide glasses.* Journal of Non-Crystalline Solids, 2004. **345-346**: p. 276-283.
34. Devyatykh, G., et al., *Recent developments in As–S glass fibres.* Journal of Non-Crystalline Solids, 1999. **256**: p. 318-322.
35. Snopatin, G., et al., *High purity arsenic-sulfide glasses and fibers with minimum attenuation of 12 dB/km.* Optoelectronics and advanced materials-rapid communications, 2009. **3**(7): p. 669-671.
36. Sanghera, J.S., L.B. Shaw, and I.D. Aggarwal, *Applications of chalcogenide glass optical fibers.* Comptes Rendus Chimie, 2002. **5**(12): p. 873-883.
37. Sanghera, J., et al., *Fabrication of low-loss IR-transmitting Ge30As10Se30Te30 glass fibers.* Lightwave Technology, Journal of, 1994. **12**(5): p. 737-741.
38. Churbanov, M., et al., *Optical fibers based on As–S–Se glass system.* Journal of Non-Crystalline Solids, 2001. **284**(1): p. 146-152.
39. Churbanov, M.F., et al., *Preparation of chalcogenide glasses of As-S, Ge-S, Ge-Se systems from monoisotopic elements.* Journal of Non-Crystalline Solids, 2013. **377**: p. 12-15.
40. Mazhorova, A., et al., *Thin chalcogenide capillaries as efficient waveguides in the mid-IR-THz spectral range.* arXiv preprint arXiv:1112.5079, 2011.
41. Brady, D.J., et al., *Minimum loss predictions and measurements in gallium lanthanum sulphide based glasses and fibre.* Journal of Non-Crystalline Solids, 1998. **242**(2-3): p. 92-98.
42. Guittard, M. and J. Flahaut, *Rare earth sulfide and oxysulfide glasses*, in *New frontiers in rare earth science and applications*. 1985.
43. Kumta, P. and S. Risbud, *Rare-earth chalcogenides—an emerging class of optical materials.* Journal of materials science, 1994. **29**(5): p. 1135-1158.
44. Alaluf, M., et al., *Plastic hollow fibers as a selective infrared radiation transmitting medium.* Journal of Applied Physics, 1992. **72**(9): p. 3878.
45. George, R. and J.A. Harrington, *Cu/CuI-coated hollow glass waveguides for delivery of infrared radiation.* Optical Engineering, 2006. **45**(5): p. 055004-055004-4.
46. Harrington, J.A. and C.C. Gregory, *Hollow sapphire fibers for the delivery of CO2 laser energy.* Optics letters, 1990. **15**(10): p. 541-543.
47. Iwai, K., et al., *Fabrication and transmission characteristics of infrared hollow fiber based on silver-clad stainless steel pipes.* Applied optics, 2009. **48**(32): p. 6207-6212.
48. Jelinkova, H., *Hollow waveguide delivery systems for laser technological application.* Progress in Quantum Electronics, 2004. **28**(3-4): p. 145-164.
49. Kasahara, R., *Transmission properties of infrared hollow fibers produced by drawing a glass-tube preform.* Optical Engineering, 2007. **46**(2): p. 025001.
50. Kriesel, J., et al., *Fiber delivery of mid-IR lasers*. 2011, Pacific Northwest National Laboratory (PNNL), Richland, WA (US).

51. Lin, X., et al., *Fabrication and characterization of infrared hollow fiber with multi-SiO2 and AgI inner-coating layers.* Applied optics, 2009. **48**(35): p. 6765-6769.
52. Matsuura, Y., et al., *Infrared-laser delivery system based on polymer-coated hollow fibers.* Optics & Laser Technology, 2001. **33**(5): p. 279-283.
53. Shi, Y.-W., et al., *Fabrication of a polymer-coated silver hollow optical fiber with high performance.* Applied optics, 2006. **45**(26): p. 6736-6740.
54. Temelkuran, B., et al., *Wavelength-scalable hollow optical fibres with large photonic bandgaps for CO2 laser transmission.* Nature, 2002. **420**(6916): p. 650-653.
55. Yu, F., W.J. Wadsworth, and J.C. Knight, *Low loss silica hollow core fibers for 3–4 μm spectral region.* Optics Express, 2012. **20**(10): p. 11153-11158.
56. Désévédavy, F., et al., *Chalcogenide glass hollow core photonic crystal fibers.* Optical Materials, 2010. **32**(11): p. 1532-1539.
57. Shiryaev, V. and M. Churbanov, *Trends and prospects for development of chalcogenide fibers for mid-infrared transmission.* Journal of Non-Crystalline Solids, 2013.
58. Renversez, G., P. Boyer, and A. Sagrini, *Antiresonant reflecting optical waveguide microstructured fibers revisited: a new analysis based on leaky mode coupling.* Opt. Express, 2006. **14**(12): p. 5682-5687.
59. Elliott, G.R., et al., *Chalcogenide glass microspheres; their production, characterization and potential.* Optics Express, 2007. **15**(26): p. 17542-17553.
60. Hewak, D.W., et al., *Chalcogenide glasses for photonics device applications.* GS Murugan, ed.(Research Signpost, Kerala, India, 2010) Chap, 2010. **2**.
61. Youden, K., et al., *Pulsed laser deposition of Ga-La-S chalcogenide glass thin film optical waveguides.* Applied Physics Letters, 1993. **63**(12): p. 1601-1603.
62. Mairaj, A., R. Curry, and D. Hewak, *Chalcogenide glass thin films through inverted deposition and high velocity spinning.* Electronics Letters, 2004. **40**(7): p. 421-422.
63. Frantz, J., et al., *Waveguide amplifiers in sputtered films of Er3+-doped gallium lanthanum sulfide glass.* Optics Express, 2006. **14**(5): p. 1797-1803.
64. Sámson, Z.L., et al., *Chalcogenide glasses in active plasmonics.* physica status solidi (RRL)-Rapid Research Letters, 2010. **4**(10): p. 274-276.
65. Hecht, J., *A Fiber-optic chronology*. 1999: Jeff Hecht.
66. Boys, C.V., *LVII. On the production, properties, and some suggested uses of the finest threads.* The London, Edinburgh, and Dublin Philosophical Magazine and Journal of Science, 1887. **23**(145): p. 489-499.
67. Kim, K.S. and S.E. Pratsinis, *Manufacture of optical waveguide preforms by modified chemical vapor deposition.* AIChE journal, 1988. **34**(6): p. 912-921.
68. Itoh, K., *Etchant and method for etching chalcogenide glass and optical member having smooth surface*. 2000, Google Patents.
69. Hesford, M., *The development of a chemical etch procedure for GLS glass preforms to improve strength and quality*, in *Optoelectronics Research Centre*. 1999, University of Southampton: Southampton. p. 74.
70. Morgan, S., et al., *Crystallization of gallium lanthanum sulfide glasses.* Journal of the American Ceramic Society, 1998. **81**(7): p. 1913-1918.
71. Li, R., et al., *The decisive role of oxide content in the formation and crystallization of gallium-lanthanum-sulfide glasses.* Journal of Materials Research, 1999. **14**(06): p. 2621-2627.
72. Tuniz, A., et al., *Drawn metamaterials with plasmonic response at terahertz frequencies.* Applied Physics Letters, 2010. **96**(19): p. 191101.
73. Wang, A., et al., *Fiber metamaterials with negative magnetic permeability in the terahertz.* Optical Materials Express, 2011. **1**(1): p. 115-120.
74. Tuniz, A., et al., *Stacked-and-drawn metamaterials with magnetic resonances in the terahertz range.* Optics Express, 2011. **19**(17): p. 16480-16490.
75. Singh, N., et al., *Fiber-drawn double split ring resonators in the terahertz range.* Optical Materials Express, 2012. **2**(9): p. 1254-1259.

References

76. Tuniz, A., et al., *Fabricating metamaterials using the fiber drawing method.* Journal of visualized experiments: JoVE, 2012(68).
77. Mazhorova, A., et al., *Composite THz materials using aligned metallic and semiconductor microwires, experiments and interpretation.* Optics Express, 2010. **18**(24): p. 24632-24647.
78. Argyros, A., *Microstructures in polymer fibres for optical fibres, THz waveguides, and fibre-based metamaterials.* ISRN Optics, 2013. **2013**.
79. Soukoulis, C.M. and M. Wegener, *Past achievements and future challenges in the development of three-dimensional photonic metamaterials.* Nature Photonics, 2011. **5**(9): p. 523-530.
80. Landy, N., et al., *Perfect metamaterial absorber.* Physical Review Letters, 2008. **100**(20): p. 207402.
81. Shalaev, V.M., *Optical negative-index metamaterials.* Nature Photonics, 2007. **1**(1): p. 41-48.
82. Walther, M., et al., *Terahertz metamaterials fabricated by inkjet printing.* Applied Physics Letters, 2009. **95**(25): p. 251107.
83. Kim, H., et al., *Fabrication of terahertz metamaterials by laser printing.* Optics letters, 2010. **35**(23): p. 4039-4041.
84. Jansen, K. and R. Ulrich, *Drawing glass fibers with complex cross section.* Lightwave Technology, Journal of, 1991. **9**(1): p. 2-6.
85. Souza, M., *FW: {Disarmed} RE: [Scientific_Glassblowers]*, P. Bastock, Editor. 2015, P. Bastock: Southampton. p. 1.
86. Tuncer, E., *Clad fiber capacitor and method of making same*. 2012, Google Patents.
87. Tuncer, E., *Device fabrication method for high power density capacitors*. 2009, Google Patents.
88. Tuncer, E., *Well defined structures for capacitor applications*. 2009, Google Patents.
89. Gu, J.F., S. Gorgutsa, and M. Skorobogatiy, *Soft capacitor fibers using conductive polymers for electronic textiles.* Smart Materials and Structures, 2010. **19**(11): p. 115006.
90. Creager, S., *Fibers for Textile-Based Electrical Energy Storage.* NTC Project M06-CL07, National Textile Center Annual Report, 2006. **9**.
91. Tse, C.H., et al., *Fabrication of lead-gallium-bismuth (PGB) optical fibre for mid-infrared nonlinearity applications*, in *Sixth International Conference on Optical, Optoelectronic and Photonic Materials and Applications (ICOOPMA '14)*. 2014: Leeds.
92. Nguyen, D.M., et al., *Plasmonic nanowire-cored silicate fiber spaser*, in *Nanometa 2015*. 2015: Seefeld, Austria.
93. Gholipour, B., et al., *Highly collimated broadband emission from plasmonic nanowire embedded in fiber*, in *The 5th International Conference on Metamaterials, Photonic Crystals and Plasmonics (META)*. 2014: NTU, Singapore.
94. Ahn, J.-H., et al., *Double-gate nanowire field effect transistor for a biosensor.* Nano Letters, 2010. **10**(8): p. 2934-2938.
95. Reich, D., et al., *Biological applications of multifunctional magnetic nanowires.* Journal of Applied Physics, 2003. **93**(10): p. 7275-7280.
96. Wang, Q., F. Min, and J. Zhu, *Preparation of gold nanowires and its application in glucose biosensing.* Materials Letters, 2013. **91**: p. 9-11.
97. SuongáOu, F., *Synthesis of hybrid nanowire arrays and their application as high power supercapacitor electrodes.* Chemical Communications, 2008(20): p. 2373-2375.
98. Wu, B., A. Heidelberg, and J.J. Boland, *Mechanical properties of ultrahigh-strength gold nanowires.* Nature Materials, 2005. **4**(7): p. 525-529.
99. Calleja, M., et al., *Fabrication of gold nanowires on insulating substrates by field-induced mass transport.* Applied Physics Letters, 2001. **79**(15): p. 2471-2473.
100. Ji, C. and P.C. Searson, *Fabrication of nanoporous gold nanowires.* Applied Physics Letters, 2002. **81**(23): p. 4437-4439.

101. Yaman, M., et al., *Arrays of indefinitely long uniform nanowires and nanotubes.* Nature Materials, 2011. **10**(7): p. 494-501.
102. Donald, I., *Production, properties and applications of microwire and related products.* Journal of materials science, 1987. **22**(8): p. 2661-2679.
103. Boyd, K., et al. *Novel Technique for the CO2 Laser Fabrication of Optical Devices with Sub-Micrometer Ablation Depth Precision*. in *Optical Communication (ECOC), 2014 European Conference on*. 2014: IEEE.
104. Steenberge, G.V., et al., *Laser cleaving of glass fibers and glass fiber arrays.* Journal of Lightwave Technology, 2005. **23**(2): p. 609.
105. Lévesque, L. and V. Jdanov, *Optical fiber cleaved at an angle by CO2 laser ablation: Application to micromachining.* Optics & Laser Technology, 2010. **42**(7): p. 1080-1083.
106. Abdi, O., et al., *Cleaving of solid single mode polymer optical fiber for strain sensor applications.* Optics Communications, 2009. **282**(5): p. 856-861.
107. Atakaramians, S., et al., *Cleaving of extremely porous polymer fibers.* Photonics Journal, IEEE, 2009. **1**(6): p. 286-292.
108. Burrows, J., et al., *Atmospheric remote-sensing reference data from GOME: Part 1. Temperature-dependent absorption cross-sections of NO 2 in the 231–794 nm range.* Journal of Quantitative Spectroscopy and Radiative Transfer, 1998. **60**(6): p. 1025-1031.
109. Hodgkinson, J. and R.P. Tatam, *Optical gas sensing: a review*. Measurement Science and Technology, 2013. **24**(1): p. 012004.
110. Laj, P., et al., *Measuring atmospheric composition change.* Atmospheric environment, 2009. **43**(33): p. 5351-5414.
111. Smith, D. and P. Španěl, *The challenge of breath analysis for clinical diagnosis and therapeutic monitoring.* Analyst, 2007. **132**(5): p. 390-396.
112. Liu, X., et al., *A survey on gas sensing technology.* Sensors, 2012. **12**(7): p. 9635-9665.
113. Vergara, A., et al., *Chemical gas sensor drift compensation using classifier ensembles.* Sensors and Actuators B: Chemical, 2012. **166**: p. 320-329.
114. Tong, L., A.P. Mouritz, and M. Bannister, *3D fibre reinforced polymer composites*. 2002: Elsevier.
115. Gregory, A., *RE: Chalcogenide sample [NC]*, P. Bastock, Editor. 2015: Southampton. p. 1.
116. micromaterials. *Products: LHPG Sapphire Fibers*. 2015 [cited 2015 07 April 2015]; Available from: http://www.micromaterialsinc.com/specsFiber.html.
117. Thorlabs. *MIR Multimode Fluoride Fiber Optic Patch Cables.* 2015 [cited 2015 07 April 2015]; Available from: http://www.thorlabs.de/newgrouppage9.cfm?objectgroup_id=7840.
118. Sedi. *Silver Halide (PIR).* 2015 [cited 2015 07 April 2015]; Available from: http://www.sedi-fibres.com/silver_halide__pir__fibers_5_35.html.
119. IRFlex. *Transmission Fiber Cable*. 2015 [cited 2015 07 April 2015]; Available from: http://www.irflex.com/products/transmission-fiber-cable.
120. Harrington, J.A., *A review of IR transmitting, hollow waveguides.* Fiber & Integrated Optics, 2000. **19**(3): p. 211-227.
121. Dils, R., *High-temperature optical fiber thermometer.* Journal of Applied Physics, 1983. **54**(3): p. 1198-1201.
122. Nubling, R.K. and J.A. Harrington, *Single-crystal laser-heated pedestal-growth sapphire fibers for Er: YAG laser power delivery.* Applied optics, 1998. **37**(21): p. 4777-4781.
123. Polletto, T.J., et al., *Comparison of germanium oxide fibers with silica and sapphire fiber tips for transmission of erbium: YAG laser radiation.* Lasers in Surgery and Medicine, 2006. **38**(8): p. 787-791.
124. Shibata, S., et al., *Prediction of loss minima in infra-red optical fibres.* Electronics Letters, 1981. **17**(21): p. 775-777.

References

125. Tran, D., G. Sigel, and B. Bendow, *Heavy metal fluoride glasses and fibers: a review.* Lightwave Technology, Journal of, 1984. **2**(5): p. 566-586.
126. Faucher, D., et al., *20 W passively cooled single-mode all-fiber laser at 2.8 μm.* Optics letters, 2011. **36**(7): p. 1104-1106.
127. Gal, D. and A. Katzir, *Silver halide optical fibers for medical applications.* Quantum Electronics, IEEE Journal of, 1987. **23**(10): p. 1827-1835.
128. Chen, D., et al., *Fabrication of silver halide fibers by extrusion*, in *Fiber Optics*. 1979, Springer. p. 119-122.
129. Taghizadeh, M.R., et al., *Transmission Measurement of Polycrystalline Silver Halide Fibres in the 1-11 μm Wavelength Region.* Optica Acta: International Journal of Optics, 1984. **31**(4): p. 371-377.
130. Paiss, I., F. Moser, and A. Katzir. *Core-clad silver halide fibers for CO2 laser power transmission*. in *Optics, Electro-Optics, and Laser Applications in Science and Engineering*. 1991: International Society for Optics and Photonics.
131. Wheeler, N.V., et al., *Low-loss and low-bend-sensitivity mid-infrared guidance in a hollow-core–photonic-bandgap fiber.* Optics letters, 2014. **39**(2): p. 295-298.
132. Gayraud, N., et al., *Mid-infrared gas sensing using a photonic bandgap fiber.* Applied optics, 2008. **47**(9): p. 1269-1277.
133. Amezcua-Correa, R., et al., *Broadband infrared transmission in a hollow-core photonic bandgap fibre free of surface modes.* 2006.
134. Lendl, B. and B. Mizaikoff, *Optical Fibers for Mid-Infrared Spectrometry*. 2002: Wiley Online Library.
135. Hongo, A., et al., *Transmission of kilowatt-class CO2 laser light through dielectric-coated metallic hollow waveguides for material processing.* Applied optics, 1992. **31**(24): p. 5114-5120.
136. Ikushima, A., T. Fujiwara, and K. Saito, *Silica glass: A material for photonics.* Journal of Applied Physics, 2000. **88**(3): p. 1201-1213.
137. Vacha, L., et al. *Flox Fibers: Fluoride Glasses with Oxide Overclad*. in *Materials Science Forum*. 1987: Trans Tech Publ.
138. Schott. *Optical Glass - Overview (Excel Table).* 2012 [cited 2012 20 April 2012]; Available from: http://www.schott.com/advanced_optics/english/products/optical-materials/optical-glass/optical-glass/index.html?so=uk&lang=english&tab=tabs-220880-6.
139. West, Y., et al., *Gallium lanthanum sulphide fibers for infrared transmission.* Fiber & Integrated Optics, 2000. **19**(3): p. 229-250.
140. Senior, J.M. and M.Y. Jamro, *Optical fiber communications: principles and practice*. 2009: Pearson Education.
141. Le Sergent, C. *Chalcogenide glass optical fibers-an overview*. in *Hague International Symposium*. 1987: International Society for Optics and Photonics.
142. Melling, P., *Alternative methods of preparing chalcogenide glasses.* American Ceramic Society bulletin, 1984. **63**(11): p. 1427-1429.
143. Katsuyama, T., S. Satoh, and H. Matsumura, *Fabrication of high-purity chalcogenide glasses by chemical vapor deposition.* Journal of Applied Physics, 1986. **59**(5): p. 1446-1449.
144. Blanc, D. and J. Wilson, *Plasma deposition of chalcogenide glass.* Journal of Non-Crystalline Solids, 1985. **77**: p. 1129-1132.
145. Fejer, M., et al., *Laser-heated miniature pedestal growth apparatus for single-crystal optical fibers.* Review of Scientific Instruments, 1984. **55**(11): p. 1791-1796.
146. Ohnishi, N. and T. Yao, *A novel growth technique for single-crystal fibers: the micro-czochralski (μ-CZ) method.* Japanese Journal of Applied Physics, 1989. **28**(2A): p. L278.
147. Churbanov, M., et al., *Origin of microinhomogeneities in As-S-Se glass fibers fabricated by the double-crucible method.* Inorganic Materials, 2007. **43**(4): p. 436-440.

148. Dianov, E., et al., *Crystallization kinetics of praseodymium-doped (Ga 2 S 3) 0.7 (LaS 3) 0.3 glass.* 1997.
149. Jollivet, C., et al., *Detailed Characterization of Optical Fibers by Combining S-2 Imaging With Correlation Filter Mode Analysis.* Journal of Lightwave Technology, 2014. **32**(6): p. 1068-1074.
150. Jasapara, J. and A. Yablon, *Spectrogram approach to S2 fiber mode analysis to distinguish between dispersion and distributed scattering.* Optics letters, 2012. **37**(18): p. 3906-3908.
151. Hui, R. and M. O'Sullivan, *Fiber optic measurement techniques*. 2009: Academic Press.